CHANGES IN MITOCHONDRIAL FUNCTION IN GLIOMA CELLS UNDER HYPERGLYCAEMIA

MAHALAXMI GANJOO

PhD Thesis

2022

SREE CHITRA TIRUNAL INSTITUTE FOR MEDICAL SCIENCES AND TECHNOLOGY TRIVANDRUM

Changes in Mitochondrial Function in Glioma Cells under Hyperglycaemia

A THESIS PRESENTED BY

MAHALAXMI GANJOO

TO

THE SREE CHITRA TIRUNAL INSTITUTE
FOR MEDICAL SCIENCES AND TECHNOLOGY, TRIVANDRUM
THIRUVANANTHAPURAM

IN PARTIAL FULFILMENT OF THE REQUIREMENTS

FOR THE AWARD OF

DOCTOR OF PHILOSOPHY

2022

DECLARATION BY STUDENT

I, **MS. MAHALAXMI GANJOO** hereby certify that I had personally carried out the work depicted in the thesis titled **"Changes in mitochondrial function in glioma cells under hyperglycaemia"** under the direct supervision of Dr G Srinivas, Scientist G, Head, Department of Biochemistry, Sree Chitra Tirunal Institute for Medical Sciences and Technology, Trivandrum; except where external help was sought and is acknowledged. No part of the thesis has been submitted for the award of any other degree or diploma prior to this date.

Date: 04/01/2022 Mahalaxmi Ganjoo

CERTIFICATE BY THE RESEARCH GUIDE

This is to certify that **Ms. MAHALAXMI GANJOO** has fulfilled the requirements prescribed for the PhD degree of the Sree Chitra Tirunal Institute for Medical Sciences and Technology, Trivandrum. The thesis entitled **"Changes in mitochondrial function in glioma cells under hyperglycaemia"** was carried out under my direct supervision. No part of the thesis has been submitted for the award of any other degree or diploma prior to this date.

Date: 04/01/2022

Dr G. Srinivas (Guide)

Changes in Mitochondrial Function in Glioma Cells under Hyperglycaemia

A THESIS PRESENTED BY

MAHALAXMI GANJOO

TO

THE SREE CHITRA TIRUNAL INSTITUTE
FOR MEDICAL SCIENCES AND TECHNOLOGY, TRIVANDRUM
THIRUVANANTHAPURAM

IN PARTIAL FULFILMENT OF THE REQUIREMENTS

FOR THE AWARD OF

DOCTOR OF PHILOSOPHY

GUIDE

Dr. SRINIVAS GOPALA, Ph.D
Scientist G & Head
Department of Biochemistry
Sree Chitra Tirunal Institute for
Medical Sciences and Technology
Trivandrum – 695011, Kerala

EXAMINER

Acknowledgements

I would like to express my sincere gratitude towards my PhD supervisor, Dr G Srinivas for his guidance, support and his faith in me. This process of PhD would have never been possible without him and his constant support through it all. I would also like to thank the Institute and Department of Science and Technology for the fellowship assistance I received during this tenure of PhD.

I would also like to acknowledge the immense help with regard to polishing my skill as a student and researcher that was given to me by the faculty and staff of the Department of Biochemistry, SCTIMST. The mentorship I received from the professors Dr Madhusoodanan U K and Dr Cibin T R has been valuable and their encouragement through all the highs and lows have been pivotal in keeping me motivated to accomplish this work. The other staff of the department, Dr Deepa and Dr Geetha have been immensely supportive and kind for which I sincerely acknowledge them.

I would also like to acknowledge my Doctoral Advisory Committee members, Dr Anoopkumar T from the Department of Molecular Medicine and Dr Deepti AN from the Department of Pathology, SCTIMST; for their invaluable inputs throughout this journey without which it would have been hard to generate a consolidated work. I acknowledge the tremendous help from the Division of Academic Affairs, the Registrar, the Dy Registrar, previous and current Deans and previous and current Directors for their support and assistance in all of the academic matters.

I could have not accomplished this feat without the helping hands and intellectual conversations with my seniors and peers without which I would have lacked the clarity of ideas and work that were instrumental in completing my PhD. I thank my seniors Dr Raji SR, Dr Nandhini RJ, Dr Anand CR, Dr Bhavya Bharatan and Dr Dhanya Krishnan and my peers Deepthi, Ganga, Aishwarya, Dr Pravi, Soumya Krishnamoorthy, Dr Revathi, Dr Vinu, Dr Anila Mani, Dr Sapna Mishra, Dr Sunu Thomas and countless others from various departments of the institute. I would like to give a special thanks to Ashok S, Dr Jyothi EK and Dr Manjunatha S, as they have had tremendous contribution in shaping my work, encouraging me throughout the journey and helping me accomplish my PhD.

Last but not the least I thank my family for their tremendous patience and faith in me and for imparting in me the values like work ethic, dedication and above all a scientific temperament.

TABLE OF CONTENTS

vi. **CRITICAL METHODOLOGICAL INSIGHT – II**

mTOR inhibition gives different inferences regarding mitochondrial function when assessed using different protocols

vii. CHAPTER 5**: WHAT CAUSES HG MEDIATED CHANGES IN THE MITOCHONDRIAL FUNCTION?**

Are the changes in mitochondrial function due to hyperglycaemia mediated by autophagy decline?

List of Figures

List of Abbreviations

ADP	:	Adenosine di phosphate
APS	:	Ammonium persulphate
ATCC	:	American Type Culture Collection
Atg	:	Autophagy-related genes
ATP	:	Adenosine Triphosphate
BAF	:	Bafilomycin
BCA	:	Bicinchoninic acid
BSA	:	Bovine Serum Albumin
CCCP	:	Carbonyl cyanide 3-chlorophenyl-hydrazone
CNS	:	Central Nervous System
DAF-FM	:	4-amino5-Methylamino-2',7'-Difluorofluorescein Diacetate
DMEM	:	Dulbecco`s Modified Eagle Medium
DMSO	:	Dimethyl Sulfoxide
DNA	:	Deoxy ribonucleic acid
Drp	:	Dynamin-related protein
DTT	:	Dithiothreitol
EDTA	:	Ethylenediamine tetra acetic acid
EGTA	:	Ethylene glycol-bis (β-aminoethyl ether)-N, N, N', N'-tetraacetic acid
ETC	:	Electron transport chain
$FADH_2$	:	Flavin adenine dinucleotide+hydrogen
FBS	:	Fetal Bovine Serum
FDA	:	Food and Drug Administration

G6PD	:	Glucose 6-Phosphate Dehydrogenase
HCl	:	Hydrochloric acid
HRP	:	Horse Radish Peroxidase
HRR	:	High Resolution Respirometry
LC3	:	Microtubule-associated protein1 light chain 3
LDH	:	Lactate Dehydrogenase
MiR05	:	Mitochondrial respiration buffer
MFF	:	Mitochondrial fission factor
Mfn	:	Mitofusin
MMP	:	Matrix metalloproteinase
mM	:	Milli Molar
mtDNA	:	mitochondrial DNA
mTORC1	:	Mammalian target of rapamycin complex1
MTT	:	4,5- dimethylthiazol-2-yl
NADH	:	Nicotinamide adenine dinucleotide (NAD) + hydrogen (H)
L-NAME	:	N(G) nitro-L-arginine methyl ester
$NaHCO_3$	:	Sodium Bicarbonate
nmol	:	Nano Molar
NO	:	Nitric Oxide
OCR	:	Oxygen consumption rate
Opa	:	Optic atrophy protein
OXPHOS	:	Oxidative phosphorylation
Pal	:	Palmitoyl-L-carnitine
PBS	:	Phosphate buffered saline
PCR	:	Polymerase Chain Reaction
qPCR	:	Quantitative PCR

PI		Propidium Iodide
PI3K		Phosphatidyl Inositol 3-Kinase
PGC-1α		Peroxisome proliferator-activated receptor-gamma coactivator 1α
FDG-PET	:	Fluorescent deoxy glucose Positron Emission Tomography
PKA	:	Protein kinase A
pmol	:	Pico Mole
PVDF	:	Polyvinylidene fluoride
qRT PCR	:	Quantitative Real Time Polymerase Chain Reaction
RIPA	:	Radio immuno Precipitation Assay
RNA	:	Ribonucleic acid
ROS	:	Reactive Oxygen Species
rpm	:	Revolutions per Minute
SDS-PAGE	:	Sodium dodecyl sulphate Polyacrylamide gel electrophoresis
SDH	:	Succinate Dehydrogenase
SEM	:	Standard Error of Mean
SUIT	:	Substrate-Uncoupler-Inhibitor-Titration
T2DM	:	Type 2 Diabetes mellitus
TBST	:	Tris Buffered Saline Tween 20
TCA	:	Tri carboxylic acid
TEMED	:	Tetramethyl ethylene diamine
TMPD	:	Tetramethyl-p-phenylenediamine
TMRE	:	Tetramethyl rhodamine ethyl ester
w/v	:	Weight/Volume
μm	:	Micro Meter
μM	:	Micro Mol

SYNOPSIS

Introduction:

The nervous tissue is composed of the neurons and the supporting glial cells. Glioma is the malignancy of these glial cells, and based on the severity can be Grade I to IV. Glioblastoma is the high-grade astrocytic tumour with poor prognosis. Glioma cells, like all cancers have altered metabolic phenotype with preferential utilization of glucose for the glycolytic ATP generation instead of the mitochondrial oxidative phosphorylation-based ATP generation. This altered metabolism is termed as the Warburg effect. Diabetes also manifests as an altered metabolic phenotype and there are multiple studies that have shown associative links between diabetes and cancer of various tissues. But there exists a negative correlation between diabetes and glioma stating that the individuals with Type 2 Diabetes are at a reduced risk of development of glioma. It is unknown as to how this deviation is observed in epidemiological data. We thus sought out to determine how diabetes metabolically affects glioma.

Mitochondrial fatty acid metabolism in glioma:

Diabetes can be metabolically classified into hyperglycaemic state and hyperlipidaemic state. We first needed to assess if lipid or glucose is the preferred fuel for the mitochondria in glioma. To determine we used Oroboros High resolution respirometry (oxygraphy) which can determine the mitochondrial oxygen consumption and thus the mitochondrial respiration in real time. We cultured the U251 glioblastoma cells in DMEM with 5.5mM glucose (recommended media for the cell) and upon the desired confluence, trypsinized them and added to the two chambers of the oxygraphy with one chamber receiving solely carbohydrate substrates (Glutamate, Malate and Pyruvate) while the other receiving solely fatty acid substrates (Palmitoyl carnitine and Malate) and the respiration compared between the two. This was performed following permeabilization of the cells with digitonin and with abundant ADP added to the chambers. We observed that although the glioma cells were capable of utilizing both carbohydrate and fatty acid substrate, the gain in oxygen consumption following uncoupling of the mitochondria by the uncoupler CCCP (which corresponds to the maximal respiration possible) was significantly lower with fatty acid substrates suggesting that it would not be the preferred source for metabolism. We thus focused on the hyperglycaemic stress mediated changes in glioma metabolism.

Formulation of the title and hypothesis:

Hypothesis: Hyperglycaemia effects the metabolism and mitochondrial function in glioma cells

Title: Changes in mitochondrial function in glioma cells under hyperglycaemia

Objectives of the study were to assess the following:

1. To determine if hyperglycaemia affects glioma aggressiveness
2. To determine if hyperglycaemia affects mitochondrial function in glioma
3. To determine what causes the hyperglycaemia mediated changes in the glioma mitochondrial function
4. To determine if hyperglycaemia affects the mitochondrial health in glioma cells

High glucose and Glioma aggressiveness:

Two glioblastoma cell lines were used for the study, U87 and U251. The cells were given normal glycemia i.e., 5.5 mM glucose containing media (corresponding to 90 mg/dl) and hyperglycaemia i.e., 30 mM glucose containing media (corresponding to 540 mg/dl) for 72 h. To determine aggressiveness, cell proliferation (using MTT assay and Hoechst-PI based cell counting of live and dead cells), cell migration (with scratch wound assay), invasion (with immunoblotting of Matrix metalloproteins – MMP2 and MMP9 which are invasion markers) and anoikis resistance (the capacity to survive in a non-adherent plate shown with PI staining of dead cells) were determined. It was observed that glioma cells become more aggressive with the hyperglycaemia.

High glucose and mitochondrial metabolism in glioma:

For the metabolism-based study, only one cell line was used – U251. We first assessed the glucose uptake in the HG cells with colourimetry and fluorometry and observed that the HG cells had higher glucose uptake than the control (normo-glycaemic cells). The glucose consumed enters the glycolysis and the end product pyruvate has only two metabolic fates, it can either enter the mitochondrial Kerbs' cycle and undergo oxidative phosphorylation or be converted into lactate and exit the cell thereby reducing extracellular pH. When the pH and lactate concentration of the cell culture media was assessed, the HG cells had lower pH and higher lactate suggesting utilization of the consumed glucose to drive glycolysis for energy production.

Also, the pyruvate converting to acetyl-CoA and entering the Krebs' cycle does not assure mitochondrial metabolism. The determining step for the commitment towards mitochondrial based respiration is with the conversion of citrate to aconitate by aconitase in the Krebs' cycle;

as citrate can shuttle out of the mitochondria for lipogenesis but aconitate does not support such anabolic processes. With Western blotting it was determined that the HG caused a decline in aconitase suggesting less commitment of glucose towards oxidative phosphorylation.

We then assessed if HG changes mitochondrial function for which we used the same cell culture techniques and analysed the mitochondrial function with high resolution respirometry, with three different protocols using only carbohydrate mediated substrates.

Intact cell respiration (Cellular bioenergetics): The intact cell respiration was determined wherein following addition of cells in the chambers of the oxygraphy, only inhibitors of mitochondrial electron chain transport chain were sequentially given. After the routine respiration was measured (the respiration value obtained following addition of cells alone) Oligomycin, that blocks ATP synthase, was added to measure the leak respiration not linked to ATP generation. This was followed by uncoupling with CCCP (giving maximal respiration) and finally addition of Rotenone and Antimycin (Complex I and III inhibitors respectively) to halt all respiration and getting background respiration (ROX). All values were normalized with the total protein in the chambers. It was observed that HG reduced mitochondrial respiration.

States of Respiration: The observed decline in respiration could be either due to decline in mitochondrial efficiency or due to lack of intracellular metabolites that drive the oxidative phosphorylation. To assess if the decline in the respiration was due of any decline in the capacity of the mitochondria, the cells were permeabilized using digitonin and supra-physiological concentrations of the substrates of individual complexes were added sequentially. Glutamate, Malate, Pyruvate (Complex I substrates) and succinate (Complex II substrate) were added to determine states of respiration with State3 corresponding to the respiration with no limiting substrates. Maximal respiration was obtained with uncoupler CCCP; following Complex I inhibition with Rotenone, Complex II maximal was also determined. All values were ROX negated and normalized with total protein in the chambers. States of Respiration:

- **State 1** –Routine respiration without any exogenous substrates (ADP and substrates both limiting)
- **State 2** – Substrate availability but ADP limiting
- **State 3** – All substrates are abundant, respiratory chain limiting (total oxidative phosphorylation capacity)

- **State 3 uncoupled / maximal State 3**– Following the uncoupling with the uncoupler with all substrates abundant
- **Maximal State 3 for Complex II** – Maximal respiration following Complex I inhibition with Rotenone

It was observed that HG mediated respiration was declined even with sufficient substrates thus concluding that HG caused decline in the mitochondrial capacity.

Complex Activity: To assess if the decline in mitochondrial capacity is due to the decline in any specific complex of the respiratory chain in the mitochondria, we determined the activity of complexes I, II and IV individually. The cells were permeabilized and substrates of only complex I (same as above) were added followed by inhibition of the same with Rotenone thus giving the activity of Complex I alone. To move the electron transport chain forward, substates for the next complex were added only after inhibiting the previous one. Similarly, for complex II and IV, Succinate and a mixture of Ascorbate and TMPD (electron donor to complex IV directly) respectively were added and inhibition with Malonate (Complex II inhibitor) and Azide (Complex IV inhibitor) respectively were done. It was observed that HG decreased the capacity of individual complexes with maximal inhibition of Complex II.

These results point out that HG treatment increased the observed Warburg effect i.e., the preference of glycolysis as the energy source instead of mitochondrial respiration, providing survival advantage to the cancer cells.

How does High glucose increase the Warburg effect in glioma?

We next went on to determine what mediates this HG induced enhanced Warburg effect. We assessed the reported effects that HG causes that has the potential to alter the metabolic phenotype of the cells.

HG and Nitric oxide generation:

It is known that the HG stress changes cellular Nitric oxide levels and nitric oxide has a direct effect on the mitochondria-based respiration. The NO levels were assessed with DAF-FM based fluorescent staining and HG treated cells showed high NO production at 6 h and 12 h. L-NAME, an inhibitor of cellular nitric oxide synthase was used under the HG condition and mitochondrial respiration with Oxygraph was measured using all the three protocols mentioned above. NO inhibition had a mild improvement of the mitochondrial respiration under HG. To determine if the effect was indeed due inhibition of NO production and not due

to any other pleiotropic effects of L-NAME, Sodium nitrate (a nitric oxide donor) was given with the L-NAME treatment and it was observed that the improvement in mitochondrial respiration was lost. This suggests that the NO generation under HG condition resulted in the observed decline in the mitochondrial respiration.

HG and Autophagy:

Autophagy is the bulk cellular degradative process that maintains homeostasis within the cells wherein a membrane bound structure is formed engulfing some cargo and fusing with the lysosome for its degradation. With nutrient deprivation, there is increased autophagy that degrades the non-essential molecules to provide simple building blocks required for survival of the cells; while with high nutrient availability, there is expected to be a decline in autophagy. We assessed it through LC3II accumulation following blocking the autophagy at the last step with Bafilomycin A1. We observed that autophagy was deficient in the HG cells. To assess if decline in autophagy was associated with the observed decline in mitochondrial function, we induced autophagy with Rapamycin and Torin under HG state and assessed the mitochondrial function with the above-mentioned protocols. It was observed that with autophagy induction with both these compounds under HG, the mitochondrial function improved.

The autophagy inducers that were used work at the upstream step of autophagy, by blocking mTOR, which is a negative regulator of autophagy. mTOR is the master nutrient and growth factor sensor of the cell and directs the cell through the cell cycle. mTOR thus has its own effects on the mitochondrial respiration independent of the effects it can bring about through autophagy. Thus, to evaluate if the improvement of the mitochondrial respiration is indeed due to autophagy, we used Lithium Chloride; another autophagy inducer which is independent of mTOR signalling and causes autophagy activation through increased phagophore formation. LiCl mediated autophagy induction showed some improvement of mitochondrial respiration under HG, which was not as much as observed with Rapamycin and Torin. We thus conclude that the autophagy decline that happens with HG causes a decline in the mitochondrial respiration in glioma. Rapamycin and Torin could have resulted in a synergistic effect on the mitochondrial respiration by modulating both mTOR and autophagy.

It was next determined if the NO signalling and the autophagy signalling are related, as they had the same effect on the mitochondrial respiration under HG. Immunoblot was performed to determine the autophagy with NO inhibition and it was observed that the autophagy

increased with NO inhibition. Thus, the effects observed by both NO inhibition and autophagy augmentation were the similar.

Changes in mitochondrial health with autophagy decline:

It needed to be established why autophagy decline under HG caused a decline in the mitochondrial function. As autophagy is the cellular degradative process, its decline could cause accumulation of unhealthy mitochondria. To test this hypothesis, mitochondrial content was determined by two methods; fluorescence based mitochondrial measurement using MitoTracker green dye and with Real-time PCR-based quantification of mitochondrial DNA normalized to a gene from the nuclear DNA. It was observed that HG increased mitochondrial content. To ensure it was due to accumulation of old mitochondria and not because of the formation of new mitochondria, master-regulator of mitochondrial biogenesis PGC1alpha was examined by immunoblotting and it was found that it declined under HG suggesting less stimuli for the formation of new mitochondria under HG.

The mitochondrial health was determined by analysing mitochondrial membrane potential by TMRE based fluorescence staining which accumulates in the mitochondria with high membrane potential and gives fluorescence. As the mitochondrial membrane potential is the driver of ATP formation, this was used as a measure for mitochondrial quality. It was observed that under HG the healthy mitochondria with optimum membrane potential declined.

Changes in mitochondrial network with autophagy decline:

As the mitochondrial network has a critical impact on the mitochondrial function, we analysed mitochondrial network by observing mitochondrial fragmentation and observed that HG increased the fragmentation of the mitochondria. Thus, we infer that HG stress disrupts mitochondrial architecture and causes accumulation of damaged mitochondria in the cell which may be driving the decline in the mitochondrial respiration observed under HG.

It was concluded from the previous experiments that the decline in autophagy under the HG condition mediates the decline in mitochondrial metabolism by potentially causing accumulation of inefficient mitochondria. It thus must follow that the interventions that were employed to enhance autophagy under the HG condition must also impact the mitochondrial health and network. We thus analysed the mitochondrial membrane potential and mitochondrial interconnectedness with the autophagy induction and observed that the mitochondrial membrane potential and mitochondrial network were both improved under HG condition with autophagy induction through Rapamycin, Torin, LiCl as well as NO suppressor

L-NAME. The TMRE based mitochondrial membrane potential was also assessed with autophagy induction and it was observed that when autophagy was induced under HG condition, the mitochondrial membrane potential was higher than with HG alone. This confirms that autophagy decline observed under HG causes the mitochondrial network disruption and accumulation of unhealthy mitochondria.

Summary and Conclusion:

- HG increased proliferation, migration, invasion and anoikis resistance in glioma thus making them more aggressive.
- HG alters the metabolism in glioma, with increasing the glucose uptake, glycolysis mediated energy production and declining the mitochondrial oxidative phosphorylation.
- There was increased shuttling of the glucose through the glycolysis pathway thus secreting lactate which caused changes in the microenvironment, lowering extracellular pH.
- The decline in the mitochondrial respiration under HG was mediated by lowering of mitochondrial efficiency and quality as observed through decline in mitochondrial membrane potential.
- There was also increased disruption of mitochondrial network in the glioma cells under HG.
- HG caused a decline in autophagy which resulted in the accumulation of inefficient mitochondria in the cell.
- This accumulation of inefficient mitochondria under HG impaired mitochondrial metabolism and could be the reason behind observed decreased mitochondrial oxidative phosphorylation.
- This could be one of the ways of augmentation of the Warburg effect observed under the HG stress.
- This increased Warburg effect is beneficial for cancer cell survival and thus could be the basis of increased aggressiveness of glioma.
- Interventions that target increase in the autophagy under HG condition improved the mitochondrial metabolism, mitochondrial health and architecture and had tendency

towards lowering glucose consumption and lactate secretion thus suggesting a decline in Warburg effect.

With these findings we conclude that the HG state being a nutrient rich state causes a decline in autophagy. This generalized decline in autophagy affects the clearance of damaged protein aggregates and organelles like the mitochondria. Thus, there is an accumulation of damaged mitochondria in the HG state which lowers the mitochondrial capacity for oxidative phosphorylation thus making the cells under HG relay on glycolysis even with the high glucose consumption. This increased glycolysis must be the driver of augmented Warburg effect observed in glioma cells under HG, and as the Warburg mechanism provides survival advantage to cancer cells; this could potentially result in the increased aggressiveness of glioma observed under HG.

Chapter 1

Introduction

The nervous tissue is divided into the neurons that perform the function of impulse generation and conduction and the supporting cells collectively called the glial cells. These include the astrocytes; which are the nutritionally supportive cells for the neurons as they form the part of the blood brain barrier; oligodendrocytes which form the myelin sheath that is a fatty layer surrounding the neurons and increase the speed of nerve impulses; the microglial cells that are the resident macrophages and form the immune and surveillance cells of the nervous system; the ependymal cells, forming the ciliated epithelial layer of the ventricles of the brain and help in the cerebrospinal fluid formation and homeostasis, metabolism and metabolic waste management of the central nervous system. Glioma are the tumours of the glial cells and form the most widespread tumour originating in the CNS. The origin of gliomas is debatable and it is not known whether they originate from the neural or glial precursor cells, stem cells or glial cells (Modrek et al., 2014).

Gliomas are generally classified into four groups, Grade I to Grade IV. The cells under Grade IV are highly proliferative and metastatic suggesting high aggressiveness. The tumour forms the capacity of neo-vascularization and often has a necrotic zone. The various layers of cells can have different tumour microenvironments with the outermost layer more nutrient rich while the inner layers show signs of necrosis and hypoxia. The Grade IV glioma are also called glioblastoma and are mostly astrocytic in origin.

Glioblastoma has the highest prevalence rate of all types of gliomas at an estimated 54.7% and an incidence rate of 3.2 per 100,000 individuals (Ferlay et al., 2015). The mainstream treatment of glioma is surgical resection, radiotherapy and chemotherapy with primarily Temezolomide, but they offer many complications as most gliomas are detected at later stages and become nonresectable through surgery and sometimes show resistance to radiation and chemotherapy (Edick et al., 2005). This makes the post diagnosis mean survival of 15 months (Edick et al., 2005). There thus have been much research into understanding the biochemistry of this set of tumours to provide better avenues for treatment and management.

One of the most well studied is the metabolic aspect in cancer cells. Cancer cells have and altered metabolic profile as compared to the normal tissues that they originate from. This was first described by Otto Warburg nearly a century ago and has been termed the Warburg effect (Koppenol et al., 2011). He observed that cancer cells had a high rate of glycolysis and an increased conversion of consumed glucose to lactate even with the sufficient oxygen availability. Previously the glycolysis was thought to occur only in the absence of oxygen to maintain some reserves of ATP as the normal pathway was the more energy favourable mitochondrial oxidative phosphorylation which was dependent upon oxygen availability; the means by which this pathway is operates is summarized in the Fig A below. The Warburg effect is so common among all types of cancers that this principle has been utilized in the FDG-PET scanning as a method of cancer diagnosis Fig B.

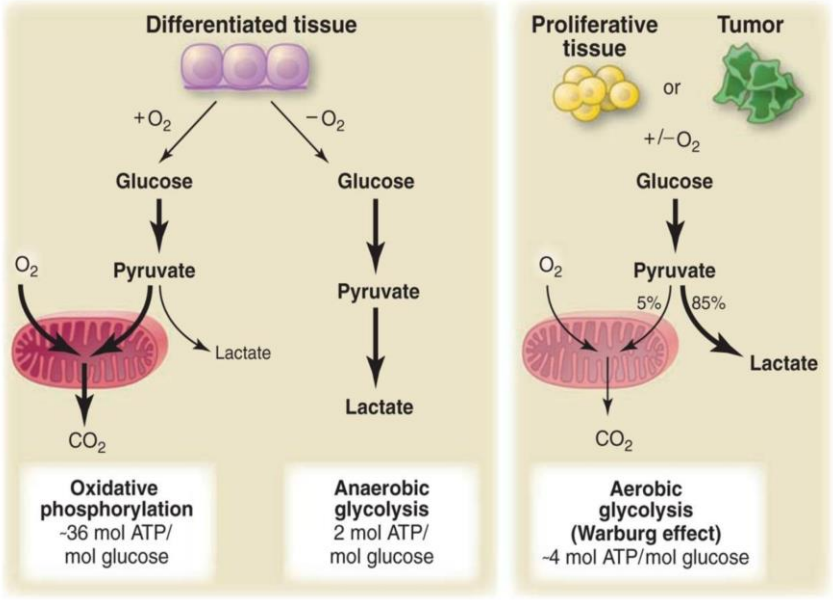

Fig A: The difference in the metabolic profile of the normal and transformed cells, with Cancer cells undergoing the Warburg effect

i 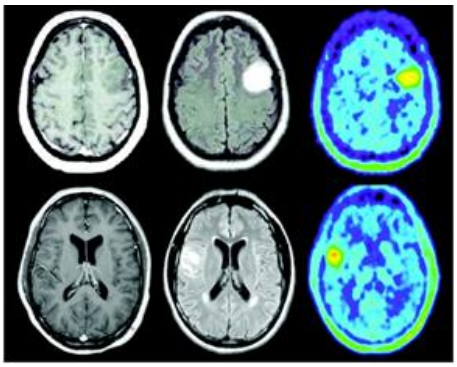 ii 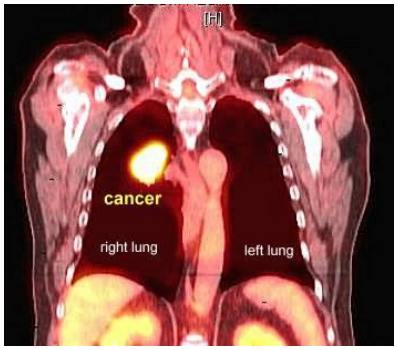

Fig B: FDG- PET based scan of the tumour mass - The over saturated bright mass observed in the brain tissue (i) and lung tissue (ii) are tumour masses and they are observed brighter than the surrounding region owing to the increased glucose uptake by the tumour as opposed to the surrounding normal tissue.

Diabetes is also a condition which is characterised by an altered metabolism. With diabetes, there have been various cellular mechanisms that become improper which forms the basis of diabetes associated complications found in various tissues like the cardiac, renal, retinal tissues etc. Overall, there are profound changes observed in mitochondrial oxidative phosphorylation leading to cellular toxicity altered calcium signalling, ROS generation, change in the metabolite pool, etc. (Boudina et al., 2007), (Bugger et al., 2008). There are many studies pointing at the associations between obesity, diabetes and cancer dating back to 19th and early 20th century wherein a patient with polyurea and sweet urine was diagnosed with carcinoma and the epidemiological survey in South Africa where diabetes was associated with an increased risk of cancer respectively (MAYNARD, 1910). The biggest link of obesity and cancer comes from the Cancer Prevention Study (CPSII) conducted in the USA between 1982 to 1996 and enrolled over a million adults and observed the height and weight versus cancer mortality. It was found that both men and women with obesity had 40-80% increased risk of cancer mortality (Calle et al., 1999). The diabetes (type II) and the cancer risk was assessed by many one such being the National Health and Nutrition Examination Survey (NHANES I), wherein the lung, colorectal, breast and prostate cancer risk was examined in 14,407 participants and it was observed that there was a 39% increased risk of cancer development in the diabetic group (Steenland et al., 1995).

There still was a debate as to causation and mere association in these studies as depicted in Fig C, which was resolved by one of the largest meta-analysis performed that selected 151 cohorts and 32 million people and came to the conclusion that there was a strong causation between Type 2 diabetes and incidence of endometrial, pancreatic, and liver cancer along with a strong causation of mortality with pancreatic cancer (Ling et al., 2020).

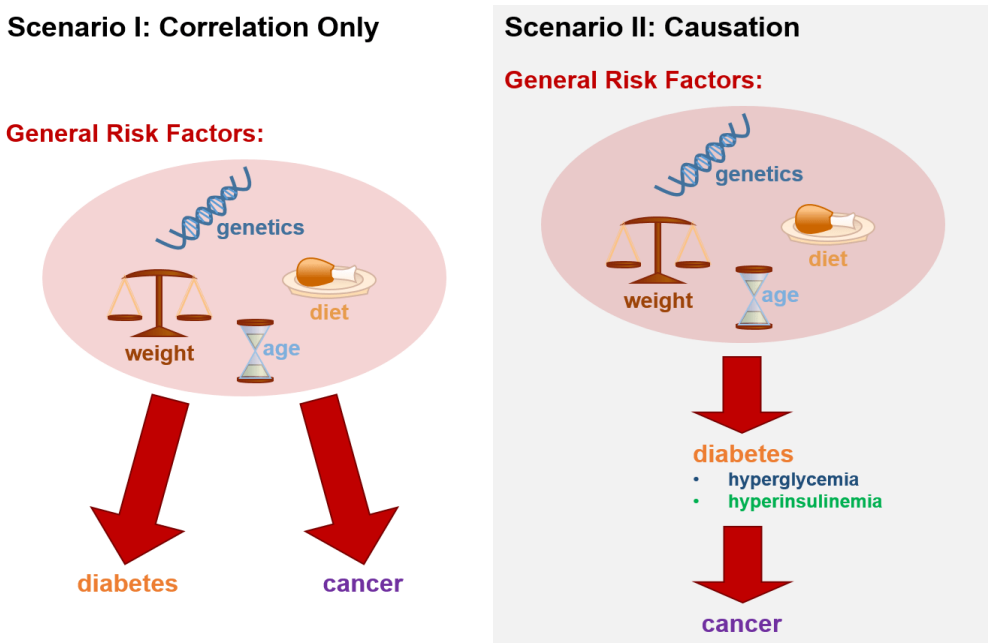

Fig C: Correlation versus Causation among the risk factors for cancer and diabetes

Although these studies have shown a positive correlation and a causation with diabetes and many types of cancers that is not the case with the gliomas. Multiple studies have tried to find correlations and associations between diabetes and metabolic syndrome and the risk of glioma with observations ranging from a trend without statistical significance towards an inverse correlation (Schlehofer et al., 1992), (Cicuttini et al., 1997), (Schlehofer et al., 1999), no relation (Wideroff et al., 1997), (Hjalgrim et al., 1997), (Campbell et al., 2012), (O'Mara et al., 1985), mixed relation (Adami et al., 1991) and highly significant negative relation between the two (Swerdlow et al., 2005), (Atchison et al., 2011), (Schwartzbaum et al., 2005), (Kitahara et al., 2014).

It is thus essential to find how diabetes metabolically affects glioma and the metabolic changes that the glioma undergoes in a diabetic environment that could shed some light on the aforementioned phenomenon. An *in vitro* model of hyperglycaemia was used for analysing its effects on mitochondrial metabolism and function.

Chapter 2

What is the likely source for glioma metabolism – Fatty acids or Glucose?

2.1 Introduction

The effects of diabetes on mitochondrial metabolism cannot be estimated in an *in-vitro* system with very accurate simulation of diabetic condition. Diabetes is a metabolically complex condition but can be predominantly differentiated into a hyper-glycaemic state and a hyper-lipidemic state. Both the glucose and lipids can form sources of fuel and can have an effect on the mitochondria. Thus, to assess how diabetes metabolically affects glioma and its mitochondria, we need to first decipher which of the two states mentioned above exerts a higher effect on mitochondria. Although, it is generally known that brain uses glucose predominantly under normal conditions, but under certain disease conditions, like cancer, the metabolic preference could be altered and cells may tend to use substrates that are not normally used as the primary metabolic source. It remains to be elucidated if such is the case in glioma, and it would thus be worthwhile to know which of the two is the preferred metabolic fuel for the glioma cells.

2.2 Review of Literature:

Whenever there is rapid proliferation in cells within a tissues, it is also accompanied with altered lipid metabolism as seen in both stem cells and cancerous cells when compared with the differentiated cells of the respective tissue (Santos and Schulze, 2012) (Beloribi-Djefaflia et al., 2016). The glioma cells are shown to have a high lipid biogenesis (Guo et al., 2013), with the studies also speculating that the lipid profile within the tumours is different corresponding with the difference in the severity of the glioma. The lipids that are taken up can either be utilized or stored as lipid droplets for use as metabolic substrates in the future. Lipid droplets are cellular organelles with a phospholipid layer enclosing triacylglycerol moiety formed when fatty acids are esterified with glycerol. The brain tissue does not undergo fatty acid beta oxidation for the production of ATP and thus have minimal levels of lipid droplets. However, recent studies have shown that the glioma cells show accumulation of these lipid droplets suggesting an alteration of the basal lipid metabolism and usage within the glioma (Welte, 2015) (Gupta et al., 2011).

The study by Tugnoli et. al. demonstrated with Nuclear Magnetic Resonance spectra that the grade of glioma had a correlation with the lipid spectra found through glioma extracts (Tugnoli et al., 2001). Different forms of lipids have shown a role in not only the cellular metabolism but in signal transduction as well with phospholipids, fatty acids, triacyl glycerol, etc. affecting physiological responses (Muro et al., 2014). Lipids can also have effects in processes other than the metabolic fuel sources. It is well documented that cancer cells require active generation of biomass including lipids which are necessary for the production of bio-membranes in the rapidly proliferating cells like cancer. These lipids can either be synthesised de novo or could be taken up from the extra cellular microenvironment and utilised for the anabolic processes. The study by Taib et.al., shows that oleic acid treatment increases the proliferation in glioma cells but not in normal astrocytic cell (Taïb et al., 2019). It has also been shown that with limiting the availability of lipids, the tumour cells increased the de novo fatty acid synthesis suggesting that the fatty acids are critical in maintaining their survival and growth (Zaidi et al., 2012). These studies indicate that the glioma cells are critically reliant on fatty acids for their growth but whether this is for the generation of ATP through beta oxidation or for the generation of new biomass that are required by the cells is not elucidated well.

2.3 Materials and Methods:

2.3.1 Reagents:

DMEM low glucose were purchased from HiMedia Laboratories (Mumbai, India). the reagents required for the isolation of mitochondria, various Substrates, Uncouplers and Inhibitors for the Mitochondrial oxygen consumption studies (SUIT protocols), like Oligomycin, CCCP, Rotenone, Antimycin, Glutamate, Sodium Pyruvate, Malate, etc. as well as common reagents like EDTA were purchased from Sigma Aldrich (MO, USA). Fetal Bovine Serum (FBS) (South American origin) was sourced from Gibco (Grand Island, USA). Trypsin was procured from PAN Biotech (Aidenbach, Germany).

2.3.2 Cell Culture and Maintenance:

U251 Glioblastoma cell line was a kind gift from Dr TR Santosh Kumar (Rajiv Gandhi Centre for Biotechnology, Trivandrum, Kerala). Cells were grown in a humidified incubator at 37°C with 5% CO_2 in low glucose DMEM (ATCC recommended media) with 10% FBS as adherent monolayer cultures. The media was changed every 48 h and the cells were re-passaged after attaining more than 80% confluence. This was done through using 0.25% trypsin-EDTA solution made in Phosphate Buffered Saline (PBS), generating non-attached cells. Cells were collected in a 15 ml tube and centrifuged to remove excess trypsin. Following a PBS wash and re-centrifugation, cells were suspended in fresh complete media (DMEM with 10% FBS) and seeded at the density of approximately $1x10^6$ cells per ml. All experiments were performed with the cells having attained nearly 80-90% confluence.

2.3.2.1 Reagents used for Cell culture

2.3.2.1.1 DMEM (low glucose) (pH 7.4)

Low glucose phenol red and pyruvate containing DMEM in powder form was used in sterile MilliQ water, filtered and stored in autoclaved bottles.

2. 3.2.1. 2. Phosphate-buffered saline (PBS) (pH 7.4)

Sodium chloride 137 mM, potassium chloride 2.7 mM, disodium hydrogen phosphate 10.14 mM, potassium dihydrogen phosphate 1.76 mM in sterile MilliQ water.

2. 3.2.1. 3. Trypsin EDTA solution (pH 7.4)

0.25% trypsin, 0.53mM EDTA in PBS.

2.3.3 High Resolution Respirometry

Mitochondrial functional analyses were performed in Oxygraph-O2k, High-Resolution Respirometry (Oroboros Instruments, Innsbruck, Austria) at 37°C with a stirring speed of 750 rpm. Amplified signals from the oxygen sensor were recorded at sampling intervals of 2 s using DatLab-6.1 Software (Oroboros). Air-calibration of the

respirometer with MIRO5 was performed at air saturation, 37°C before the commencement of each experiment. Addition of substrates, uncoupler, and specific inhibitors of mitochondrial electron transport chain (ETC) complexes was performed using Hamilton syringes manually.

2.3.3.1 Fatty acid versus Carbohydrate protocol:

Cells were trypsinized at attainment of desired confluence and centrifuged to remove trypsin, following a wash with PBS and re-centrifugation cells were suspended in mitochondrial respiration buffer (MIRO5) and equal cells were added in each of the two chambers of the Oxygraph. One of the chambers was given only carbohydrate substrates while the other was given only fatty acid substrates following cell permeabilization with Digitonin; and the respiration was recorded. For carbohydrate substrates glutamate (10 mmol/L), malate (M) (2 mmol/L) and pyruvate (5 mmol/L) were added while for fatty acid substrates, palmitoyl- L-carnitine (Pal) (25 μmol/L) and malate (M) (2 mmol/L) were used. After addition of ADP (5 mmol/L) to the medium, State 3 respiration was achieved. Uncoupler CCCP was titrated to assess the maximal respiration with both substrate types followed by the addition of Rotenone and the experiment was culminated with the addition of Antimycin A. The respiration obtained following Antimycin A addition was taken as Residual Oxygen Consumption (ROX) and was subtracted from all obtained values. All values were normalized for the total protein in the chamber.

Mitochondrial respiration medium (MiR05)

	FW	Final Conc (mM)	Addition to 1 litre final Vol:
EGTA	380.4	0.5	0.190 g
$MgCl_2.6H_2O$	203.3	3	0.610 g
K-lactobionate	358.3	60	120 mL of 0.5 M stock
Taurine	125.1	20	2.502 g
KH_2PO_4	136.1	10	1.361 g

HEPES	238.3	20	4.77 g
Sucrose	342.3	110	37.65 g
BSA (FA free)		1 g/L	1 g

Table 1: Composition of mitochondrial respiration medium

Preparation of MiR05 stock solution

- Weighed given amounts of the listed chemicals (expect BSA and lactobionic acid) and transferred to a 1000 mL glass beaker.
- The big lumps were mechanically disrupted. (It was recommended to do this before adding water, because during dissolution these lumps do not disintegrate easily).
- Added ~ 800 mL H_2O and dissolved using a magnetic stirrer at ~30ºC.
- Added 120 mL of K-lactobionate stock solution.
- Adjusted the pH to 7.1 with 5 N KOH at 30ºC.
- Dissolved the BSA in a subsample of the MiR05 stock solution and added to the final MiR05 (Separate preparation of the BSA solution is recommended, since BSA produces foams that do not dissolve easily).
- Added H_2O to a final volume of 1000 mL and checked the pH and finally MiR05 was prepared.
- Divided into 4 mL portions in plastic vials and stored at -20ºC.
- Each vial was warmed to 37^0C before use and foam formation was avoided by gentle shaking. (It was recommended to use the stock solution on a single day only, to avoid microbial contamination of the respiration medium).

Preparation of K-lactobionate stock solution

Dissolved 35.83 g lactobionic acid in 100 mL H_2O, adjust pH to 7.0 with KOH, and adjusted volume to 200 mL with H_2O. pH - 7.1 (5 N KOH), divided and frozen at -20º C in falcon tube.

SUIT Protocol			
S/ U/ I	**Event**	**Volume (μL)**	**State**
Palmitoyl- Carnitine Malate	PCM	5 5	State 2 for fatty acid substrates
Glutamate Malate Pyruvate	GMP	10 5 5	State 2 for carbohydrate substrates
Adenosine 5' diphosphate	ADP	20	State 3
Carbonyl cyanide p-trifluoro-methoxy phenyl-hydrazone	CCCP	1+1..	ETS
Rotenone	Rot	1	State 3 CII ($FADH_2$ respiration)
Antimycin A	AA	1	ROX

Table 2: Protocol for mitochondrial oxygen consumption study

Chemicals for mitochondrial substrate-uncoupler-inhibitor titration (SUIT) protocols:

Substrates

Substrate	*FW*	*Stock solution Conc. (mM)*	*Stock solution Amount*	*Final concentration in 2ml (Volume within the Chambers)*

G: L- Glutamic acid	169.1	2000	3.382 g/ 10 mL H_2O	10 mM
M: L-Malic acid	134.1	400	536 mg/10 mL H_2O	2 mM
P: Pyruvic acid sodium salt	110	2000	44 mg/ 0.2 mL H_2O	5 mM
Pal: Palmitoyl-DL-carnitine-HCl	436.1	10	8.72 mg/ 2 mL H_2O	25 µM
D: ADP (Adenosine 5' diphosphate, potassium salt)	501.3	500	0.501 g/ 2 mL H_2O	5 mM

Table 3: Substrates used for the mitochondrial respiration experiments

Uncouplers

Uncouplers	*FW*	*Stock solution Conc (mM)*	*Stock solution Amount*	*Final concentration in 2ml (Volume within the Chambers)*
CCCP: Carbonyl cyanide 3-chlorophenylhydrazone	254.2	1	2.54 mg/ 10mL ethanol	0.5+0.5 µM

Table 4: Uncoupler used for the mitochondrial respiration experiments

Inhibitors

Inhibitors	FW	Stock solution Conc. (mM)	Stock solution Amount	Final concentration in 2ml (Volume within the Chambers)
AA: Antimycin A	540	5	11 mg/ 4mL ethanol	2.5 µM
Rot: Rotenone	394.4	1	3.94 mg/10mL ethanol	0.05 µM

Table 5: Inhibitors used for the mitochondrial respiration experiments

2. 4. Statistical analysis

All statistical calculations and preparation of graphs were carried out in Microsoft EXCEL 2020 software. Values are the average of a minimum of n=3 and expressed as the mean ± standard error of the mean (SEM). The significance of the difference from the respective control for each experimental test condition was assayed by Student's *t*-test as the distributions were normal. For all statistical analysis, differences between means were considered statistically significant at a *p*- value of less than 0.05.

2.5 Results:

2.5.1 Respiratory Measurements:

The respiratory measurements observed that there was oxygen flux in both the fatty acid and the carbohydrate chambers. The Routine respiration is the observed respiration without the addition of any substrates, which is solely dependent upon the basal metabolites within the cells. as there was no separate treatment given to the cells

prior to commencement of experiment with the only difference being in the substrates provided, the Routine respiration showed similar results (Fig 1A).

The Leak respiration was measured following permeabilization with digitonin. In that state, the cell cytoplasm becomes continuous with the extracellular buffer and thus, the mitochondria have negligible substrate availability. The oxygen flux recorded at that state corresponds to the oxygen consumption by the mitochondrial enzymes which does not result in the electron transport chain function, thus termed leak respiration. As both the chambers had similar cells, the Leak respiration showed no difference between the two groups (Fig 1B). Total oxidative phosphorylation corresponded to the respiration measurement with the addition of all substrates (all carbohydrate substrates – Glutamate-Malate-Pyruvate) in the carbohydrate chamber and all fatty acid substrates -Palmitoyl Carnitine-Malate- in the fatty acid chamber) with sufficient ADP. This ensured that the utilization of substrates was not limited by the lack of ADP. Both the substrate types were utilized by the cells though carbohydrate had a slight better utilization (Fig 1C).

The substrates given only had NADH as the reducing equivalent generated following the Krebs cycle, although there is the potential for $FADH_2$ generation with each round of beta-oxidation of fatty acids. Thus, following the inhibition of Complex I which utilizes NADH, only fatty acid mediated respiration could drive the oxygen flux. It was confirmed that the glioma cells were undergoing the beta oxidation with the oxygen flux measurement mediated by $FADH_2$ following addition of Rotenone (Fig 1G). The maximal respiration was obtained with the uncoupler CCCP, which dissipated the proton gradient between the mitochondrial membranes and thus required all the complexes of the electron transport chain to function at their maximal capacity in order to bring to homeostasis the mitochondrial membrane potential. The maximal respiration observed showed that the carbohydrate substrates had a higher potential in driving the electron transport chain (Fig 1D). The reserve capacity is the respiratory reserve of the mitochondria arrived at by the formula Maximal – Routine respiration. The reserve capacity was also shown to be higher in the carbohydrate group (Fig 1E) correspondingly seen by the gain in oxygen consumption rate (OCR) following uncoupling (Fig 1H).

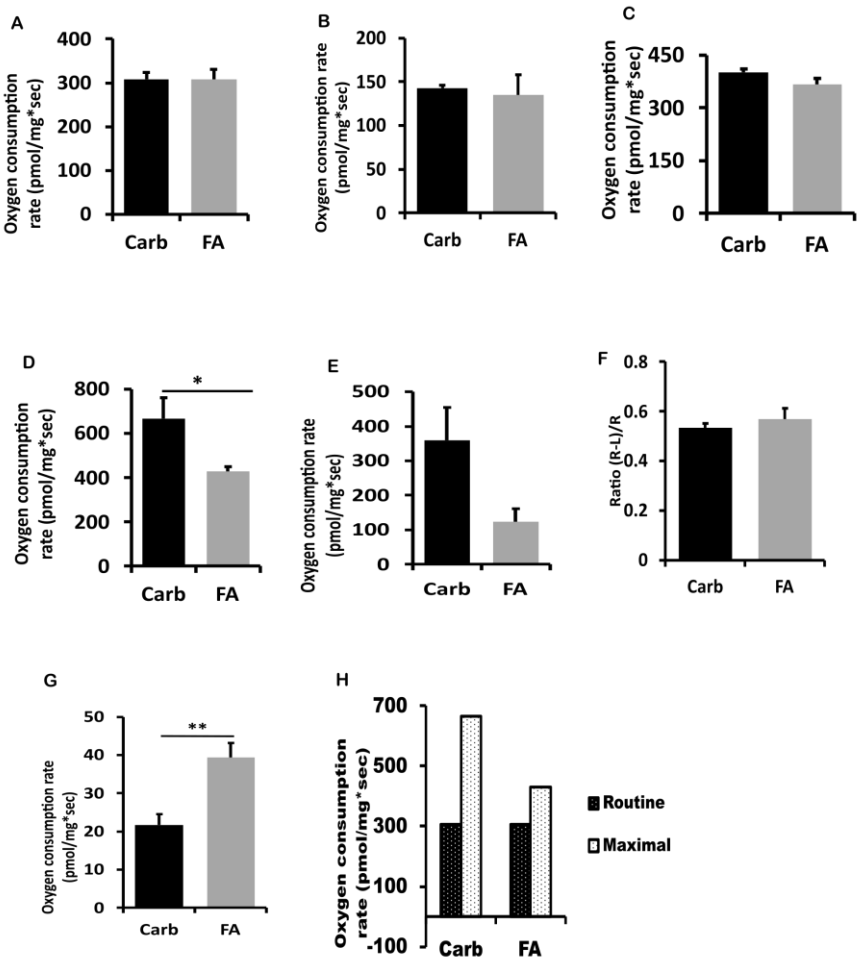

FIG 1: **Respiration measurements between Carbohydrate and Fatty Acid Substrates**
A- Routine Respiration, **B** - Leak respiration (following cell permeabilization with digitonin), **C** - Total oxidative phosphorylation capacity (following substrate addition), **D**- Maximal Respiration (following uncoupling), **E** - Reserve capacity (Maximal - Routine), **F** - Coupling efficiency ((R-L)/R), **G** - $FADH_2$ mediated respiration (following inhibition of Complex I), **H** - Gain in Oxygen Consumption Rate (OCR) following uncoupling

Both the substrates had the potential to be utilized for the mitochondrial respiration but there was a significantly reduced reserve respiratory capacity with fatty acid substrates, implying that carbohydrate would be a preferred substrate for the mitochondria in the glioma cells.

2.6 Discussion:

These *in vitro* results confirm that both the substrates, glucose and fatty acids that are in excess in the diabetic condition are utilized in glioma cells. But the fatty acid substrates did not have eminent effect on the reserve capacity and thus are less likely to be the preferred substrate. Also, the *in vitro* simulation of diabetes is generally done with the high glucose. Our results suggest that the high glucose model would be apt for the further studies to assess the effect of diabetic-phenotype on mitochondria in glioma cells. The metabolic alterations and effects of high glucose would be a closer approximation of the metabolic alterations on the glioma under diabetes condition as the fatty acid though utilized is an efficient substrate and is thus less likely to be used with the presence of abundance of glucose. There are multiple studies showing the ability of glioma to metabolise fatty acids and thus their metabolic plasticity, but they are seldom preformed in high glucose environment. The study by Sperry et. al., that in glucose limiting conditions, glioma cells adjust their metabolic preference and become capable of utilizing fatty acids and ketone bodies for ATP generation (Sperry et al., 2020). But our studies point out that with high glucose condition, the glucose must be the likely fuel source.

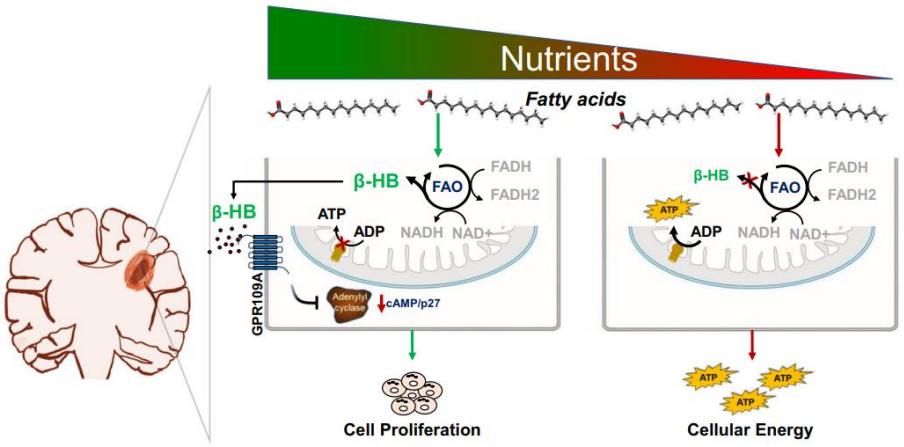

Fig D: In nutrient favourable conditions the fatty acids are utilize to generate biomass through the cAMP-p27 pathway observed in the glioma cells; while in the nutrient limiting conditions, the glioma cells adapt their metabolic profile and utilise the fatty acids for beta oxidation in the mitochondria to generate ATP.

(Kant et al., 2020)

2.7 Conclusion and Inference:

Glioma cells can utilize both fatty acid and carbohydrate substrates but the fatty acid substrates are less advantageous for metabolic needs. As the preferential substrate was glucose for the mitochondrial metabolism, the hyperglycaemia would have a stronger impact on the mitochondrial metabolism than hyperlipidaemia in glioma cells under a diabetic environment. Thus, to assess how diabetes metabolically affects mitochondrial capacity in glioma a hyperglycaemic state was used for *in vitro* simulation.

Rationale: Diabetes has shown to affect many cancers positively being considered a causative agent in some forms of cancer but it affects glioma negatively. The metabolic profile of the cells has a determining role on the tumourigenesis, with mitochondria playing a major role in shaping the metabolic landscape within the cells. As it was shown that the glioma has reduced potential to use fatty acid substrates for mitochondrial respiration, we speculate that the high glucose environment would likely have an effect on the glioma mitochondria and thus glioma metabolism. Based on the above results the following hypothesis was formulated for experimental evaluation.

Hypothesis: Hyperglycaemia would have an effect on the metabolism and mitochondrial function in glioma cells

Title: Changes in mitochondrial function in glioma cells under hyperglycaemia

Objectives of the study were to assess the following:

1. To assess if hyperglycaemia affects glioma aggressiveness
2. To evaluate if hyperglycaemia affects mitochondrial function in glioma
3. To determine what causes the hyperglycaemia mediated changes in the glioma mitochondrial function
4. To determine if hyperglycaemia affects the mitochondrial health in glioma cells

Chapter 3

Hyperglycaemia and Glioma Aggressiveness

3. 1 Introduction

There are numerous studies that suggest that cancer cells behave highly tumourigenic under high glucose and thus, diabetes and metabolic syndrome have been taken as a risk factor for various types of cancers. But, the epidemiological data points towards there being a negative correlation between diabetes and glioma formation and aggressiveness (Seliger et al., 2016), (Kitahara et al., 2014). It is well known that tumour cells have altered metabolism and with our previous experiments in Chapter 2 it was confirmed that the glioma cells have preference for glucose as the metabolic fuel. We thus needed to elucidate how hyperglycaemia affect glioma aggressiveness.

Aggressiveness is the ability of a greater number of cells formed per unit time and the capacity of these cells to undergo metastasis and was thus defined as having the following components:

1. Increased proliferation: One of the main components of aggressiveness is increase in the total number of cells within a given time.
2. Increased migration: In metastatic tumours, the ability of the cells to migrate is a critical means for metastasis. The high-grade glioma cell lines that were used in this study, both have high metastatic rate, so to assess aggressiveness it becomes critical to also assess the changes in the migration capacity of the cells.
3. Increased capacity for invasion: The metastasis or aggressiveness can only be accomplished if the cells that have the capacity for migration also develop the capacity for invasion, that would entail the over-expression of various invasion specific markers, primarily MMPs (Matrix Metalloproteinases) which have the capacity of digesting the basement membrane of the tumour mass and the other tissue whereupon following migration, the tumour cells can initiate a secondary tumour formation.
4. Anoikis resistance: The metastasis capacity of tumour cells requires the cells to undergo a change from endosomal to mesenchymal characteristics. The endosomal cells require attachment to a basement membrane for the cells to be viable. In metastatic tumours, the tumour cells attain the capacity for transition

from the endosomal to mesenchymal type wherein they can survive without the need for substratum and can freely flow in circulation (Systemic, lymphatic or in the case of glioma the CSF) to another region where it can initiate a new solid tumour mass, forming secondary tumour.

3. 2 Review of Literature:

Glioma are very aggressive brain tumours of astrocytic origin. Glioblastoma are Grade IV tumours with poor survival rate of merely 26.5% even after standard procedure of therapy, i.e., surgery, radiotherapy and chemotherapy combined (Stupp et al., 2005). It thus becomes critical to understand the risk factors and the potential therapeutic targets which has driven research in this field for past many decades. Diabetes and poor glycaemic control have shown to be a positive predictor in the cancers of breast, oesophagus, etc but not so with glioma. Rather, the incidence of diabetes often is associated with a negative risk for the development of glioma in some studies (Swerdlow et al., 2005), (Atchison et al., 2011), (Schwartzbaum et al., 2005), (Kitahara et al., 2014), while in others there were non-significant (Schlehofer et al., 1992), (Cicuttini et al., 1997) (Schlehofer et al., 1999) or mixed relation between the two (Adami et al., 1991). We thus first sought to elucidate how hyperglycaemia affected glioma aggressiveness.

3. 3 Materials and methods:

3. 3. 1 Reagents

DMEM low glucose were purchased from HiMedia Laboratories (Mumbai, India). The common reagents like EDTA, MTT were purchased from Sigma Aldrich (MO, USA). Fetal Bovine Serum (FBS) (South American origin) was sourced from Gibco (Grand Island, USA). Trypsin was procured from PAN Biotech (Aidenbach, Germany). Antibodies against MMP2, MMP9 and β-actin were obtained from Cell Signalling Technology (Beverly, MA, USA). Horse Raddish Peroxidase conjugated anti-rabbit IgG- #7074 were obtained from Cell Signaling Technology, Inc. (MA, USA). Clarity ECL kit #1705061, ClarityMax ECL Kit #1705062, and 29:1

Acrylamide: Bisacrylamide (40%) solution were procured from Bio-Rad Laboratories (CA, USA).

3. 3. 2 Cell culture and maintenance

Glioblastoma cell U87MG were purchased from NCCS, Pune and U251MG was provided by Dr TR Santosh Kumar (Rajiv Gandhi Centre for Biotechnology, Trivandrum, Kerala). Cells were cultured in low glucose DMEM, with 5.5 mM glucose (HiMedia Laboratories, Mumbai, India). The control cells were kept in 5.5 mM media containing 1% FBS (here after referred to as normal glucose media/ control) while the hyperglycaemic cells were given 30 mM DMEM containing 1% FBS (hereafter referred to as high glucose media/ hyperglycaemia). The media was changed every 48 h and the culture maintained for 72 h and all experiments were performed at that time point (unless otherwise specified).

3. 3. 2. 1 Reagents used

3. 3. 2. 1. 1 DMEM -low glucose preparation (1 litre) (pH 7.4)

5.5 mM glucose containing DMEM, Sodium bicarbonate (2.7 g) in sterile MilliQ water, filtered and stored in autoclaved bottles.

3. 3. 2. 1. 2 DMEM -high glucose preparation (1 litre) (pH 7.4)

25 mM glucose containing DMEM with the addition of 0.9 gm Dextrose, Sodium bicarbonate (2.7 g), Sodium pyruvate (0.11 g) in sterile MilliQ water, filtered and stored in autoclaved bottles.

3. 3. 2. 1. 3. Phosphate-buffered saline (PBS) (pH 7.4)

Sodium chloride 137 mM, potassium chloride 2.7 mM, disodium hydrogen phosphate 10.14 mM, potassium dihydrogen phosphate 1.76 mM in sterile MilliQ water.

3. 3. 2. 1. 4. Trypsin EDTA solution (pH 7.4)

0.25% trypsin, 0.53mM EDTA in PBS.

3. 3. 3 Cell proliferation analysis:

3. 3. 3. 1 MTT assay for cell viability assessment:

Cells were seeded in a 96 well plate at a density of 5000 cells per well. After the desired confluency was reached, the media was changed to low glucose and high glucose media. The 3-(4,5-dimethylthiazol-2-yl)-2,5-diphenyltetrazolium bromide (MTT) (Sigma Aldrich, MO, USA) salt was dissolved in PBS at a concentration of 1mg/ml and after the media was aspirated, the PBS containing tetrazolium was added to the plate and incubated for 3hrs. Following which the formazan crystals were dissolved by addition of DMSO (Sigma Aldrich, USA) and incubating for 1hr at 37 °C and the absorbance was read on an ELISA plate reader at 570 nm wavelength. The reading in the control was taken as 100% viability and the high glucose condition was compared with it and results plotted as percentage rise.

3. 3. 3. 1. 1 Reagents Used

3. 3. 3. 1. 1. 1 MTT:

1mg MTT in each ml of sterile PBS solution, prepared fresh.

3. 3. 3. 2 Hoechst –PI staining procedure

Cell death analysis was performed by means of Hoechst/PI double staining method. Optimal number of cells were seed on to 96 well plates, and after the desired treatments were done for 72 h, the cells were incubated with 1µg/mL Hoechst (Sigma-Aldrich, Gillingham, UK) at 37˚C for 15 min, washed with PBS and incubated with 1µg/mL Propidium Iodide (PI) (Sigma-Aldrich, Gillingham, UK) for 3-5 min. The fluorescent images (Hoechst- Ex/Em:350/460 nm; PI- Ex/Em:530/640 nm) were obtained from multiple different fields for each group and cells were counted using ImageJ version 1.49a (NIH, USA). Cell death after C and HG treatment was analyzed by fluorescence microscopy (Olympus, Tokyo, Japan) after staining with Hoechst/PI. Multiple fields were captured for each of the groups. The cell counting was performed using ImageJ software and the average number of live cells per field were computed.

The cell death percentage was then calculated as,

$$\%Cell\ death = \frac{\text{No. of PI (HG)/No. of Hoechst (HG)}}{\text{No. of PI (C)/No. of Hoechst (C)}} X100$$

3. 3. 3. 2. 1 Reagents Used

3. 3. 3. 2. 1. 1 Hoechst 33342 stock (10 mM)

2 mg in 1 mL DMSO

3. 3. 3. 2. 1. 2 Propidium iodide stock (10 mg/mL)

5 mg in 500 µL DMSO

3. 3. 4 Cell migration analysis:

3. 3. 4. 1 Scratch wound assay

Cells were cultured in 12 well plate at the density of 20000 cells per well in complete media. After 70% confluency, the media was changed to either normal or high glucose media for 48 h and a scratch was made with a 200 ul pipette tip at the end of 48 h. The scratch was observed for the next 24 h and imaged with a phase contrast microscope Olympus IX 51(Tokyo, Japan) at various time points and the migration quantified through ImageJ.

3. 3. 5 Cell invasion analysis:

3. 3. 5. 1 Immunoblot analysis

3. 3. 5. 1. 1 Whole cell lysate preparation

Cells were treated for respective time course described. After the treatment periods, the cells were washed with ice-cold PBS and scrapped in ice cold RIPA (Radio Immuno Precipitation Assay) buffer containing proteinase inhibitor and phosphatase inhibitor cocktail. The lysate was then gently vortexed at 4 ^{0}C for 30 min followed by centrifugation at 13,000 rpm for 20 min at 4 ^{0}C. The supernatants were then aliquoted in to equal volumes and stored at -80 ^{0}C for use.

3. 3. 5. 1. 2 Protein quantification

Protein quantifications were performed using BCA-assay kit (Pierce Biotechnology, MA, USA). Pre-diluted BSA protein standards in range of 125 to 2000 µg/mL were

used to generate a standard curve of Absorbance versus Micrograms of protein, and the concentration of proteins in the cell lysates were determined.

3. 3. 5. 1. 3 SDS PAGE

Whole cell lysates were quantified and (20-40 µg) proteins were heat denatured with β- Mercaptoethanol, for 5 minutes, and resolved on Sodium Dodecyl Sulphate- Poly Acrylamide Gel Electrophoresis (SDS-PAGE) at 100V. Resolved proteins were transferred on to PVDF membrane at 10V for 40 minutes in a semi dry transfer apparatus or 100V for 30- 60 min (depending upon the percentage of the gel used and the molecular weight of the protein to be assessed) in a wet transfer apparatus. The membrane was blocked for 60 min at room temperature with blocking buffer (5 % Milk in TBST). The membrane was then probed with antibodies against MMP2, MMP9 and β- Actin (1:1000 dilution) at 4 ^{o}C overnight. HRP conjugated anti rabbit (1:5000 dilution) secondary antibody used for the study.

3. 3. 5. 1. 4. Chemiluminescent detection

femtoLUCENT™ PLUS-HRP Chemiluminescence Detection Kit (GBiosciences, MO, USA) was used for visualizing protein bands. Equal volumes of luminol and peroxide solutions were mixed and added on to the membranes. An X-ray film was used to capture light emitting bands. The film was then developed and documented in Gel Doc™ XR Imaging System (Bio-Rad Laboratories, Hercules, CA, USA) and quantified using Image J Analysis Software (NIH).

3. 3. 6 Anoikis Resistance

The cells were cultured in complete medium and following 70% confluence the treatment of normal glucose and high glucose were given for 48 h. The cells were trypsinized with 0.25% trypsin (Pan Biotech) and EDTA (Sigma Aldrich, USA) solution which was inactivated by adding complete media (5.5 mM glucose containing media with 10% FBS). After washing the cells off the trypsin using complete media, cells were resuspended in the respective normal glucose and high glucose media and added to 96 well low attachment plates. After 48 h following re-seeding, cells were given PI in PBS and incubated for 5 min at 37 °C in 5% CO_2. The cells were imaged

using fluorescence microscopy and multiple fields were imaged for each group attempting to cover the entire well. The dead cells were counted using ImageJ and average number for each group was calculated.

3. 4 Statistical analyses:

All experiments had n equal to or more than 3 for both the cell lines and the values represented are the mean with the standard error of mean indicated. Appropriate statistical tests were used to make the graphs. The p value of less than 0.05 was considered significant.

3. 5 Results:

3. 5. 1 Hyperglycaemia increases glioma cell proliferation:

The MTT assay showed that under the HG condition, there was an increase in the total number of cells (Fig 2A-B). The results obtained from the MTT assessment was confirmed with the cell counting performed with live dead cell staining using Hoechst-PI. It was observed that in both the cell lines, by the 72 h there were a higher number of cells in the HG group as compared to control group (Fig 2C-F) indicating that there was increased proliferation under HG.

3. 5. 2 Hyperglycaemia increases glioma cell migration:

The scratch wound assay showed that the scratch created was narrower in the HG group than in the control group (Fig 3A-B). This could also be due to the increased cell proliferation thus filling in the scratch. To mitigate this, the time to determine the migration was thus chosen to be final 24 h which less than the doubling time of the cells (U251 doubling time is 24 h and U87 doubling time is 34 h). The scratch wound assay suggests that there was a higher migration in the cells under the HG group.

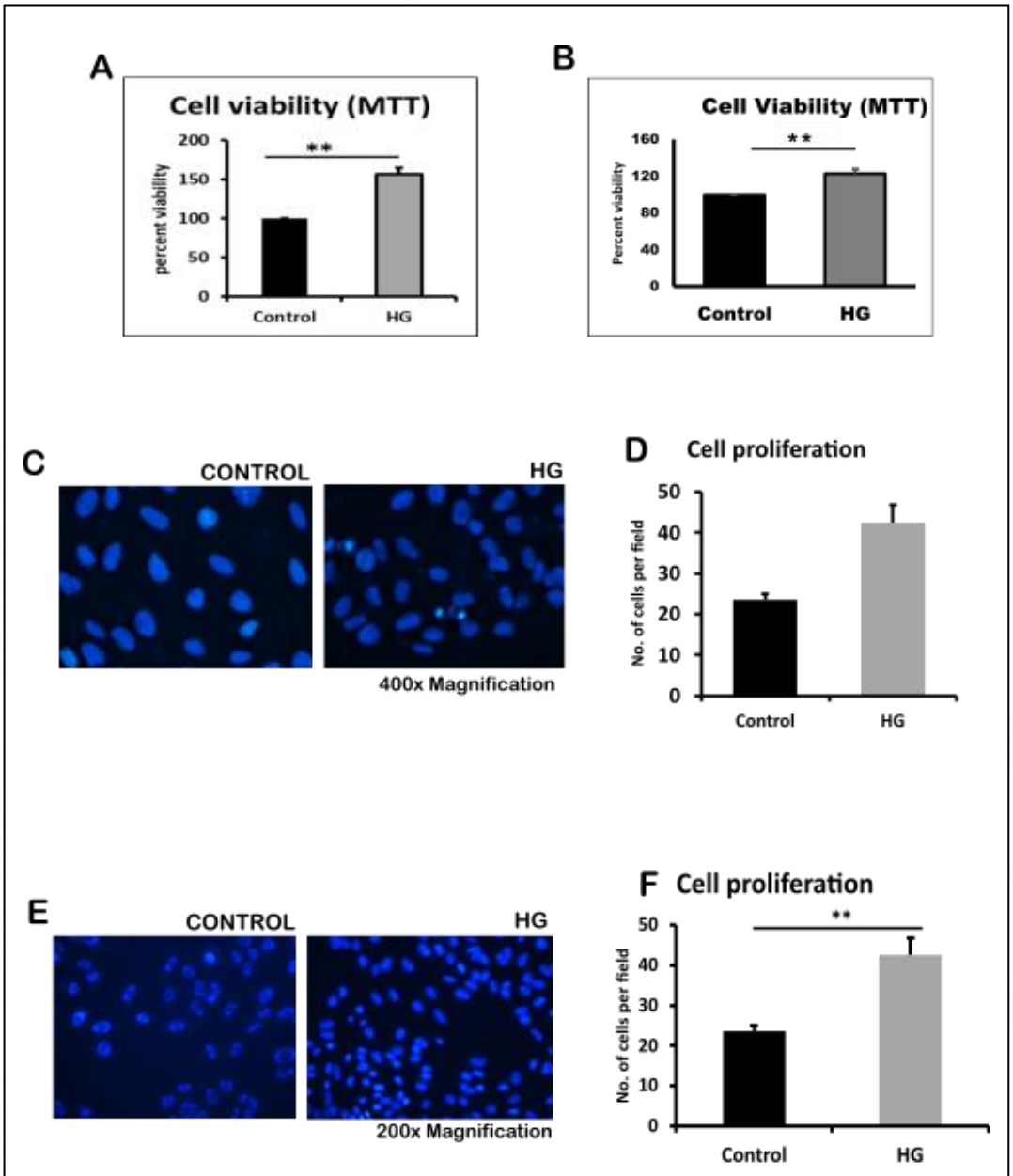

FIG 2 : Hyperglaycaemia and glioma proliferation

A - MTT assay for U251 cells, **B** - MTT assay for U87 cells, **C** - Hoechst-PI staining for U251 cells, **D** - Hoechst-PI proliferation assessment -U251 cells, **E** - Hoechst-PI staining in U87 cells, **F** - Hoechst-PI proliferation assessment -U87 cells

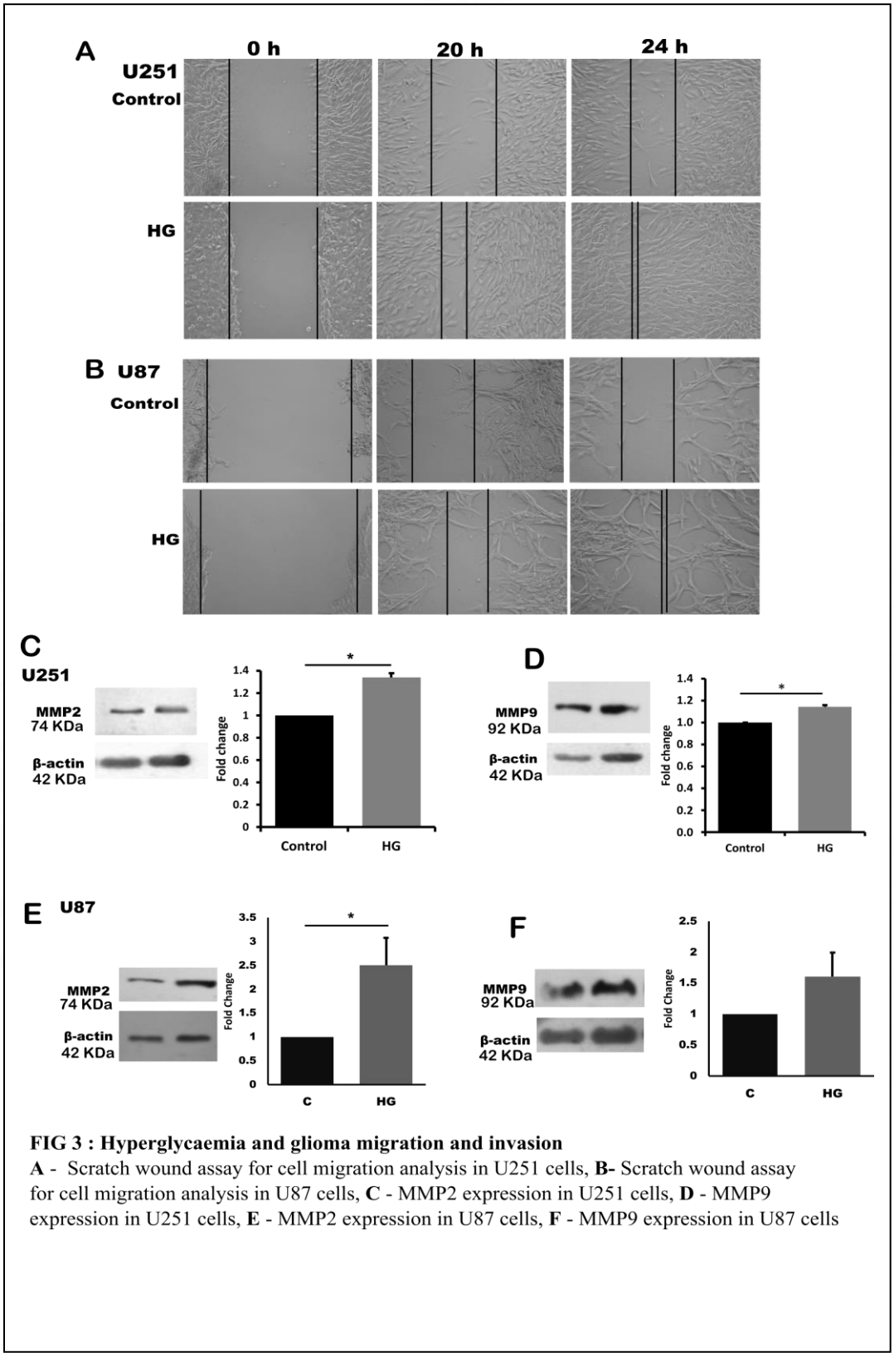

FIG 3 : Hyperglycaemia and glioma migration and invasion

A - Scratch wound assay for cell migration analysis in U251 cells, **B-** Scratch wound assay for cell migration analysis in U87 cells, **C** - MMP2 expression in U251 cells, **D** - MMP9 expression in U251 cells, **E** - MMP2 expression in U87 cells, **F** - MMP9 expression in U87 cells

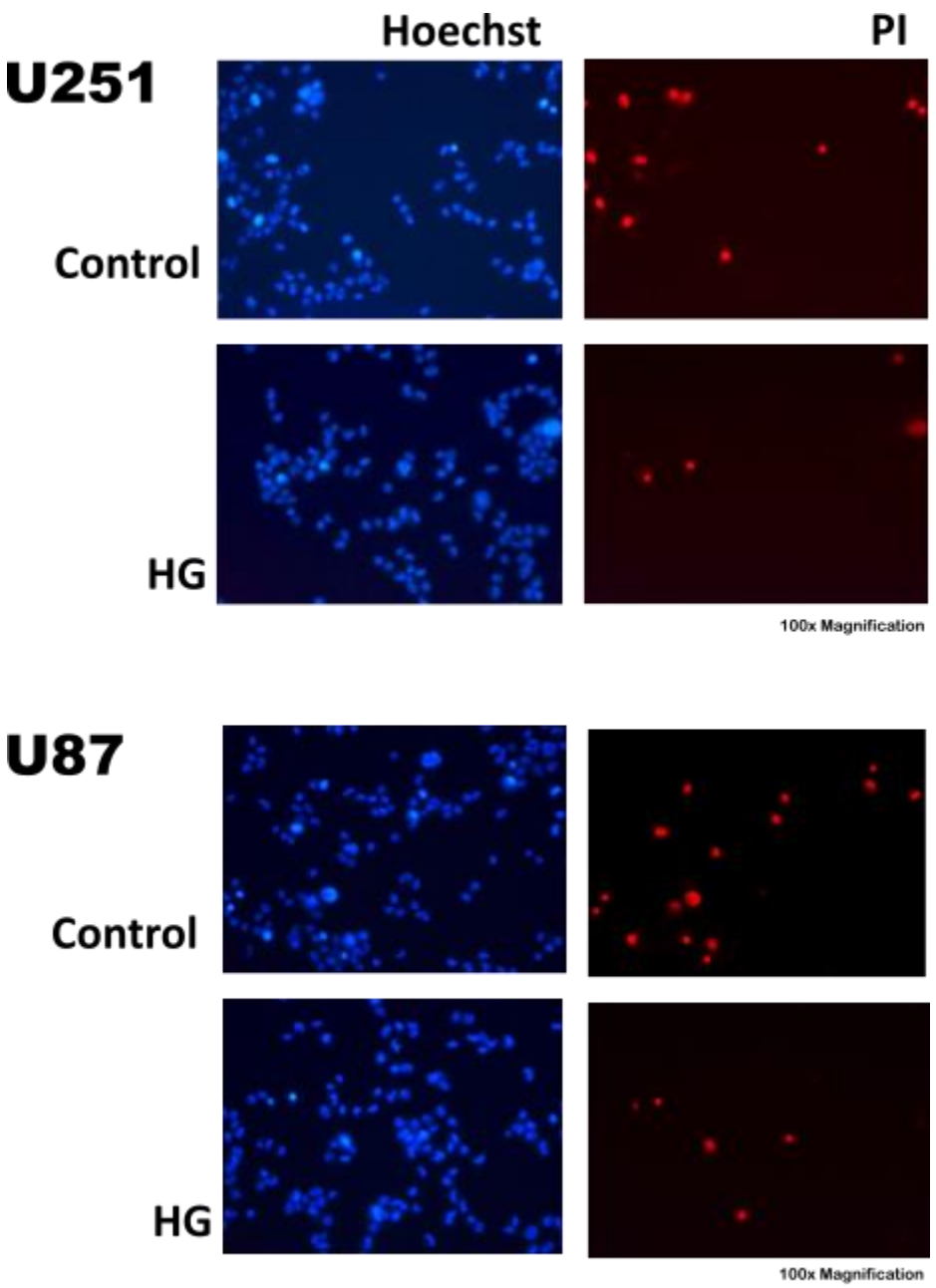

FIG 4: Hyperglycaemia and Anoikis Resistance

3. 5. 3 Hyperglycaemia increases the expression of invasion markers in glioma:

The Western Blot analysis showed that there was an increased expression of both MMP2 and MMP9 in the HG group as compared to the control group (Fig 3C-F). This suggests that there is likely an increased capacity for invasion of the basement membrane for the glioma cells under HG.

3. 5. 4 Hyperglycaemia increases anoikis resistance in glioma:

The fluorescence imaging showed that there are more dead cells, fluorescing red with the uptake of PI stain in the control group as compared to the HG group (Fig 4). This suggests that more cells survived the low attachment conditions under the HG group providing evidence for anoikis resistance increased under the HG treatment.

3. 6 Discussion:

The results point out that the HG condition is a growth favourable condition of the glioma cells. It regulates cell cycle and increases proliferation suggesting an increase in the tumour mass given the same time. It was also observed that the HG caused improved migration capacity in the glioma cells along with an increase in the expression of invasion specific markers. With the increase in the expression of matrix metalloproteinases, there would be increased capacity for the cells in the tumour mass to digest the basement membrane and leave the tumour bulk thus creating a potential for metastasis. The anoikis resistance is required for the cells that leave the tumour mass and initiate a secondary growth. It was observed that the anoikis resistance was improved in the cells with HG treatment. These results thus implies that HG makes glioma more aggressive.

This *in vitro* data did not correlate with the epidemiological data presented by many groups that show a negative association between the development of glioma in patients and diabetes. The study published by Bao et. al. also had similar observations in their in vitro model systems (Bao et al., 2019) they used U87 as their in vitro model system and found corresponding results with cell proliferation and migration. They also observed enhanced Vascular endothelial growth factor (VEGF) production mediated through the EGFR upregulation and other cytokines promoting cell cycle progression.

Our results also bring the same inference with cell culture studies. An interesting component of their work was that done with xenografts of U87 cells in the normal and diabetic mice models, which showed that the cancer had increased metastasis in the diabetic mice which again differed from the epidemiological data. There have been many theories put forward for this discrepancy observed observation; could be due to the confounding variables like use of anti-diabetic drugs in the patient groups; as these have been shown to reduce the aggressiveness of multiple cell lines in vitro.

3. 7 Conclusion:

The parameters that were used to measure glioma aggressiveness; proliferation, migration, invasion and anoikis resistance all showed that the HG condition had a higher tendency towards enhancing the aggressiveness in the glioma cell lines.

Critical Methodological Insight – I

Albumin binds to uncoupler CCCP to diminish depolarization of mitochondria

1. Introduction:

Mitochondria are the dynamic organelles that are primarily involved in the ATP generation from ADP and P_i by Complex V with the utilization of the potential gradient ($\Delta\psi m$) established by pumping of electrons by Complexes I, III and IV ("Mitochondrial electron transport chain, ROS generation and uncoupling (Review) - PubMed," n.d.). Carbonyl cyanide 3-chlorophenylhydrazone (CCCP) is a commonly used mitochondrial uncoupler that reduces this potential gradient; achieved by making the mitochondrial inner membrane leaky to the protons which dissipates the proton gradient. The reduced mitochondrial membrane potential marks the mitochondria for the clearance of its damaged fragments through mitochondria specific autophagy (mitophagy).

BSA forms one of the constituents of buffers used in mitochondrial structure or functional assessments; while serum is commonly used for *in vitro* experiments. There are experimental methods utilizing isolated mitochondria, where the use of BSA (essentially fatty acid free BSA) is vital, as it preserves their integrity and membrane potential (Salabei et al., 2014) . Also, BSA and serum have surfactant property that makes them suitable in formulations for isolating mitochondria (Ikuma, 1970). The albumin in serum serves in the transport of the substrates and proteins to the cell which could be later utilized for metabolism. This property of serum makes it routinely employed in the experimental protocols for metabolic studies.

Although the uncoupling efficiency of CCCP is widely known, there exists a discrepancy between the concentrations required to induce uncoupling of cellular mitochondria and that required for uncoupling isolated mitochondria. *Soutar et al.* showed that in presence of serum greater concentrations of CCCP were required for mitochondrial recruitment of Parkin, suggesting higher concentrations required for CCCP to induce uncoupling (Soutar et al., 2019). Multiple studies in the previous decades demonstrated that the presence of serum hinders the depolarization capacity

of commonly used uncouplers like FCCP, CCCP, 2,4- DNP (Layton and Symmons, 1973) (Skogh et al., 1983b) (Skogh et al., 1983a). The cause for this remains elusive. Mitophagy can be induced by the generation of mitochondrial superoxide, which is induced by the presence of FCCP while reduced by the presence of BSA, owing to the activation of GSH mediated mitochondrial antioxidant system. It remains to be determined whether the presence of serum, or its main constituent, albumin, protects the mitochondria through activating any such signalling mechanisms (Cantin et al., 2000) (Kane et al., 2018) or if there is a direct physical interaction between the components of serum and CCCP.

We thus performed this study to check the instantaneous effect of presence of serum or BSA on the CCCP induced mitochondrial depolarization and demonstrate that mitochondrial depolarization is hindered in the presence of serum and BSA due to the molecular interaction between CCCP and albumin, thereby reducing its effective concentration.

2. Materials and methods:

2.1 Cell Culture and chemicals:

HEK293T (Human embryonic kidney cells), a kind gift from Department of Pathology, Sree Chitra Tirunal Institute for Medical Sciences and Technology (SCTIMST), Trivandrum and H9c2 (rat embryonic cardiomyoblasts), from ATCC were used. The cells were cultured in high glucose DMEM with 10% FBS and maintained in humidified incubator at 37^0 C with 5% CO_2. Other chemicals and reagents used in the following study have been discussed earlier.

2.2 Measurement of Mitochondrial Membrane Potential:

H9c2 cells were seeded at appropriate density in 8-well chamber cover-slips from Ibidi, (Munich, Germany). On attaining 50-60% confluence the media was changed to serum and BSA free DMEM for the control group and DMEM with 0.5% and 1% BSA for the test group. cells were incubated for 15 min at 37^0 C with 5% CO_2 with Hoechst and TMRE as per manufacturer's recommendations. The vehicle control group formed of 0.5% BSA alone without the addition of CCCP. The experiment was

divided into two sub-groups with the first determining of CCCP induced depolarization at increasing concentrations of BSA and the other sub-group determining the same at fixed concentration of BSA but increasing concentrations of CCCP. In the uncoupler group, cells were treated with CCCP at the mentioned concentrations (1 µM, 2 µM, 5 µM and 10 µM) in serum and BSA free media or with 0.5% or 1% BSA and incubated for 15 min with Hoechst and TMRE. The fluorescence distribution was captured using fluorescence microscope (Olympus IX 51, Tokyo, Japan) and mitochondrial depolarization was assessed as the decline in TMRE mediated fluorescence (excitation, 530 ± 21 nm; emission, 592 ± 22 nm).

2.3 Measurement of mitochondrial uncoupling:

Mitochondrial uncoupling was determined in Oroboros O2K high-resolution respirometry (Oroboros Instruments, Innsbruck, Austria). The respiration media used for the experiments was the cell culture media as control or with the 1%, 5% or 10% of serum or 0.1%, 0.5% or 1% of BSA in the experimental groups. HEK293T cells, at 80-90% confluence, were harvested and added to the respirometer. The addition of CCCP was performed with manual micro titrations using Hamilton syringes, and the maximal respiration recorded was taken as the fully uncoupled respiration. The concentration of CCCP required for uncoupling was normalized to the total protein content added to the chambers.

2.4 Spectrophotometric measurements for molecular interactions:

Albumin residues in BSA have an intrinsic fluorescence imparted by tryptophan residues at positions 134, 212 and 583 (“A Spectroscopic Approach to Investigate the Molecular Interactions between the Newly Approved Irreversible ErbB blocker ‘Afatinib’ and Bovine Serum Albumin,” n.d.). These residues undergo selective excitation at 280 nm wavelength and generate emission spectra at 290 nm to 500 nm wavelength. The interaction of BSA with CCCP quenched the fluorescence and the drop of fluorescence was measured spectrophometerically. The BSA was dissolved in phosphate buffered saline (pH 7.4) at 1 µM concentration while CCCP was prepared in absolute ethanol at 1 mM concentration and was serially diluted from 1 to 4 µM, and the drop in fluorescence was measured at these different dilutions.

2.5 Docking Studies

The BSA binding property of CCCP was studied by *in silico* methods. Schrodinger suite (Maestro) was used for the molecular docking studies. The crystal structure of BSA in complex with 3, 5-diiodosalicylic acid (pdb ID:4jk4) from Protein database (PDB) was used as the protein input structure. The structure was prepared for docking studies using the protein preparation wizard of Schrodinger software using OPLS_3 force field. A grid of dimension 12 Å was generated around the bound ligand, 3, 5-diiodosalicylic acid in the crystal structure in such a manner that it could cover the entire active site cleft. The structure data files (SDF) of Carbonyl cyanide 3-chlorophenylhydrazone were downloaded from pubchem database. The downloaded ligand file was prepared using ligprep module of Schrodinger suite. Docking simulations were carried out using extra precision (XP) method of glide module.

2.6 Statistical analysis:

All *in vitro* experiments were performed with minimum of three biological replicates and the values were averaged. Pearson's Correlation coefficient was calculated to assess the real time mitochondrial uncoupling with varying concentrations of Serum or Albumin, while Student's unpaired t-test with the two tailed and homoscedastic distribution was used to assess the mitochondrial depolarization with fluorescence measurements. A p- value of less than 0.05 was taken as significant.

1. Results and discussion:

3.1 BSA interferes with the depolarization of the mitochondria by CCCP:

To assess the polarization potential of the mitochondria, TMRE fluorescence measurements were carried out. The cells in the control group showed high TMRE fluorescence while the cells given 1 and 2 µM CCCP showed decline in the fluorescence intensity suggesting a decline in mitochondrial potential gradient ($\Delta\Psi m$). In the presence of BSA, either 0.5% or 1% in the CCCP treated group, the TMRE fluorescence showed results comparable to control in the presence of BSA (Fig 5) suggesting interference in CCCP mediated depolarization of the mitochondria. With

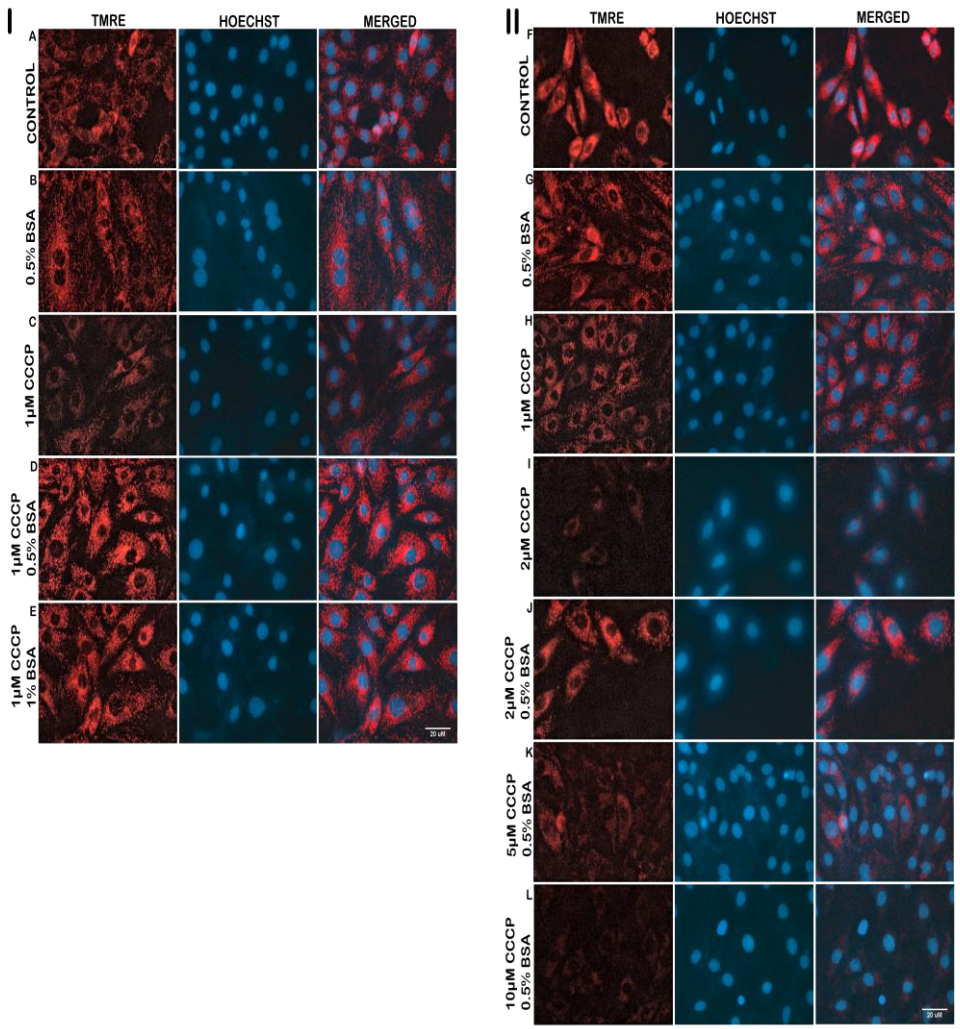

Figure 5: TMRE staining for mitochondrial membrane potential at various concentrations of CCCP and BSA

further increase in the concentrations of CCCP added (up to 5 μM and 10 μM), BSA could not protect the mitochondria from CCCP-induced depolarization. This decline in the mitochondrial uncoupling in the presence of BSA could be either due to the activation of signalling cascade that protects mitochondria from depolarization; or due to the reduced availability of CCCP as a result of its molecular interaction with BSA. To assess the same, we performed real time mitochondrial depolarization experiments.

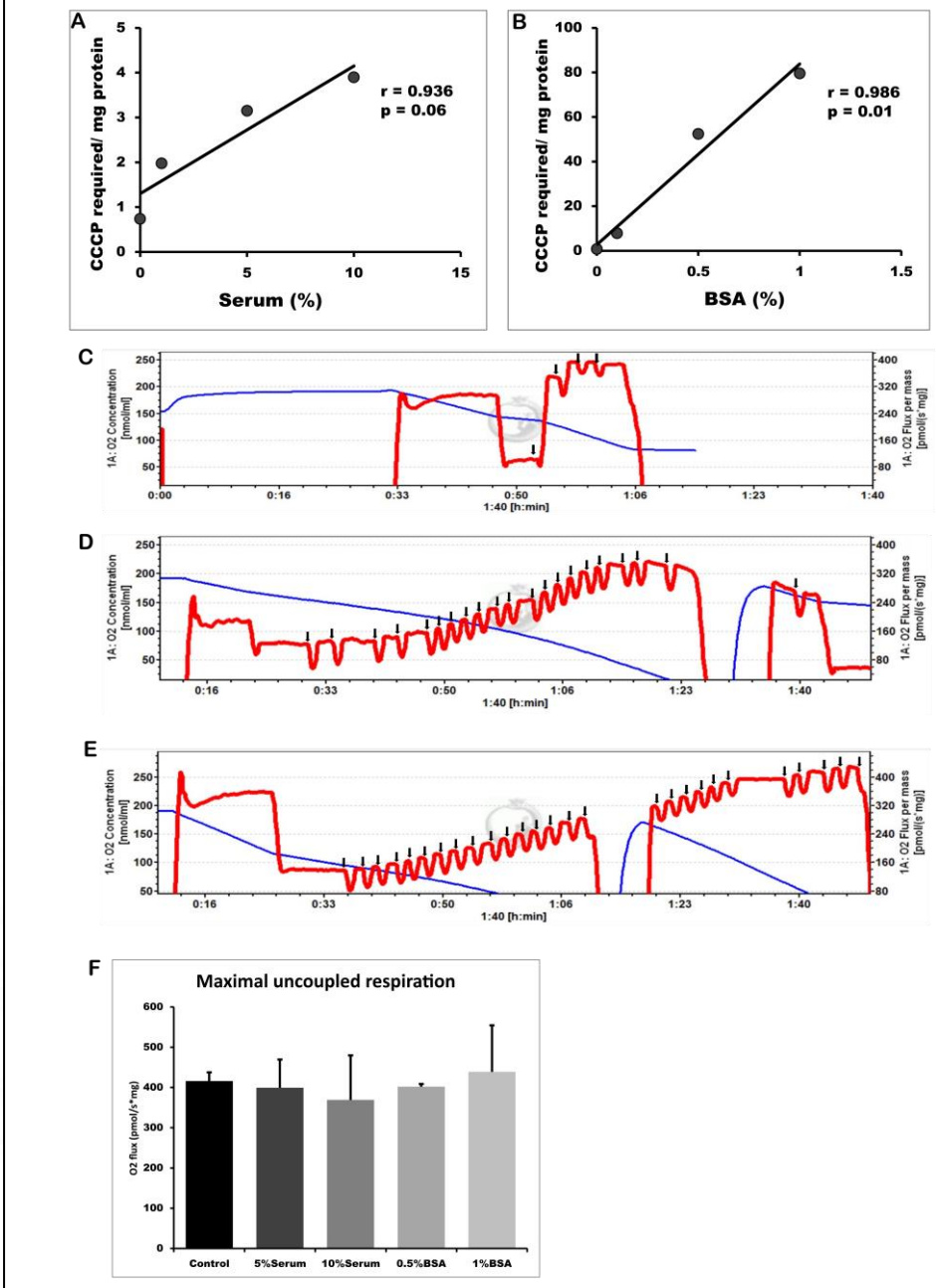

Figure 6: A, B – Correlation of the concentration of CCCP required for complete uncoupling with serum or BSA, **C, D, E** – Datlab data of effect of serum or BSA on the mitochondrial respiration measurements, **F** – Maximal respiration following mitochondrial uncoupling at various concentrations of serum and BSA

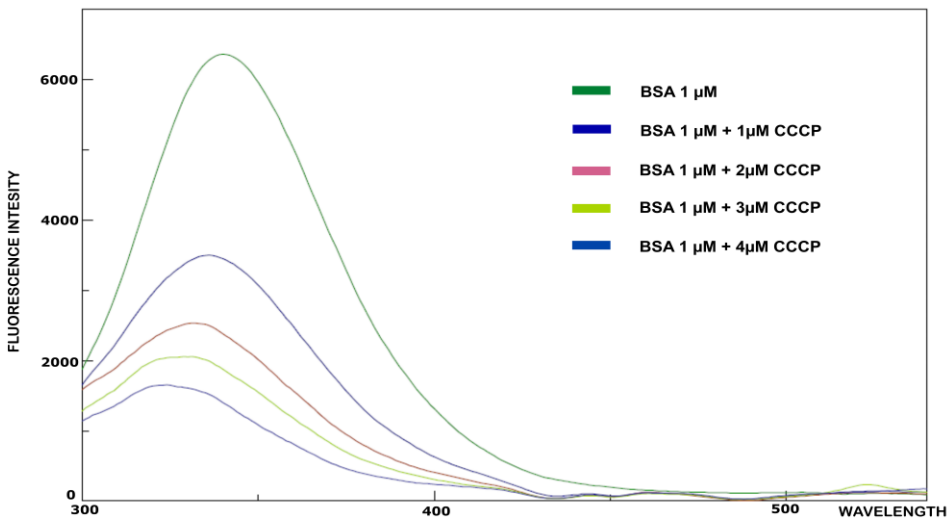

Figure 7: Spectrophotometric analysis of CCCP binding to BSA

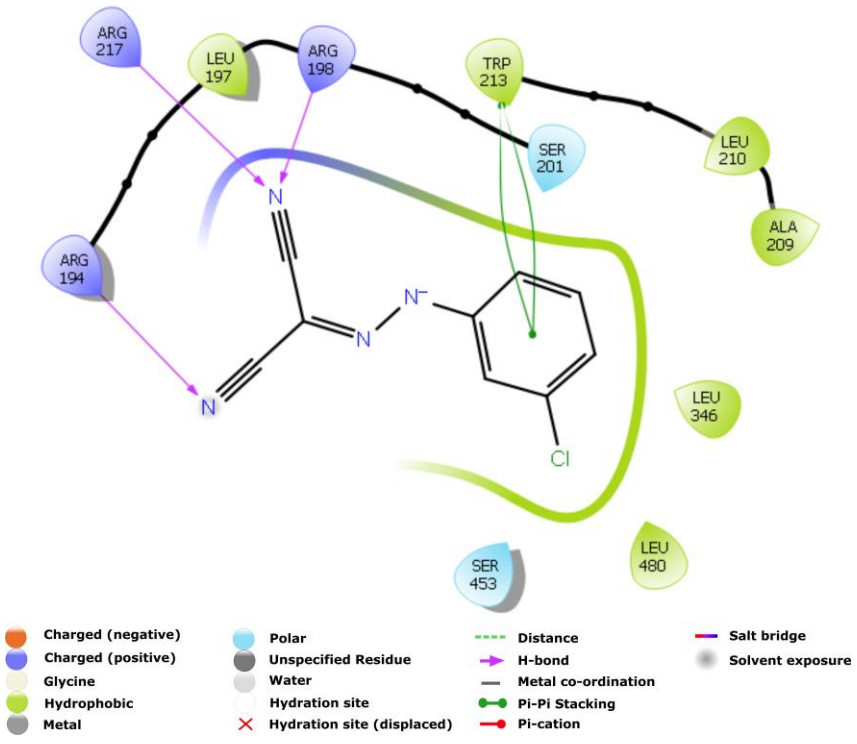

Figure 8 a: Docking of CCCP to BSA

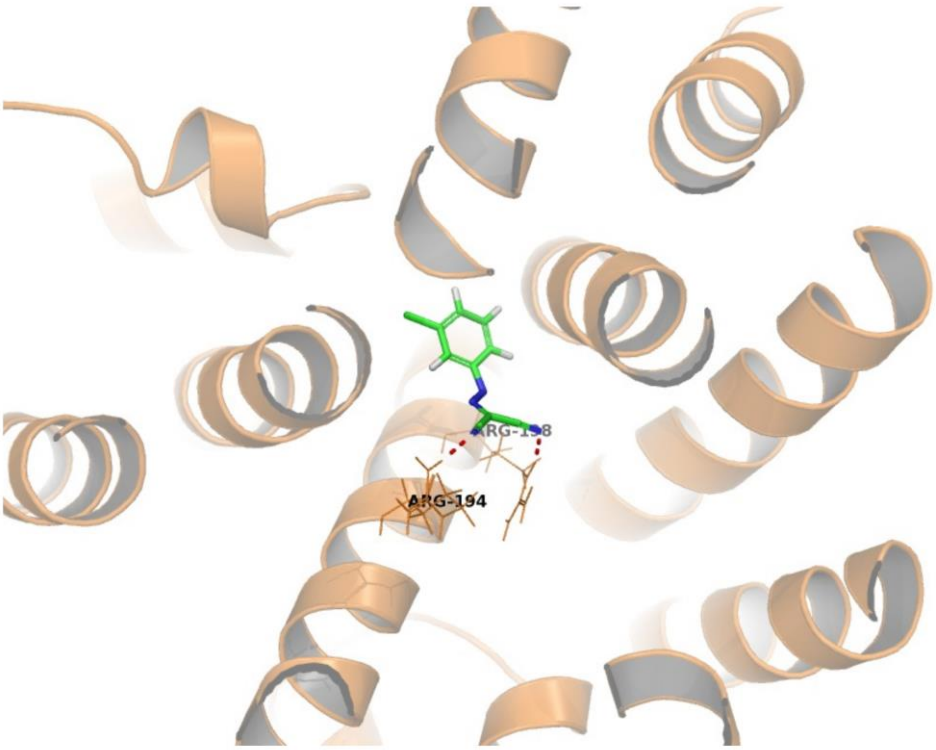

Figure 8 b: Docking of CCCP to BSA

3.2 Serum and BSA increases the uncoupler required for mitochondrial uncoupling:

To perform the real time mitochondrial experiments, we used Oroboros O2K high-resolution respirometry with data acquisition every 2 sec. It was observed that in DMEM without serum or BSA lower concentration of CCCP was required to achieve complete mitochondrial uncoupling. As the concentration of serum or BSA increased in the medium, the CCCP required for uncoupling also increased (Fig 6). The Pearson's plot showed that there was a significant correlation with a linear relationship between the concentration of CCCP required for attaining uncoupling and the concentration of serum and BSA in the media.

3.3 The albumin in serum and BSA interacts with the CCCP:

As there was an instantaneous effect of the presence of serum and BSA on the depolarization capacity of CCCP, and since there was a linear relationship between CCCP required for uncoupling and the concentration of serum or BSA; activation of any signalling pathways for this observation was less likely. We proceeded to study if there was any molecular interaction between the two. Towards that, the fluorescence spectra of BSA and the quenching effects of different concentrations of CCCP were determined. CCCP quenched the BSA fluorescence in a linear manner with increasing concentrations, suggesting a direct molecular interaction (Fig 7). It was observed that at higher concentrations of CCCP, there was a proportional decline in the BSA fluorescence spectra suggesting a likely molecular interaction between the two molecules.

To confirm if there existed a molecular interaction, we performed *in silico* docking studies, which revealed that CCCP has high affinity towards BSA. The glide score obtained was -4.36 Kcal/mol. The compound formed three hydrogen bonds with ARG 194, ARG 217 and ARG 198. The chlorophenyl moiety also interacts with TRP 213 by pi-pi stacking contacts (Fig 8).

2. Conclusion:

Recent studies have shown that presence of serum or BSA could interfere with mitochondrial depolarization with CCCP (Soutar et al., 2019). This being so, there is a need to standardize the concentration needed for obtaining desired mitochondrial uncoupling with CCCP accounting for the buffer and media formulations; nonetheless, there are many protocols where a titration of the precise concentration of CCCP to induce the required uncoupling is not possible. With less-than-optimal CCCP concentration employed, complete depolarization is not obtained giving a partially uncoupled respiration value which is lower than fully uncoupled respiration measurements. This makes it erroneous to extrapolate the methodologies or to make comparisons between studies with the same cell type and experimental method while performing intact cell respiration measurements; even where all other experimental

conditions are kept constant; if there is serum or BSA in the media or buffers. In such a scenario, the CCCP concentration to be employed must be optimized to each experimental setting and buffer formulations, to negate the non-availability of CCCP resulting from its interactions with serum and BSA.

To conclude, as CCCP binds to the serum or albumin, the use of these compounds during the mitochondrial functional assessments were eliminated where the bioenergetic studies were performed and cell culture media was used as the resuspension medium; while in the experiments with permeabilization, the use of MIRO5 warranted the addition of BSA and thus, careful titration of CCCP was performed to obtain complete uncoupling.

Chapter 4

Does hyperglycaemia affect mitochondrial function in glioma?

4.1 Introduction:

It has been demonstrated from the experiments described in the previous sections that the fatty acids do not form as optimal a source of metabolic substrate as glucose for the glioma cells and there seems to be a preference for glucose metabolism. The metabolism of glucose in the cells is through two prominent pathways, glycolysis in which glucose is taken up in the cells and converted to pyruvate (the end product of glycolysis) generating 2 molecules of ATP which under some circumstances gets converted to lactate through lactate dehydrogenase enzymes. This lactate can be shuttled outside the cell through monocarboxylate transporters at the cell membrane. The Pyruvate can also be converted to acetyl-CoA which then enters mitochondrial Krebs Cycle to generate reducing equivalents (NADH primarily) which is fed into the electron transport chain situated at the mitochondrial inner membrane which utilize the flow of electrons to reduce O_2 to H_2O also generating a potential gradient across the mitochondrial membrane which is utilized by ATP synthase to produce ATP. This generates a total of 36 ATP per molecule of glucose, thus making it an energy favourable pathway. But cancer cells have enhanced glycolytic metabolism to support biomass generation. So, in the presence of excessive glucose in the extracellular media, could the glioma cells utilize the glucose for mitochondrial respiration after dedicating some glucose towards glycolysis?

4. 2 Review of literature:

Otto Warburg reported in sarcoma cells a phenomenon of increased glycolytic ATP generation even in the presence of sufficient O_2, a phenomenon known as Warburg Effect (Warburg, 1925). The end product of glycolysis is lactate production and with this pathway NADH is generated, which can be used to generate biomass. But when observed closely in glioma and other tumour types, it was discovered that the glycolytic ATP generation was not sufficient for meeting the energy demands of the cells and (Heiden et al., 2009). In MCF-7 breast cancer cell line, it was revealed that there is a distribution of the ATP generation through both the glycolytic and OXPHOS pathways and the glycolytic ATP amounted for about 20% while that from oxidative phosphorylation generated nearly 80% thus challenging that the mitochondria are

redundant and do not contribute to energy metabolism in cancer cells (GUPPY et al., 2002). One could argue that the glioma being of primarily astrocytic in origin, would have a higher glycolytic phenotype; as astrocytes are known to undergo glycolysis, shuttles the lactate outside the cells through monocarboxylate transporters which are taken up by neurons for oxidative phosphorylation, to support their demands for ATP generation (Bangsbo et al., 2002). This theory was also tested with primary culture of human glioblastoma cells that the cells had a high oxidative phosphorylation capacity (Lin et al., 2017). It therefore is confirmed that both aerobic glycolysis and the mitochondrial OXPHOS are active in glioma cells and requires further research to determine what pathway is upregulated in the state of hyperglycaemia.

4. 3. Materials and Methods:

4. 3. 1. Reagents

All reagents were as mentioned in Chapter 2 and 3. In addition to that, the phenol red free DMEM both low glucose (HiMedia Laboratories, India) and High glucose (Sigma Aldrich, MO, USA) were used for Glucose and Lactate estimation; while Aconitase antibody was obtained from CST (MA, USA).

4. 3. 2. Cell culture and maintenance

The cell culture and maintenance techniques were similar to that mentioned in Chapter 2.

4. 3. 3 Glucose estimation:

The cells were cultured as previously mentioned and treated with Control or HG media (phenol red free) for 72 h without media change. The media was collected and concentration of glucose was determined by Glucose estimation Kit as per manufacturer's instructions. Briefly, the estimation was performed using the hexokinase method for detection. The glucose is converted to glucose-6-phosphate (G-6-P) by the enzyme hexokinase provided in the reaction mixture.

Glucose + ATP → G-6-P + ADP (enzyme involved – hexokinase)

The G-6-P is later oxidised in the presence of glucose 6-phosphate dehydrogenase (G6PD) to gluconate 6- phosphate in the presence of NADPH. This is NADPH has a specific UV absorbance and it formation which is proportional to the concentration of glucose in the sample is measured using UV absorbance

G-6-P + $NADP^+$ → Gluconate-6-phosphate + NADPH + H^+

The corresponding media alone was also assayed for the glucose concentration and used as blank. The glucose consumption was calculated by the following equation

Glucose consumption = Blank – Glucose concentration of the sample

4. 3. 4 Lactate estimation:

The cells were cultured as previously mentioned and treated with Control or HG media (phenol red free) for 72 h without media change. The media was collected and concentration of secreted lactate was determined by Lactate estimation Kit. Briefly, the L-Lactate present in the sample was oxidised to pyruvate by the enzyme lactate oxidase provided in the kit with concomitant generation of H_2O_2. This reaction peroxidase enzyme is used as a second step to utilize this peroxide to generate a coloured compound measured spectrophotometrically. The corresponding media alone was also assayed for the lactate concentration and used as blank. The lactate secretion was calculated by the following equation

Lactate secretion = Lactate concentration of the sample – Blank

4. 3. 5 pH determination:

The cells were treated as mentioned above without media change and media collected at the final hour and centrifuged to remove debris. The clear supernatant was used and pH estimated. All measurements for pH were finished in less than 5 min following media collection, to limit the pH change.

4. 3. 6 Immunoblot analysis: Whole cell lysate preparation, Protein quantification, SDS PAGE, Chemiluminescent detection

The method for immunoblotting was similar to that mentioned in Chapter 3.

4. 3. 7 High Resolution Respirometry

Mitochondrial functional analyses were performed in Oxygraph-O2k, High-Resolution Respirometry (Oroboros Instruments, Innsbruck, Austria) at 37 °C with a stirring speed of 750 rpm. Amplified signals from the oxygen sensor were recorded at sampling intervals of 2 s using DatLab-6.1 Software (Oroboros). Air-calibration of the respirometer at specific media was performed at air saturation, 37 °C before the commencement of each experiment. Addition of substrates, uncoupler, and specific inhibitors of mitochondrial electron transport chain (ETC) complexes was performed using Hamilton syringes manually.

4. 3. 7. 1 Analysis of Mitochondrial bioenergetics (Intact cell respiration)

U251 cells cultured with Control or HG for 72 h were harvested using 0.1% Trypsin-EDTA, washed, and resuspended in cell culture media (Control media without FBS), and added to the 2 ml glass chambers (1–2 million cells/ml) of O2k-Respirometer.

Intact cell respiration was measured using serum free cell-culture media. In accordance with Oroboros guidelines ("MiPNet08.09 CellRespiration - Bioblast," n.d.), coupling control protocol for intact cells with oligomycin was used and respiration in different coupling control states, ROUTINE (R), LEAK (L), and Maximal electron transfer capacity (E) was derived from the O_2 flux values. 'R' corresponds to the physiological respiration of intact cells with endogenous substrates and is measured after adding cells to the chambers. 'L' respiration means the residual respiration independent of ATP synthase and corresponds to the proton leak, proton slip, and cation cycling across the inner mitochondrial membrane; Oligomycin (2.5 μM), complex-V inhibitor, was used to induce leak-state. Here, the Oligomycin sensitive respiration, i.e., the difference between 'R' and 'L', represents the ATP-linked respiration (R-L). Hereafter, the maximal respiration, 'E' was established experimentally by stepwise titration of CCCP (Carbonyl cyanide 3-chlorophenylhydrazone), 0.5 μM each time. The Spare-capacity of mitochondria was calculated as a difference between the Maximal-capacity and the Routine respiration (E-R). Residual oxygen consumption, ROX is the respiration connected to non-mitochondrial oxygen-consuming processes and instrument background; Rotenone (5

nM), an inhibitor of Complex-I and Antimycin A (2.5 mM), an inhibitor of Complex-III, were added to the system to inhibit mitochondrial oxygen consumption, giving ROX.

4. 3. 7. 2 Analysis of States of Respiration:

U251 cells cultured with Control cell culture medium (normal glucose levels) or HG for 72 h were harvested using 0.1% Trypsin-EDTA, washed, and resuspended in respiration buffer (MIRO5) consisting of 110 mM sucrose, 60 mM potassium-lactobionate, 20 mM taurine, 10 mM monobasic potassium phosphate, 3 mM magnesium chloride, 20 mM HEPES, 1 mM EGTA, and 0.1% (w/v) BSA at pH 7.1; and added to the 2 ml glass chambers (1–2 million cells/ml) of O2k-Respirometer. The SUIT (Substrate-Uncoupler-Inhibitor-Titration) protocol mentioned by Pesta et al., was followed with slight modification (Pesta and Gnaiger, 2012). Following addition of the cells, the Routine respiration was measured which was designated as State 1 respiration. The cells were permeabilized with titration of Digitonin – 0.5µl of 10mg/ml concentration each time. Upon the complete permeabilization, the cell cytoplasm becomes continuous with the respiration buffer and thus there is a sharp decline observed in the O_2 flux corresponding to the State 2 respiration. The substrates for the mitochondrial complexes were added sequentially. The Glutamate(5mM) and Malate (2mM) were added in the presence of ADP (5mM) which gives Glutamate-Malate State 3, Pyruvate (5mM) was added which forms substrates for Complex I and thus generates the value for Complex I mediated State 3 respiration. Malate, though not a substrate in itself is required as without malate addition, there would not be sufficient oxaloacetate generation to push the TCA cycle forward even in the presence of sufficient concentrations of other substrates. This, with an abundant Pyruvate present would activate the negative feedback loop and halt the respiration, thus giving erroneous inferences. This was followed by the addition of Succinate (10mM) which forms the substrate for Complex II, this activates the electron transport chain and initiates the flow of electrons through it at both the Complex I and Complex II routes, thus giving the total oxidative phosphorylation activity. The mitochondrial uncoupler CCCP was used in titrations for complete mitochondrial uncoupling. The mitochondrial complexes not only move the electrons sequentially through the

complexes but also help in generating an electrochemical gradient by pumping protons in the mitochondrial inter-membrane space. The uncoupling makes the mitochondrial inner membrane leaky to protons and causes backflow into the matrix, this makes the mitochondrial complexes perform at their maximal potential for restoration of the homeostasis; generating Maximal State 3 Respiration. The Complex I was then inhibited with Rotenone (0.1 μM) which gives the Maximal State 3 Respiration of Complex II. The experiment was terminated with Antimycin addition which blocks Complex III and generates the residual oxygen consumption. All values were ROX negated and normalized to the total protein content.

States of Respiration:

- State 1 –Routine respiration without any exogenous substrates (ADP and substrates both limiting)
- State 2 – Substrate availability but ADP limiting
- State 3 – Substrates are abundant, respiratory chain limiting
- State 3 uncoupled / maximal – Following the uncoupling with the uncoupler with all substrates abundant.
- Maximal State 3 Complex II – Maximal respiration following Complex I inhibition with Rotenone.

4. 3. 7. 3 Analysis activity of mitochondrial complexes:

Cells were permeabilized and analysis of the mitochondrial activity following exogenously given substrates in cells was carried out in mitochondrial respiration buffer (MiRO5). Following cell permeabilization and addition of ADP, the substrates for Complex I were added and respiration measured. The Complex I was then inhibited with Rotenone and the change in respiration measurement was taken as Complex I activity. This was followed for the other complexes, for Complex II Succinate was used as the substrate and Malonate (5 mM) was used as its inhibitor. Complex IV activity was determined following inhibition of Complex III with Antimycin A1 and addition of TMPD (Tetramethyl phenylenediamine), 0.5 mM, as electron donor

(donates electrons to cytochrome c that later passes it to Complex IV and keeps the electron flow moving) in the presence of Ascorbate (2 mM) to keep it in a reduced state while it was inhibited using Azide (100 mM).

Mitochondrial respiration medium (MiR05)

The preparation of MiRO5 was similar to that mentioned in Chapter 2.

Chemicals for mitochondrial substrate-uncoupler-inhibitor titration (SUIT) protocols

Substrates

Substrate	FW	Stock solution Conc. (mM)	Stock solution Amount	Final concentration in 2ml Volume within the Chambers
G: L- Glutamic acid	169.1	2000	3.382 g/ 10 mL H_2O	10 mM
M: L-Malic acid	134.1	400	536 mg/10 mL H_2O	2 mM
P: Pyruvic acid sodium salt	110	2000	44 mg/ 0.2 mL H_2O	5 mM
S: Succinate disodium salt, hexahydrate	270.1	1000	2.701 g/ 10 mL H_2O	10 mM
TMPD: (tetramethyl phenylenediamine)	237.2	200	47.4 mg/ ml H_2O	0.5 mM
ASC: Ascorbate	198.1	800	1.584 g/ 10 mL H_2O	2 mM
D: ADP (Adenosine 5' diphosphate, potassium salt)	501.3	500	0.501 g/ 2 mL H_2O	5 mM

Table 6: Substrates used for the mitochondrial functional analysis for hyperglycaemic experiments

Inhibitors

Inhibitors	FW	Stock solution Conc. (mM)	Stock solution Amount	Final concentration in 2ml Volume within the Chambers(A&B)
AA: Antimycin A	540	5	11 mg/ 4mL ethanol	2.5 µM
Omy: Oligomycin	800	5	4 mg/ 1mL ethanol	2.5 µM
Rot: Rotenone	394.4	1	3.94 mg/10mL ethanol	0.05 µM
Az: Sodium Azide	65.01	4000	260 mg/ ml	100 mM

Table 7: Inhibitors used for the mitochondrial functional analysis for hyperglycaemic experiments

4. 4 Statistical analyses

All statistical analysis were performed as mentioned in Chapter 2.

4. 5 Results:

4. 5. 1 Glucose estimation:

To first determine if the cells that are under HG condition are utilizing the extra glucose, we performed the glucose uptake assay which showed that the higher glucose in the extracellular media was being taken up in the cell (Fig 9A).

4. 5. 2 Lactate estimation:

It was then determined if he glucose that was being taken up by the cells was being utilized for glycolytic pathway or was being forwarded to the mitochondria for

oxidative phosphorylation. On performing the lactate estimation, it was determined that the cells under HG condition had higher lactate generation (Fig 9B).

4. 5. 3 pH determination:

The pH of the extra-cellular media in the HG state showed significant reduction suggesting an increase in acidity (Fig 9C). This could be due to the conversion of lactate to lactic acid thus affecting the pH, also validating that the lactate generation and secretion was higher in the cells under HG.

4. 5. 4 Immunoblot analysis:

The expression of aconitase is significantly lower in the cells under HG condition, suggesting that there is decline in the secretion of the critical enzyme responsible for the allocation of citrate towards oxidative phosphorylation. This further points towards reduced mitochondrial respiration and increased glycolysis under HG (Fig 9D-E).

4. 5. 5 High Resolution Respirometry:

4. 5. 5. 1 Analysis of Mitochondrial bioenergetics (Intact cell respiration):

The intact cell measurements of mitochondrial bioenergetics confirmed that the mitochondrial function had a drastic decline in the HG state. There was a decline in all respiratory parameters measured including Routine respiration (Fig 10A), leak respiration (Fig 10B), maximal respiration (Fig 10C), ATP linked respiration (Fig 10D) and Reserve Capacity (Fig 10E). Although, the coupling control ratios were similar among Control and HG (Figure 10F-I)

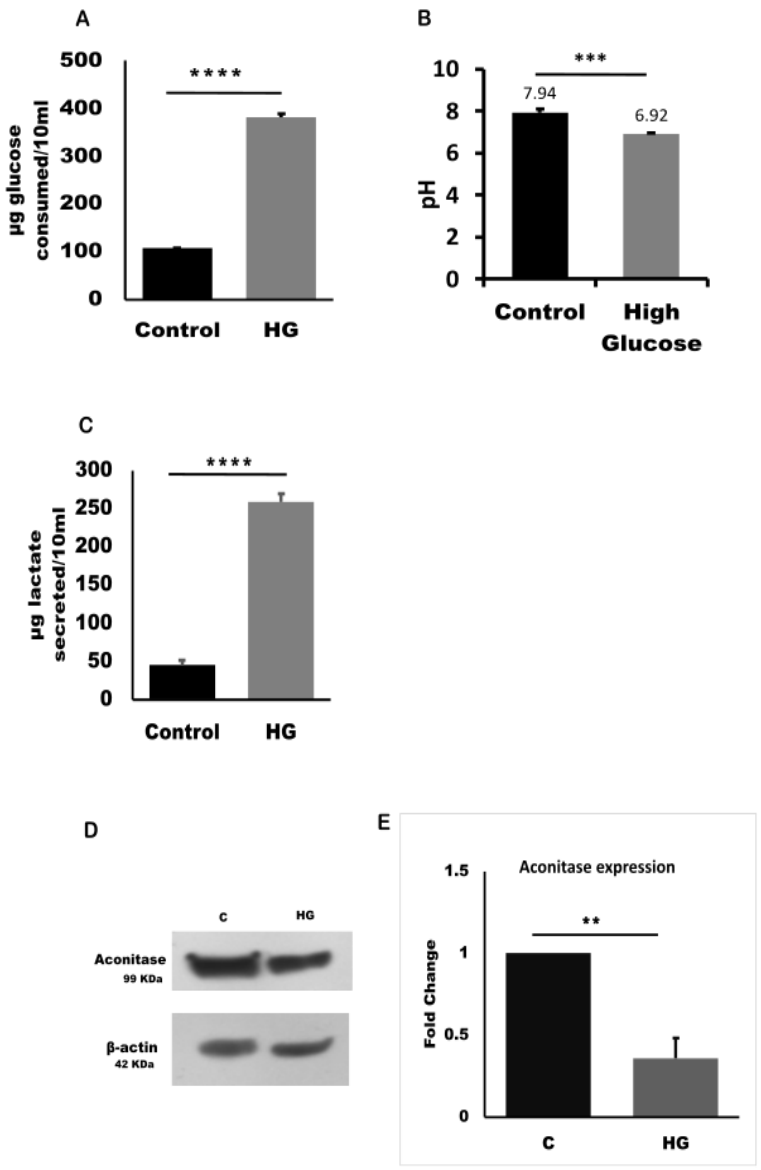

FIG 9: **A** - Glucose consumption, **B** - pH analysis, **C** - Lactate secretion, **D - E** - Aconitase expression

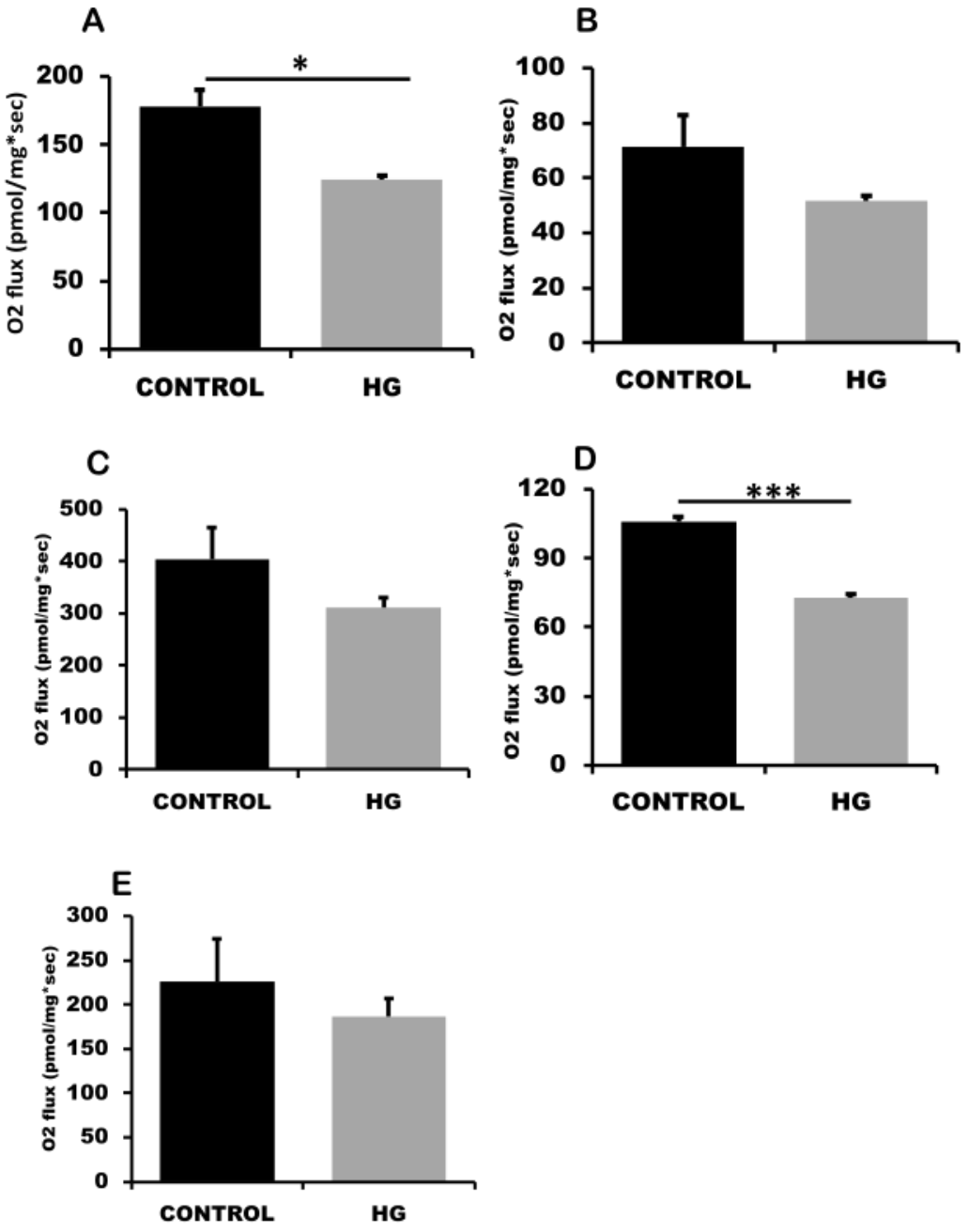

FIG 10: **A-** Routine Respiration, **B** - Leak respiration (following ATP synthase inhibition), **C** - Maximal Respiration (following uncoupling), **D**- ATP linked respiration (Routine - Leak), **E** - Reserve capacity (Maximal - Routine), **F** - Coupling efficiency ((R-L)/R), **G** - Leak/ Maximal (the proportion of maximal respiration contributed by proton leak), **H** - Leak/Routine (the proportion of Routine contributed by leak), **I** - ((Routine-Leak)/Maximal) (the proportion of Maximal contributed by ATP linked Respiration

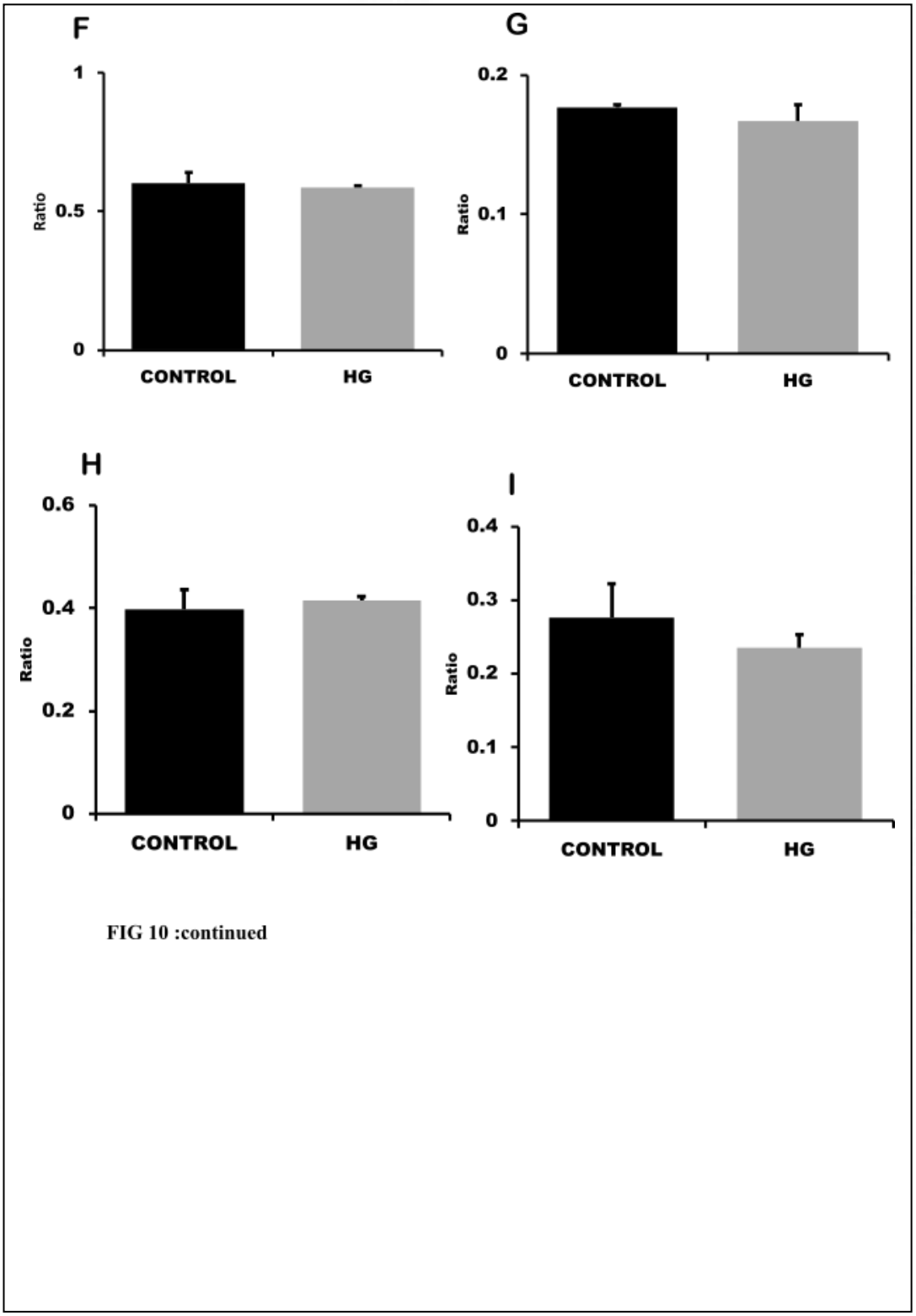

FIG 10 :continued

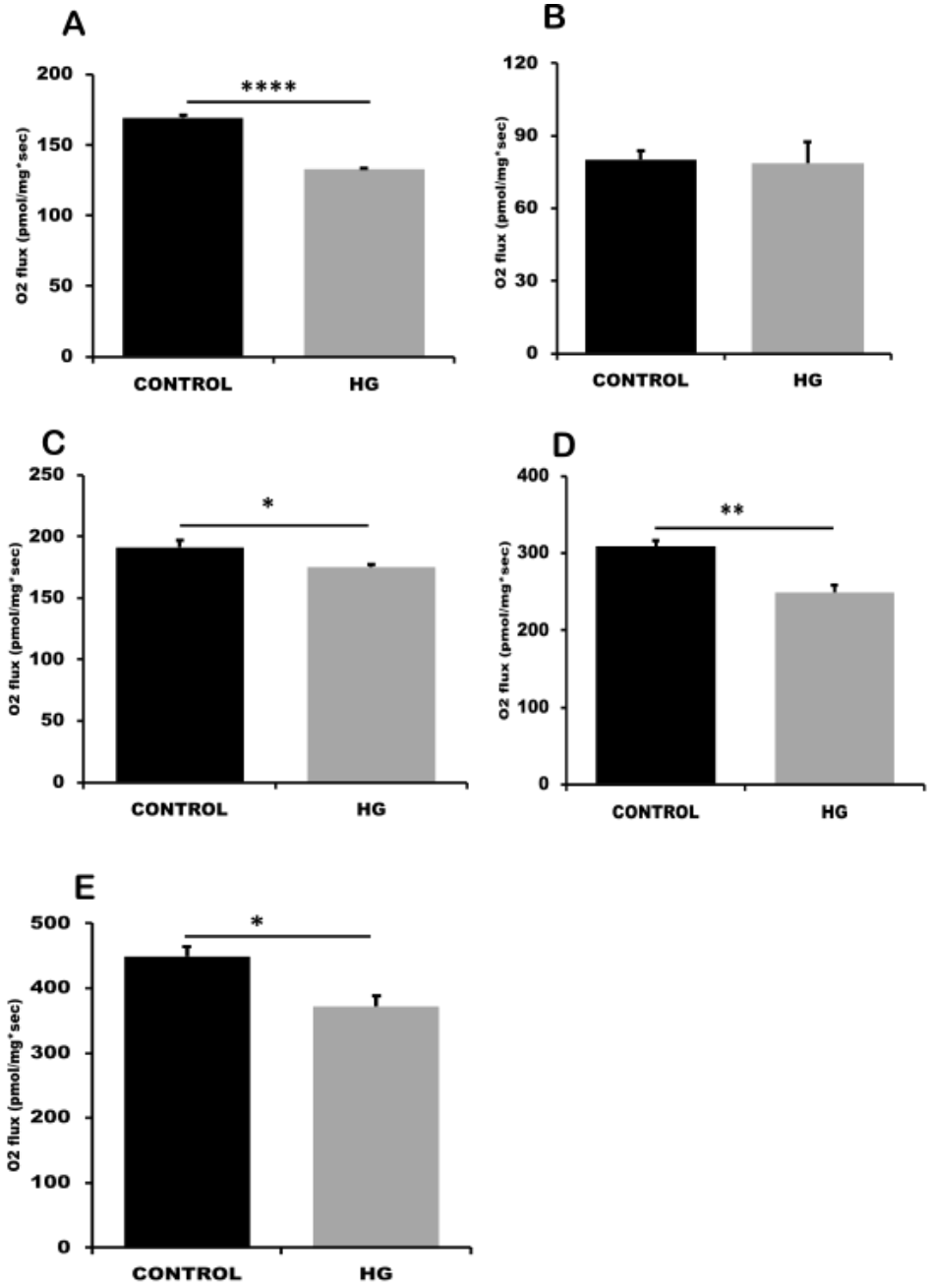

FIG 11 - Mitochondrial States of Respiration
A - State 1 respiration (Routine), **B** - State 2 respiration (following permeabilization with Digitonin, **C** - Glutamate-Malate-State 3, **D** - Complex I- State 3 (Glutamate-Malate-Pyruvate), **E** - Total oxidative phosphorylation capacity (Glutamate-Malate-Pyruvate-Succinate), **F** - Maximal State 3 respiration (following uncoupling), **G** - Complex II Maximal State 3 respiration (following inhibition of Complex I)

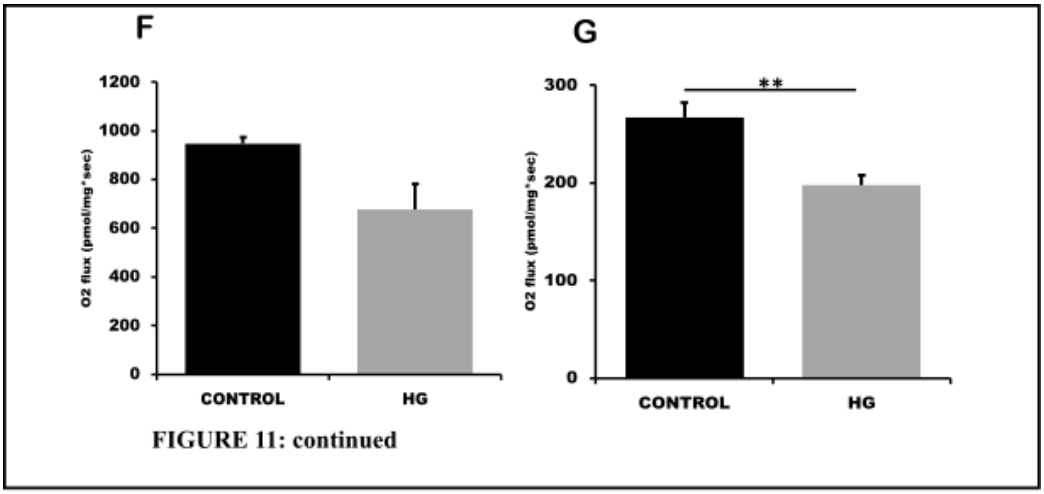

FIGURE 11: continued

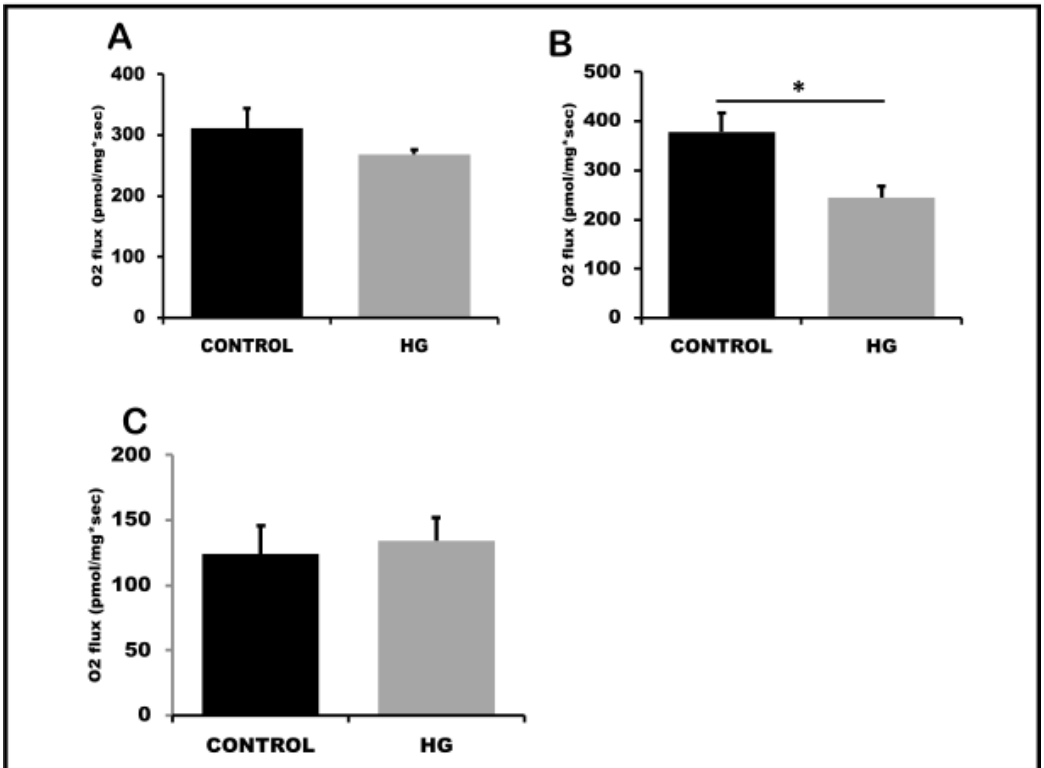

FIG 12 - Activity of Mitochondrial Complexes
A - Complex I function, **B** - Complex II function,
C - Complex IV function

4. 5. 5. 2 Analysis of States of Respiration:

To determine of the decline in respiration was due to decline in the respiratory intermediates within the cells or due to a decline in the functional capacity of the mitochondria, we analysed the States of Respiration with exogenously provided substrates.

The State 1 respiration showed similar pattern with the Routine respiration observed in the bioenergetics protocol (Figure 11A) as no substrates were added but even upon permeabilization with digitonin and addition of substrates, the states of respiration showed a significant decline in the HG group. State 3 for Glutamate-Malate (Fig 11C), State 3 respiration for Complex I mediated substrates (Glutamate-Malate-Pyruvate) (Fig 11D), the total OXPHOS (State 3 with both Complex I and Complex II substrates) (Fig 11E) and Complex II mediated maximal (Fig 11G) showed significantly diminished respiration in the HG group. The Maximal State 3 respiration (Fig 11F) which although not significant showed a trend towards decline. This confirms that the decline in respiration is due to the decline in the capacity of mitochondria in the HG group.

4. 5. 5. 3 Analysis activity of mitochondrial complexes:

It was further analysed if the decline in total mitochondrial performance was due to decline in any of the specific mitochondrial complexes. The activity of Complex I showed a trend towards a decline that was not observed in the activity of Complex IV (Fig 12A, C). there was maximal decline observed in the activity of Complex II (Fig 12B).

4. 6 Discussion:

There is the requirement to ensure that the glucose in the surrounding media under the HG state is taken up by the cells without which there would not be any biochemical changes to metabolism. It was confirmed that under HG there was higher glucose consumption, which seems likely as the cells of the central nervous tissue have Glut 3 as their main glucose transporter, which is constitutively expressed on the cell

membranes and is rather insensitive to insulin. Thus, the extra glucose was taken up by the cells. The lactate secretion in the extracellular media pointed towards a highly active glycolytic pathway, which was further established by assessment of the media pH. This acidification of the extracellular environment by lactate in the cancer cells has been proven to help their invasion capacity (Heiden et al., 2009). To fully confirm that the glioma in the HG state had a rise in glycolytic respiration and not OXPHOS, mitochondrial function was assessed through total cellular bioenergetics and substrate mediated respiration and was observed that the mitochondria had reduced efficiency under the HG condition and there was significant decline in the oxidative capacity suggestive of the glucose being used for aerobic glycolysis.

The determining step that commits the Acetyl-Co-A that enters the Krebs Cycle towards the OXPHOS is its conversion to aconitate, as citrate generated by combining Acetyl-Co-A with oxaloacetate in the first step of the Krebs cycle can have other metabolic destiny and may contribute in anabolic process of lipogenesis by moving out of the mitochondria (Currie et al., 2013). Our results indicate that there was reduced expression of aconitase and thus reduced Acetyl-CoA being carried forward through the TCA cycle further contributing to the reduced mitochondrial metabolism.

It has been well documented that the glucose utilized by the cells if not contributing towards OXPHOS, gets shuttled to other pathways that provide survival advantage to the cancer cells. the Pentose Phosphate Pathway is fed by the glucose-6-phosphate generated at the first step of glycolysis and which traps the glucose inside the cell. The end product of this pathway is the production of 5 carbon ribose-5-phosphate molecules which are utilized to form nucleotides; as the with the association and addition of glycine, glutamine, aspartate, tetrafolate and CO_2, ribose-5-phosphate gets converted into purine nucleotides; while with glutamine, aspartate and bicarbonate it generates pyrimidines. Even the telomerase reverse transcriptase, which is critical in maintaining the proliferative nature of cells, was shown to increase the transcription of enzymes of this pathway (Ahmad et al., 2016). Thus, the Warburg effect and increased glycolysis provides materials for DNA, RNA and energy currency in the form of ATP, GTP, etc. which would help in the rapid proliferation of the cells. We thus believe that the observed augmentation of Warburg could be the driver of

increased aggressiveness observed in the HG state. The study by Xu et al., gives insight into the importance of the glycolytic pathway in maintaining the cancer cell metabolism, as when the glycolytic enzymes were blocked it was observed that the mitochondria were not able to regain the capacity of metabolism and there ensues a severe ATP depletion causing growth arrest and further apoptosis in the colon cancer and lymphoma cells. there was also an increased re-localization of BAX onto the mitochondria causing the initiation of the cell death (Xu et al., 2005) Many clinical studies also suggest a high association of overexpression of glycolytic enzymes and poor prognosis in cancers, which led to the Yu et al., propose after analysing 86 clinical studies that the glycolytic enzyme expression could for a good prognostic marker for cancer survival and could form a basis for individualized therapy regimes (Yu et al., 2019). It has also been documented that the lactate secretion and subsequent tumour micro-environment change has a profound impact on the tumourigenesis, with one such research stating that lactate in the surrounding media influences the cancer associated fibroblasts to secrete hepatocyte growth factor in an NF-kB dependent pathway (Apicella et al., 2018). This further increases the growth factor availability for the cancer cells and favours proliferation.

One critical observation with the assessments of activities of mitochondrial complexes, was a decline in Complex II (Succinate dehydrogenase - SDH) function. With the mutation of SDH in many cancer cell lines, it was observed that the metabolites of Krebs cycle would accumulate as there would be less passage of electrons through Complex II and these would later be escape outside the mitochondria and inhibit prolyl hydrolase (PHD); which is a negative regulator of HIF1-α; thus, stabilizing HIF1-α and inducing hypoxia signalling (King et al., 2006). Although there are no SDH mutations reported in glioma, the HIF1-α mediated signalling has been shown to have pro-malignant effects in glioma (Gao et al., 2016). Thus, accumulating succinate which is plausible with reduced SDH activity, can behave as an oncometabolite. The succinate dehydrogenase subunits B, C and D are known to have anti-tumour properties, it is seen in multiple tumour models that when any one or more of these subunits are mutated causing a reduction in its activity, thereby causing a reduction in the activity of the SDH complex, there is a potential succinate

accumulation which leads to tumourigenic phenotype. SDH mutation caused a pseudo-hypoxic phenotype in the fibroblast and caused nuclear translocation of HIF1-α (Brière et al., 2005). This implies that with reduced Complex II function, there is a potential for activation of pro-tumourigenic cellular pathways.

4. 7 Conclusion:

Our results show that the increased glucose present in the HG condition is taken up by the glioma cells. there seems to be upregulation of the glycolytic pathways and the final generation of lactate than the increase of the mitochondrial OXPHOS by this extra glucose consumed. The decline in the aconitase expression suggests that the pyruvate in the form of Acetyl Co-A which enters the TCA cycle had reduced commitment towards utilization for OXPHOS and likely there would be shuttling of citrate outside the mitochondria for lipogenesis, which would further support the requirement of bio-membrane generation in the proliferating cells.

Critical Methodological Insight – II

mTOR inhibition gives different inferences regarding mitochondrial function when assessed using different protocols

1. Introduction:

mTOR inhibition and autophagy activation through the use of Torin and Rapamycin is a well-accepted and routine used method in multiple studies. The way it affects the cellular metabolism and mitochondrial respiration is also documented. The methodology for the determination of the mitochondrial function is not completely established as the real time functional studies have been underway only in the recent past. Thus, multiple methods for mitochondrial functional assessments are used in different studies like cellular bioenergetics that determines the capacity of the mitochondria by the utilization of its own biochemical substrates while other methods determine the functional capacity of the mitochondria with non-limiting substrates given and assessing the capacity to utilize them through electron transport chain. Yet another method employs analysis of the function of individual mitochondrial complexes through enzymatic procedures. It is seldom gauged how the treatments given affect these parameters differently. As mTOR is a master switch that governs multiple cellular processes including metabolism, growth and sustenance etc. it is ideal to weigh the mitochondrial metabolic studies against multiple determinants by using the more than one protocols.

2. Materials and Methods:

2.1 Reagents:

All reagents were as mentioned in Chapter 2 and 3.

2.2.2 Cell culture and Treatments:

Cell culture and maintenance were similar to that mentioned previously. Briefly U251 cells were cultured in recommended media and the treatments consisted of Rapamycin (25 nM) and Torin (100 nM) reconstituted in the same media as control and given for 72 h.

2.2 High Resolution Respirometry

Mitochondrial functional analyses were performed in Oxygraph-O2k, High-Resolution Respirometry (Oroboros Instruments, Innsbruck, Austria) at 37°C with a stirring speed of 750 rpm. Amplified signals from the oxygen sensor were recorded at sampling intervals of 2 s using DatLab-6.1 Software (Oroboros). Air-calibration of the respirometer at specific media was performed at air saturation, 37°C before the commencement of each experiment. Addition of substrates, uncoupler, and specific inhibitors of mitochondrial electron transport chain (ETC) complexes was performed using Hamilton syringes manually.

2.2.1 Analysis of Mitochondrial bioenergetics (Intact cell respiration): Methodology same as that mentioned in Chapter 4.

2.2.2 Analysis of States of Respiration: Methodology same as that mentioned in Chapter 4.

2.2.3 Analysis activity of mitochondrial complexes: Methodology same as that mentioned in Chapter 4.

3. Statistical analysis:

All statistics were done as pre the methods mentioned previously in Chapter 2.

4. Results and discussion:

4.1 High Resolution Respirometry:

4.1.1 Analysis of Mitochondrial bioenergetics (Intact cell respiration):

The intact cell measurements of mitochondrial bioenergetics showed that the mitochondrial function had a drastic decline in the treated groups. There was a decline in all respiratory parameters measured including Routine respiration (Fig 13A), leak respiration (Fig 13B), maximal respiration (Fig 13C), ATP linked respiration (Fig 13D) and Reserve Capacity (Fig 13E). As the leak respiration also showed a decline it is suggestive of an overall diminished oxidative phosphorylation in the treated groups. The coupling efficiency showed a decline in the treated groups while the

L/Max and L/R showed an increase implying that the proportion of leak respiration towards the Maximal and Routine were high.

This could be due to the substantial decline in the routine and maximal respirations observed. This illustrates that there was a considerable decline in the bioenergetics along with a diminished mitochondrial capacity.

4.1.2 Analysis of States of Respiration:

To validate the mitochondrial functional decline with mTOR inhibition, we analysed the mitochondrial function with another widely used method of assessment of the States of Respiration with exogenously provided substrates.

The State 1 respiration showed similar pattern with the Routine respiration observed in the bioenergetics protocol (Figure 14A) as no substrates were added but upon permeabilization with digitonin and addition of substrates, the states of respiration showed a different pattern in the treated group. State 3 for Glutamate-Malate (Fig 14C), State 3 respiration for Complex I mediated substrates (Glutamate-Malate-Pyruvate) (Fig 14D), the total OXPHOS (State 3 with both Complex I and Complex II substrates) (Fig 14E) and Complex II mediated maximal (Fig 14G) showed significantly enhanced respiration in the treated groups. The Maximal State 3 respiration (Fig 14F) although did not show any significant difference, the rest of the parameters clearly suggested an improvement in the respiration. This assessment protocol implies that the mitochondria under mTOR inhibition had improvement in the oxidative phosphorylation capacity with highly efficient electron transport chain function.

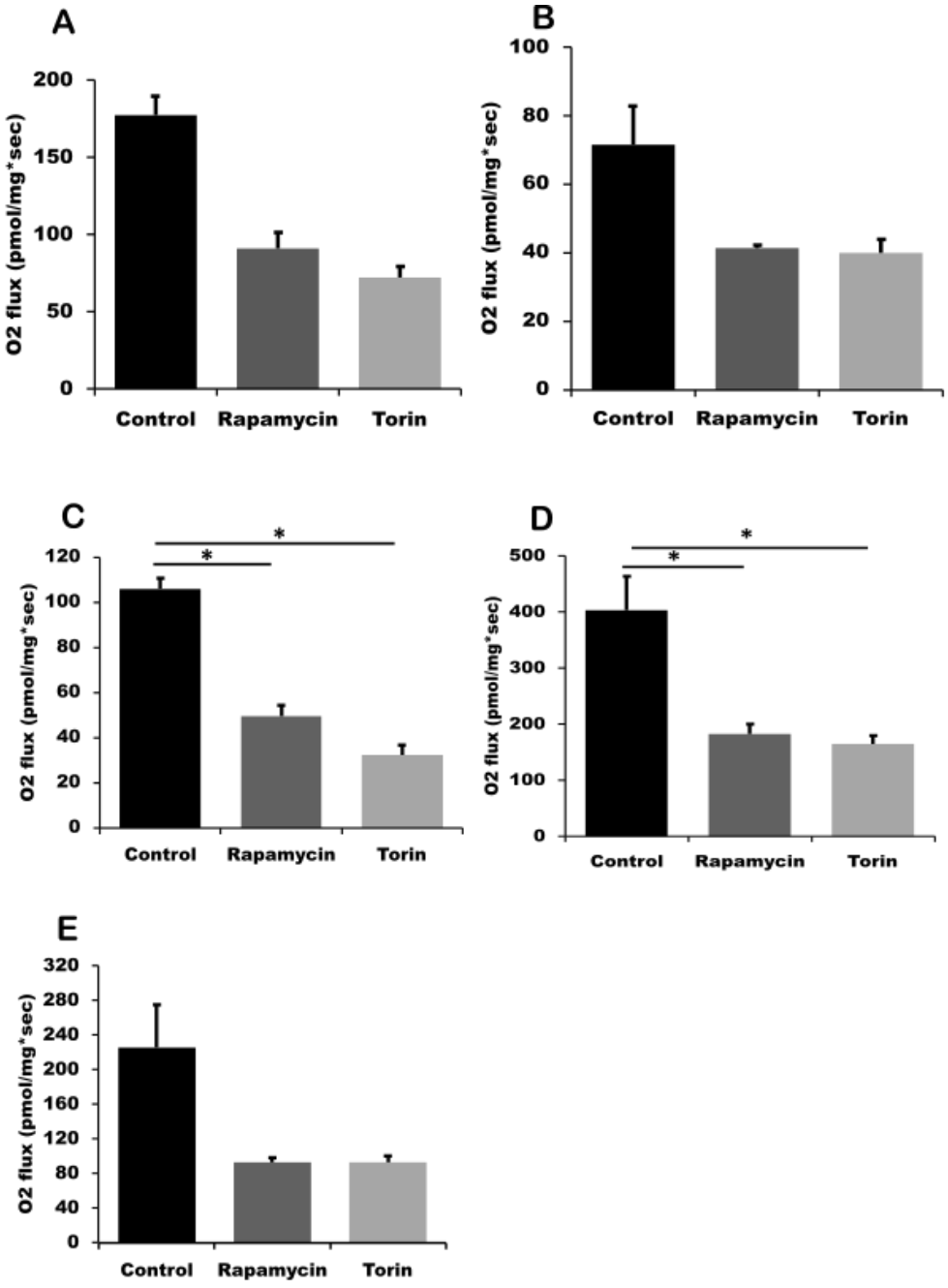

FIG 13: **A-** Routine Respiration, **B** - Leak respiration (following ATP synthase inhibition), **C** - ATP linked respiration (Routine - Leak), **D**- Maximal Respiration (following uncoupling), **E** - Reserve capacity (Maximal - Routine), **F** - Coupling efficiency ((R-L)/R), **G** - Leak/ Maximal (the proportion of maximal respiration contributed by proton leak), **H** - Leak/Routine (the proportion of Routine contributed by leak), **I** - ((Routine-Leak)/Maximal) (the proportion of Maximal contributed by ATP linked Respiration

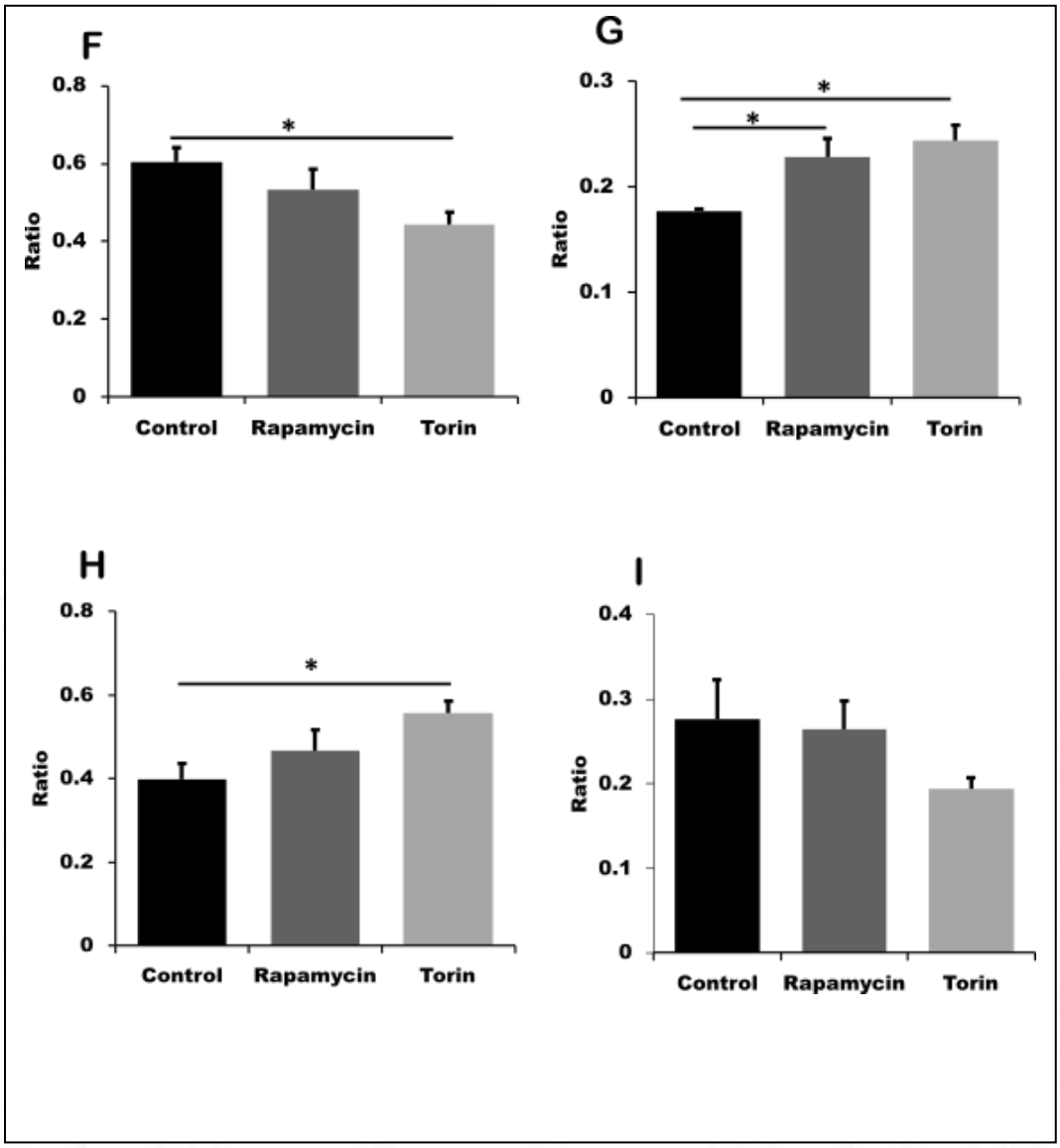
F
0.8
0.6
0.4
0.2
0
Ratio
*
Control
Rapamycin
Torin
G
0.3
0.2
0.1
0
Ratio
*
*
Control
Rapamycin
Torin
H
0.8
0.6
0.4
0.2
0
Ratio
*
Control
Rapamycin
Torin
I
0.4
0.3
0.2
0.1
0
Ratio
Control
Rapamycin
Torin

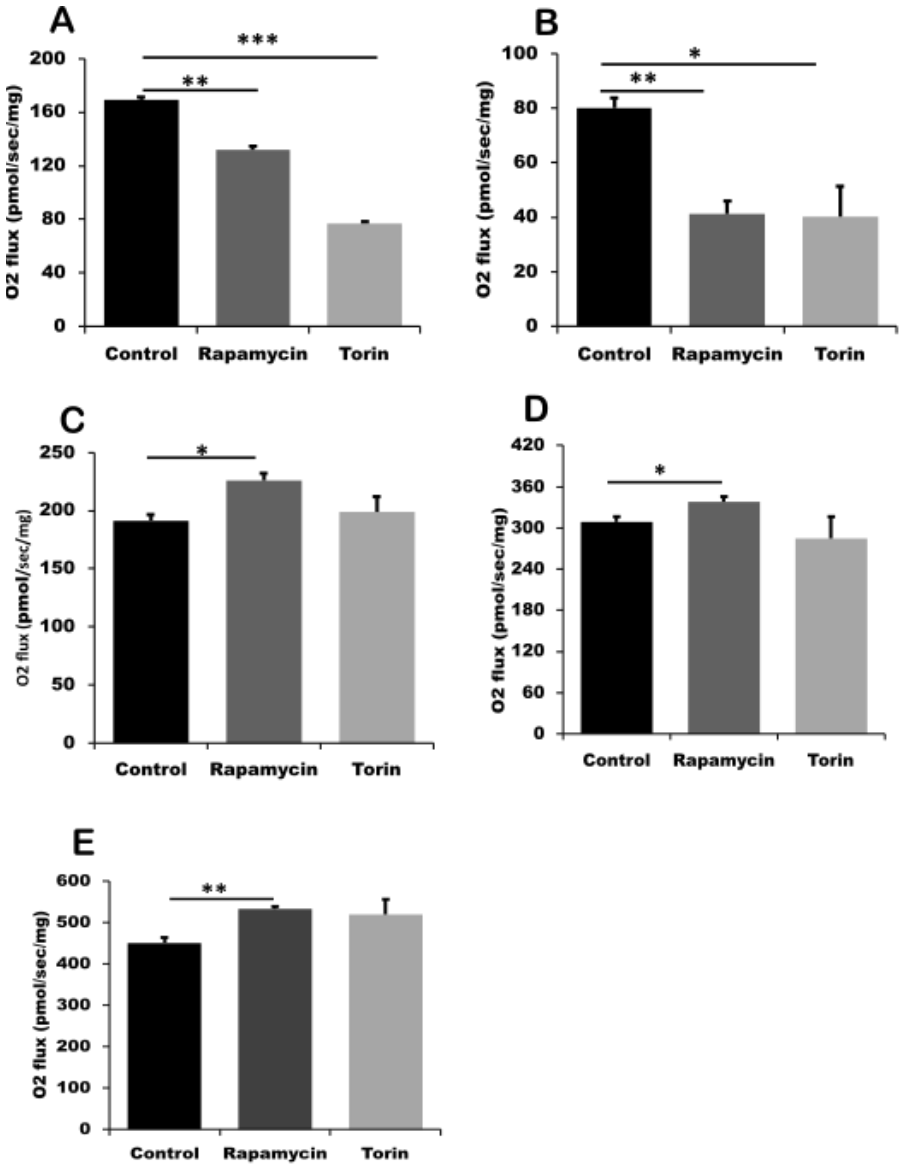

FIG 14 - Mitochondrial States of Respiration

A - State 1 respiration (Routine), **B** - State 2 respiration (following permeabilization with Digitonin, **C** - Glutamate-Malate-State 3, **D** - Complex I- State 3 (Glutamate-Malate-Pyruvate), **E** - Total oxidative phosphorylation capacity (Glutamate-Malate-Pyruvate-Succinate), **F** - Maximal State 3 respiration (following uncoupling), **G** - Complex II Maximal State 3 respiration (following inhibition of Complex I)

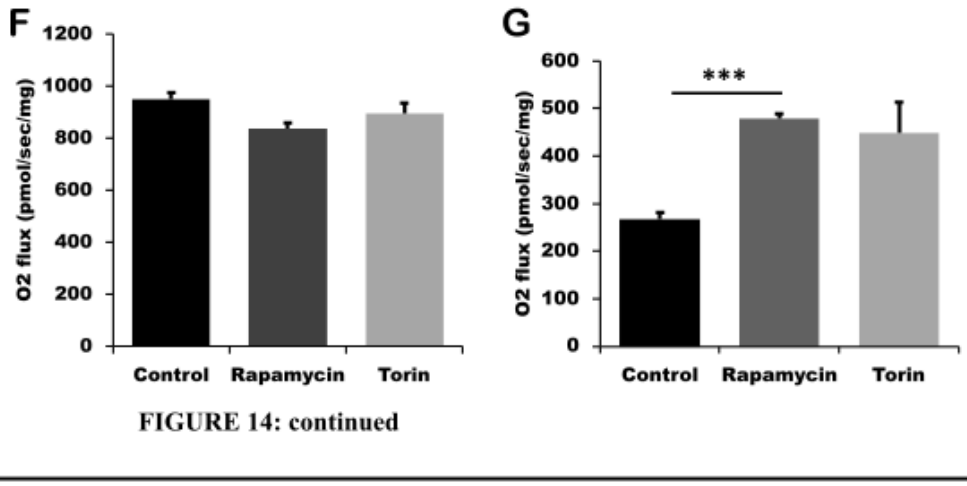

FIGURE 14: continued

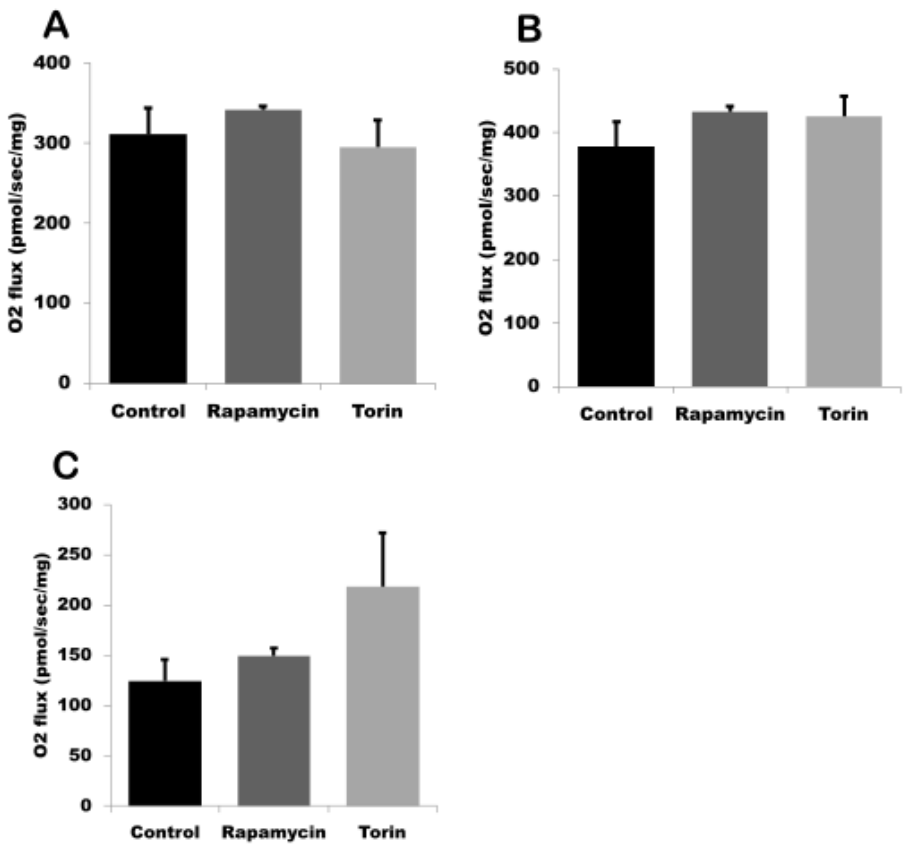

FIG 15 - Activity of Mitochondrial Complexes
A - Complex I function, **B** - Complex II function,
C - Complex IV function

4.1.3 Analysis activity of mitochondrial complexes:

The third commonly employed protocol for assessment of mitochondrial function is through the assessment of activities of individual mitochondrial electron chain Complexes. This method although failed to give any significance in the recorded observations, showed more correlation with the observations with the permeabilized and substrate addition protocol for states of respiration than with cellular bioenergetics. The activity of all three Complexes, Complex I, II and IV showed a trend towards improvement in the mTOR inhibited groups (Fig 15A-C).

5. Conclusion:

The mitochondrial functional assessments are done utilizing various accepted protocols and most often by utilizing a single protocol. The cellular bioenergetics and the permeabilized protocols wherein the substrates were given exogenously differ fundamentally in the underlying function being assessed. The bioenergetics shows how the mitochondria behave with the metabolites available within the cell and while the other protocols determine the capacity of the mitochondria to perform the electron transport chain function or assess the functional capacity of individual mitochondrial complexes separately. Our results display that the cellular bioenergetics is reduced while the mitochondrial functional capacity with substrate mediated respiration improved; this could be due to changes in the metabolites that fuel the mitochondrial oxidative phosphorylation with mTOR inhibition; since mTOR forms a major junction of various cellular signalling pertaining to metabolism and growth.

As the different methodologies adopted to assess mitochondrial function with mTOR inhibition gives different inferences, to come to a comprehensive conclusion, both the cellular bioenergetics and the substrate mediated respiration must be evaluated. We thus followed this strategy and determined mitochondrial efficiency with the three states protocols for all appropriate experiments.

Chapter 5

Objective 3: What causes HG mediated changes in the mitochondrial function?

Are the changes in mitochondrial function due to hyperglycaemia mediated by autophagy decline?

5.1 Introduction:

Macroautophagy (commonly referred to as autophagy) is a bulk cellular degradative process that is enhanced under the conditions of nutrient and growth factor depletion. It is mediated by five stages namely; a) nucleation also known as the formation of phagophore which begins the autophagy process, b) Atg5-Atg12 conjugation and association with the Atg16-L, c) processing of the LC3 molecule and insertion in the growing phagophore membrane, d) the capture of cargo which could be either random fragments of cytoplasm or random subcellular organelles or selective mediated by association with adaptor proteins, e) fusion with the lysosome that causes the degradation of the contents of the cargo through lysosomal proteases (Glick et al., 2010) as shown in the Fig E. mTOR works at the direct upstream step of autophagy initiation and it phosphorylates the first Atg protein Atg1 from interacting with Atg 13 thus inhibiting phagophore formation.

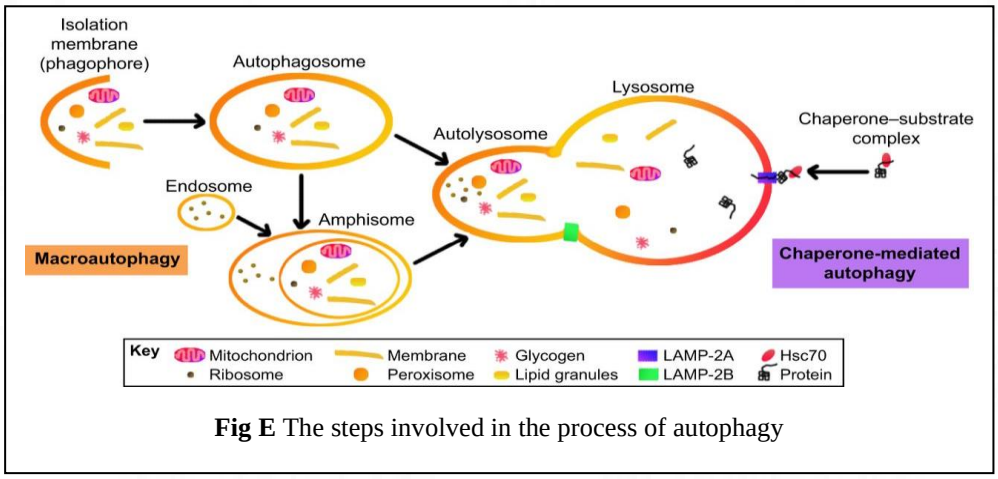

Fig E The steps involved in the process of autophagy

In a starvation stress, the autophagy is enhanced to meet the cells requirements for basal building blocks required for the cell survival and maintenance. This brings to notice that under the nutrient excess state, as the one created by the HG stress, the autophagy would be again dysregulated but in reverse, meaning autophagy would be declined. The dysregulation in autophagy has shown to impact mitochondrial activity.

We thus hypothesize that there is a decline in autophagy under HG state and this contributes the decline in mitochondrial function.

5.2 Review of Literature:

After the discovery of the process of autophagy and the associated Atg proteins, various types of autophagy have been identified along with the mechanisms through which it functions to maintain cellular homeostasis or mitigate cellular stress response (Nakatogawa et al., 2009), (Yang and Klionsky, 2010). Various cytosolic substrates which may include the misfolded or damaged proteins, cytoplasmic constituents, organelles like mitochondria (mitophagy) or endoplasmic reticulum or even pathogens like viruses or bacteria (Mizushima et al., 2008). With excess or damaged mitochondria there is selective elimination of the mitochondrial subunits through mitophagy thus retaining the quality of the mitochondrial pool (Narendra et al., 2008), (Twig et al., 2008). But when there is a dysregulation of cellular autophagy, there is observed decline in the mitochondrial quality; suggesting that correcting for that dysregulation could potentially correct the mitochondrial dysfunction.

Autophagy induction is possible by inhibition of its master upstream regulator mTOR. mTOR is present as two complexes mTOR-C1 and mTOR-C2 as depicted in the Fig F below, with mTOR-C1 activation having a direct inhibitory role on autophagy while mTOR-C2 has shown to be more indirect in its regulation of autophagy. Thus, for a

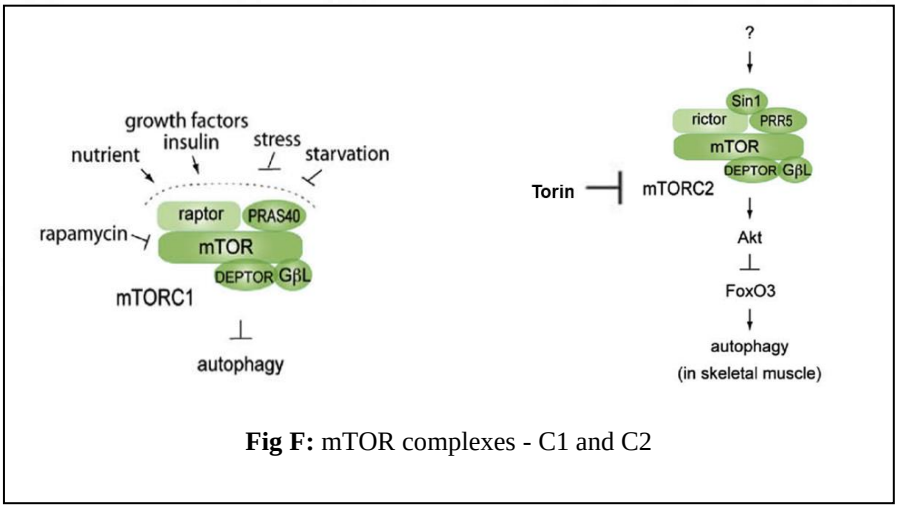

Fig F: mTOR complexes - C1 and C2

comprehensive understanding of autophagy induction, both mTOR Complex inhibitors must be utilized.

Also, mTOR complex 1 being a master regulator of cellular growth factor and nutrient signalling as depicted in Fig C; it has its own impact on mitochondrial metabolism and structure. This could be a confounding variable in estimating the role of autophagy induction on mitochondrial function with the use of mTOR modulators.

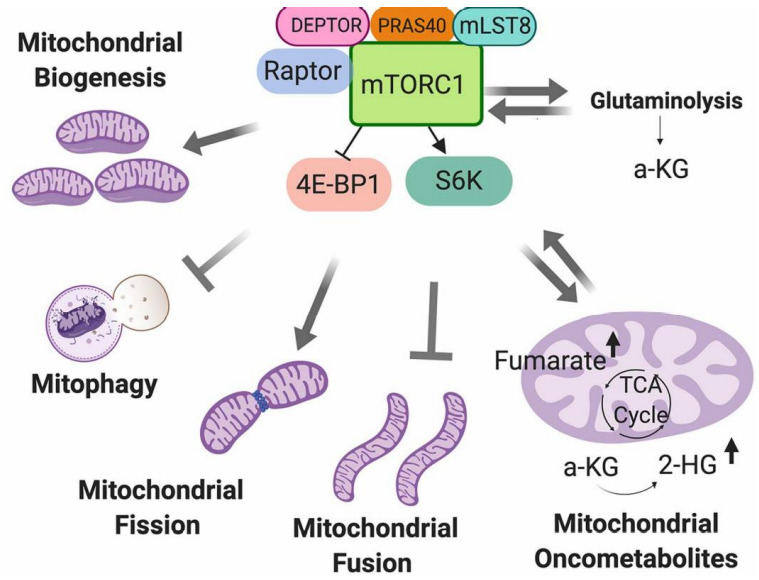

Fig G – mTOR regulates mitochondrial dynamics and metabolism

(de la Cruz López et al., 2019, p. 1)

5.3 Materials and Methods:

5.3.1 Cell Culture and Maintenance:

Cell culture and maintenance techniques were similar to that mentioned in Chapter 4.

5.3.2 Reagents used for Cell culture:

All reagents as mentioned in Chapter 4 along with Rapamycin, Torin and Bafilomycin A1 (Cayman Chemicals, MI, USA) were used. Acridine orang stain and Chloroquine

was obtained from Sigma (MO, USA). The treatments used were the same as that used for the cell culture in Chapter 4. The additional groups were added to the treatments with Rapamycin and Torin given as autophagy inducers, for which 25 nM Rapamycin and 100 nM Torin was used for 72h in HG media. LC3II antibody was obtained from CST (MA, USA) while

5.3.3 Acridine Orange staining:

Cells were cultured in a 96 well plate and treated with control and HG media in two batched for 72 h as mentioned previously. For the last 4 h of the treatment the corresponding media with 50 µM of Chloroquine was added to one of batch each of control and HG. Cells were stained with Acridine Orange which stains the acidic vacuoles, was added at a concentration of 2 µg/ml for 10 min and incubated in the CO_2 incubator. Cells were washed with PBS and the fluorescence images were acquired with a Olympus IX 51 Fluorescent microscope (Tokyo, Japan).

5.3.4 Immunoblotting:

For autophagy estimation, the Control and HG groups were given Bafilomycin A1 for the last 2 h of the 72 h treatment duration. The other methodology for immunoblotting was same as mentioned in Chapter 4.

5.3.5 Glucose consumption and Lactate secretion:

The glucose consumption and lactate experimental methods were same as that mentioned in Chapter 4.

5.3.6 Mitochondrial Respiration measurements:

All mitochondrial respiration methods were same as that mentioned in Chapter 4.

5.4 Statistical analysis:

The comparisons were made between HG and HG with Rapamycin or Torin using Student's T-Test (two tailed, uniform variance) without making within group comparisons. For assessment of autophagy through immunoblot, the group and its respective Bafilomycin treated groups were compared with Student's T-Test with one tailed distribution. All other statistics were performed as mentioned in Chapter 2.

5.5 Results:

5.5.1 Determination of Autophagy:

5.5.1.1 AO staining:

AO stain localizes in the nucleus and fluoresces in the yellow-green range while it localizes in the acidic compartments like lysosomes and fluoresces in orange. With the inhibition of the final step of autophagy, the autophagolysosome accumulate in the cells and the cells with high autophagy have more autophagosome accumulation while cells with lower levels of autophagy have lower accumulation of such vesicles. The AO imaging is a valid preliminary step in assessing the autophagy in the cells, and with high autophagic flux data show higher orange vacuoles while with lower autophagy there are fewer orange vacuoles. The flux data showed more vacuole in the Control group than in the HG (Fig 16A) pointing towards a potential decline in autophagy under HG.

5.5.1.2 Immunoblotting for LC3II flux:

To confirm the autophagic status, autophagy flux was assessed by the accumulation of LC3II following autophagy inhibition using Bafilomycin A1. The densitometric measurements showed that there was a significantly higher LC3II accumulation in the Control+Baf group than in the HG+Baf group suggesting that the autophagy was declined in the HG group (Fig 16B).

5.5.2 Glucose consumption and Lactate secretion:

The glucose consumption was significantly declined with both the autophagy inducers given under HG condition (Fig 16C) and also the secretion of lactate in the extra cellular media significantly declined in these groups (Fig 16D). This suggests that there was less glucose utilization and less glycolytic end product lactate expulsion. This effect was more pronounced for Torin than for Rapamycin.

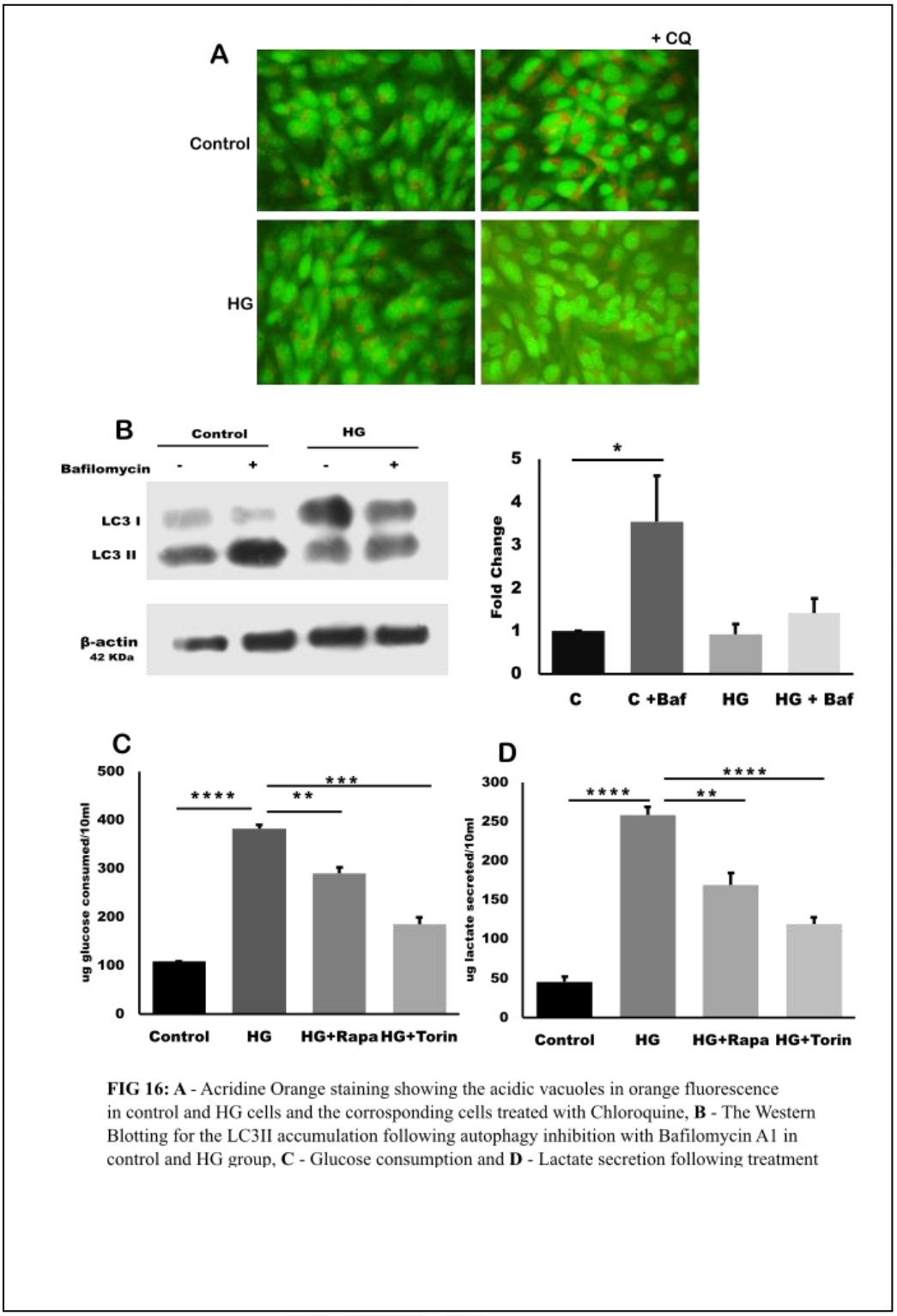

FIG 16: A - Acridine Orange staining showing the acidic vacuoles in orange fluorescence in control and HG cells and the corrosponding cells treated with Chloroquine, **B** - The Western Blotting for the LC3II accumulation following autophagy inhibition with Bafilomycin A1 in control and HG group, **C** - Glucose consumption and **D** - Lactate secretion following treatment

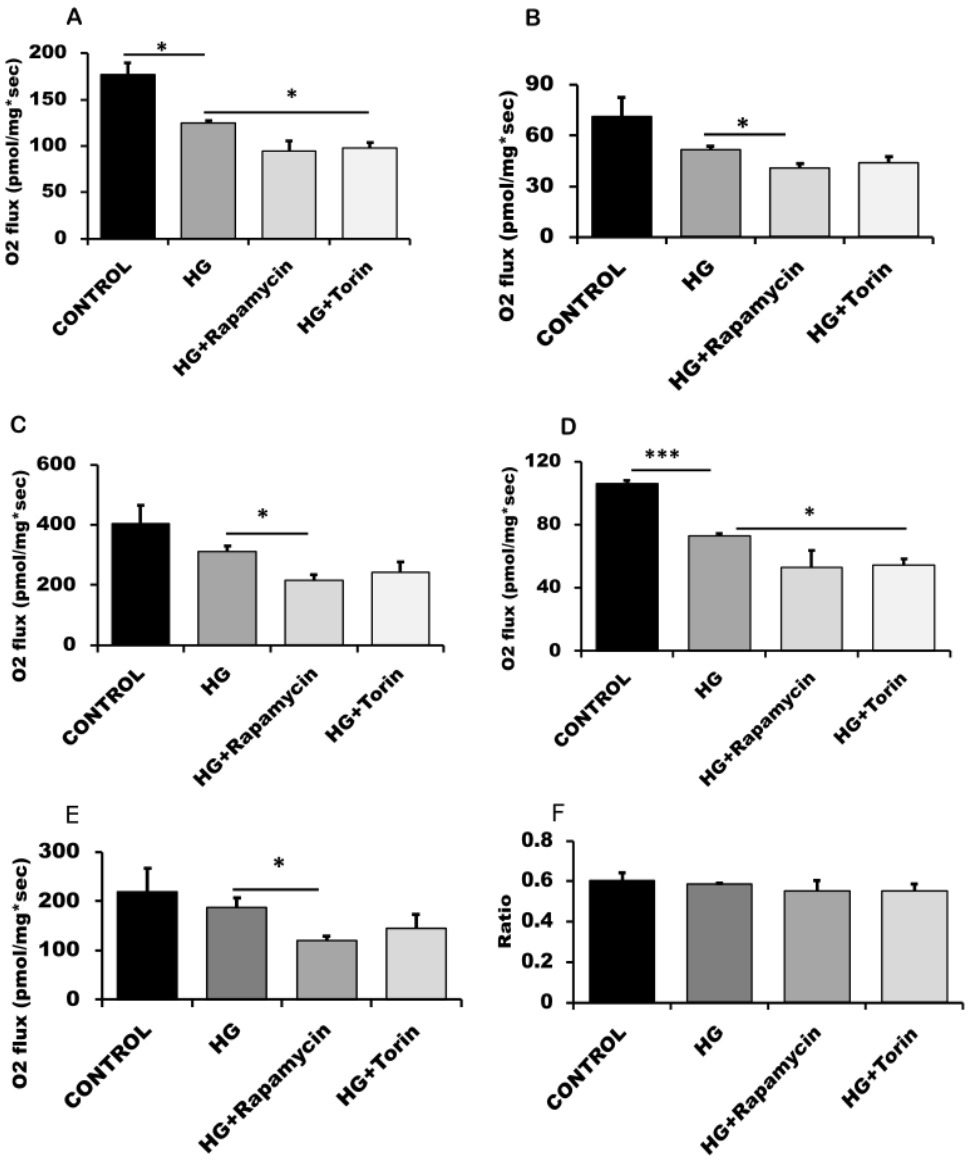

FIG 17: **A-** Routine Respiration, **B** - Leak respiration (following ATP synthase inhibition), **C** - Maximal Respiration (following uncoupling), **D-** ATP linked respiration (Routine - Leak), **E** - Reserve capacity (Maximal - Routine), **F** - Coupling efficiency ((R-L)/R), **G** - Leak/ Maximal (the proportion of maximal respiration contributed by proton leak), **H** - Leak/Routine (the proportion of Routine contributed by leak), **I** - ((Routine-Leak)/Maximal) (the proportion of Maximal contributed by ATP linked Respiration

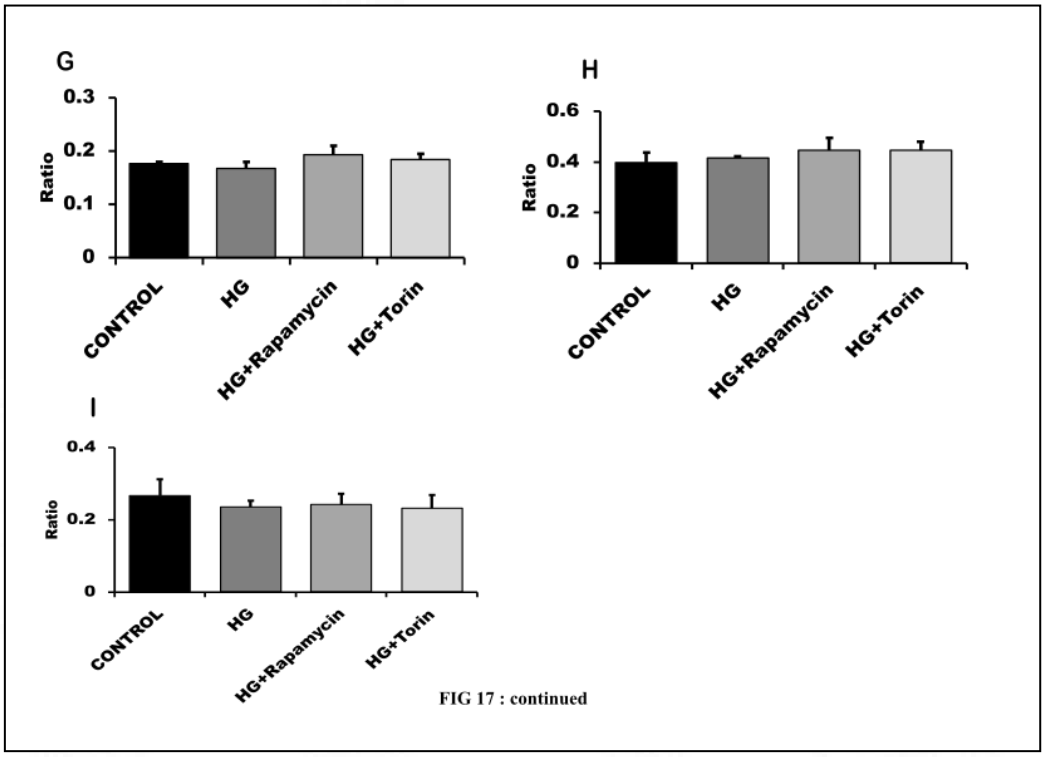

FIG 17 : continued

5.5.3 Mitochondrial Respiration measurements:

Intact cell respiration: All respiratory parameters measured within the Control, HG and HG with Rapamycin and HG with Torin showed there was a steady decline in respiration with induction of autophagy as observed in the values for Routine respiration (Fig 17A), leak respiration (Fig 17B), maximal respiration (Fig 17C), ATP linked respiration (Fig 17D) and Reserve Capacity (Fig 17E). As the leak respiration was also significantly reduced, it could imply that there is overall diminished respiration in the treated groups. The coupling control ratios were observed to be similar to the ones seen in Control and HG (Figure 17F-I), also pointing out that there may not be much damage to the mitochondrial population in the Rapamycin and Torin treated groups.

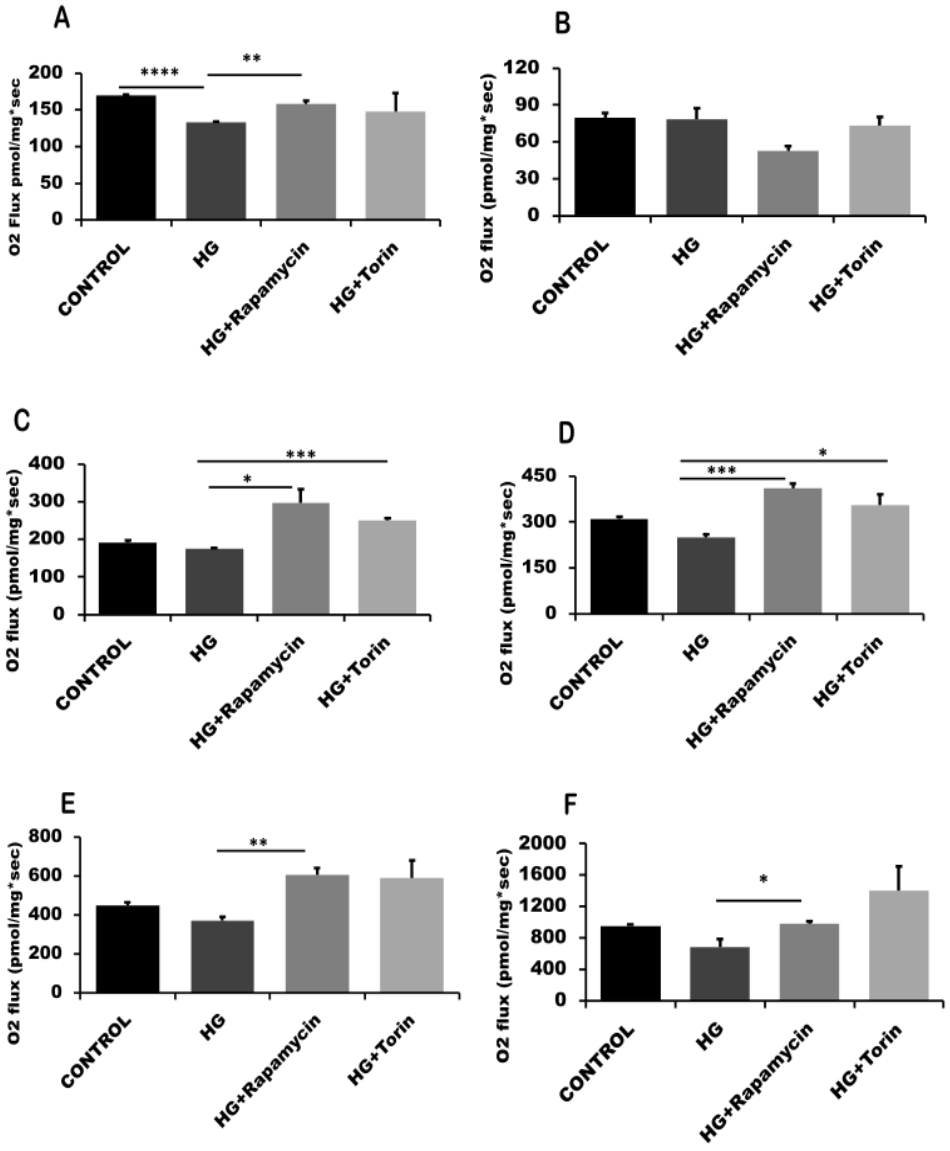

FIG 18 - Mitochondrial States of Respiration
A - State 1 respiration (Routine), **B** - State 2 respiration (following permeabilization with Digitonin, **C** - Glutamate-Malate-State 3, **D** - Complex I- State 3 (Glutamate-Malate-Pyruvate), **E** - Total oxidative phosphorylation capacity (Glutamate-Malate-Pyruvate-Succinate), **F** - Maximal State 3 respiration (following uncoupling), **G** - Complex II Maximal State 3 respiration (following inhibition of Complex I)

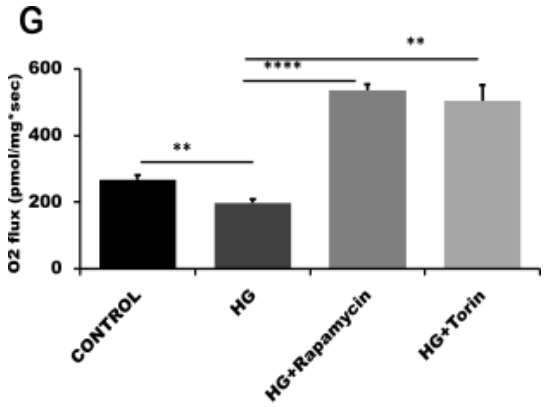

FIGURE 18: continued

States of Respiration: With the states of respiration, it was observed that there was an improvement in the respiratory assessments. The State 1 showed enhanced respiration with autophagy induction (Figure 17A). State 3 for Glutamate-Malate (Fig 17C), State 3 respiration for complex I mediated substrates (Glutamate-Malate-Pyruvate) (Fig 17D) both showed significant increase, suggesting better capacity at the Complex I junction. The total OXPHOS (State 3 with both Complex I and Complex II substrates) (Fig 14E) showed significant improvement in the total oxidative electron transport chain capacity also observed with Maximal State 3 respiration (Fig 17F). The Complex II mediated maximal respiration showed significant improvement with both Rapamycin and Torin (Fig 17G) suggesting that the succinate accumulation and succinate mediated tumorigenesis can possibly be hindered by autophagy induction.

Activities of mitochondrial complexes: The results with the permeabilized protocol with exogenously given substrates pointed at there being a betterment in the capacity of the mitochondrial electron transport chain enzymes. We thus analysed the activities of individual mitochondrial complexes, and observed that both Rapamycin and Torin addition improved the activity of all the three complexes assessed i.e., Complex I, II and IV (Fig 19A-C); a significantly higher activity for Complex II and Complex IV.

This confirmed that when substrates were provided exogenously, it was observed that the decline in the complex activities observed in the HG condition was reversed with the autophagy induction by Rapamycin and Torin.

5.6 Are these results due to enhanced autophagy?

The results suggested that the autophagy decline played a role in HG mediated decline in mitochondrial function and autophagy induction could remedy that effect. But the autophagy inducers used were the mTOR inhibitors, as mTOR is the direct upstream

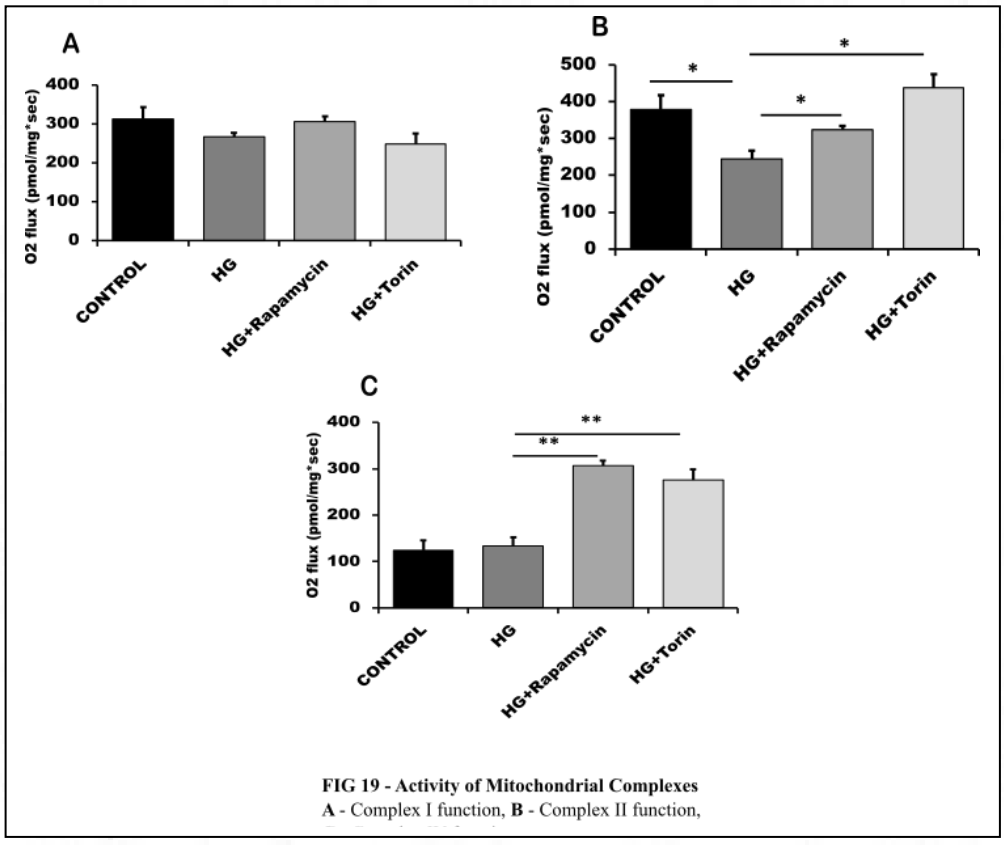

FIG 19 - Activity of Mitochondrial Complexes
A - Complex I function, **B** - Complex II function,

negative modulator of autophagy. mTOR is a cellular nutrient sensor and through the modulation of transcription factors plays a fundamental role in cellular response to nutrient availability and growth factor signalling. It thus has a direct impact on the mitochondria along with the indirect influence through autophagy modulation as depicted in Fig H. To assess if the effects observed were due to autophagy activation or mTOR inhibition, we used Lithium Chloride based autophagy induction. LiCl

causes enhanced phagophore formation which causes autophagy induction without having any direct effect on mTOR activation, Fig I.

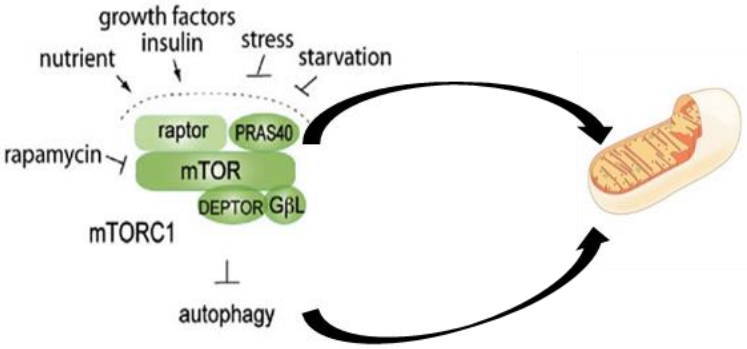

Fig H – Regulation of mitochondrial activity by mTOR

5.6.1 Reagents used:

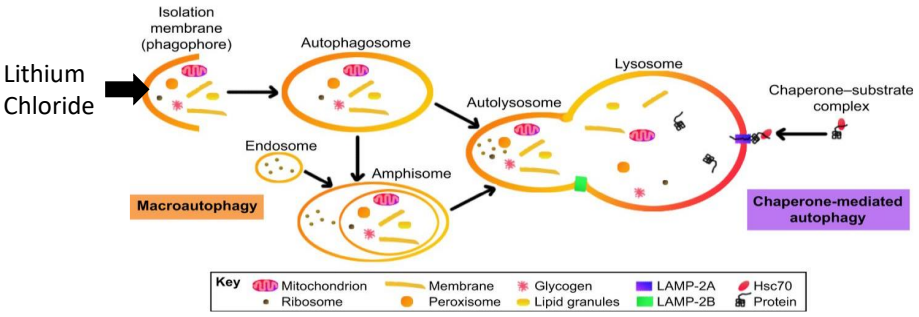

Fig I: Autophagy induction by Lithium Chloride

Same as that mentioned above alone with an additional treatment group having 5µM LiCl (Sigma Aldrich, USA) reconstituted in HG media.

5.6.2 Results:

5.6.2.1 Glucose consumption and Lactate secretion:

The glucose consumption was not affected by LiCl mediated autophagy induction (Fig 20A) and also the secretion of lactate in the extra cellular media did not show any decline (Fig 20B).

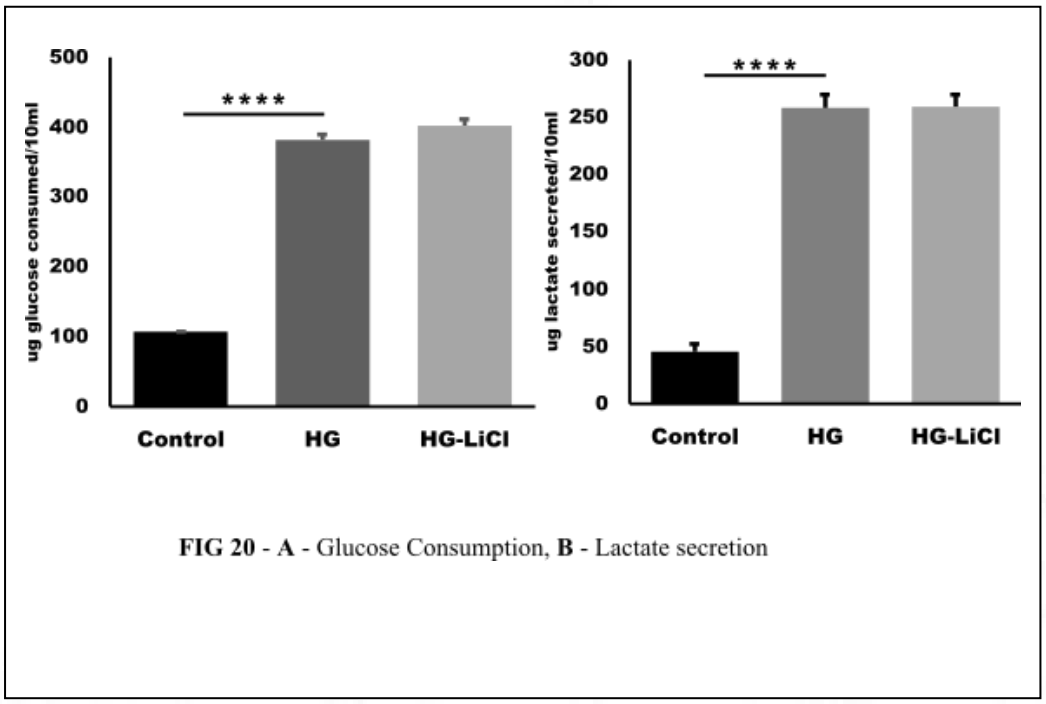

FIG 20 - **A** - Glucose Consumption, **B** - Lactate secretion

5.6.2.2 Mitochondrial Respiration measurements:

Intact cell respiration: All respiratory parameters measured within the Control, HG and HG with LiCl showed there was a steady decline in respiration with induction of autophagy as observed in the values for Routine respiration (Fig 21A), leak respiration (Fig 21B), maximal respiration (Fig 21C), ATP linked respiration (Fig 21D) and Reserve Capacity (Fig 21E). although there was significance observed only for Routine and ATP linked respiration, there was a marked trend towards a decrease in other values. As the leak respiration was also significantly reduced, it could imply that there is overall diminished respiration in the treated group. The coupling control ratios were observed to be similar to the ones seen in Control and HG (Figure 21F-I), also pointing out that there may not be much damage to the mitochondrial population in the LiCl treated groups.

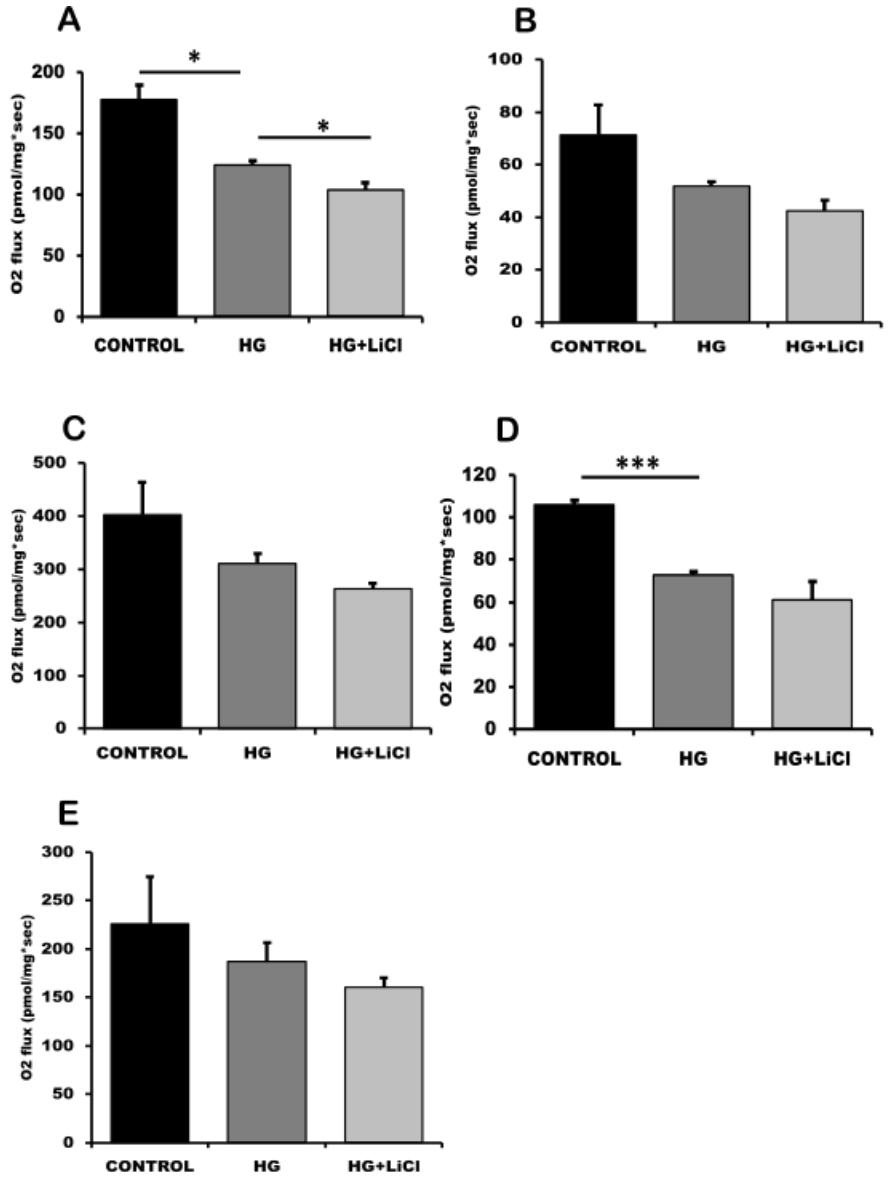

FIG 21: **A-** Routine Respiration, **B** - Leak respiration (following ATP synthase inhibition), **C** - Maximal Respiration (following uncoupling), **D**- ATP linked respiration (Routine - Leak), **E** - Reserve capacity (Maximal - Routine), **F** - Coupling efficiency ((R-L)/R), **G** - Leak/ Maximal (the proportion of maximal respiration contributed by proton leak), **H** - Leak/Routine (the proportion of Routine contributed by leak), **I** - ((Routine-Leak)/Maximal) (the proportion of Maximal contributed by ATP linked Respiration

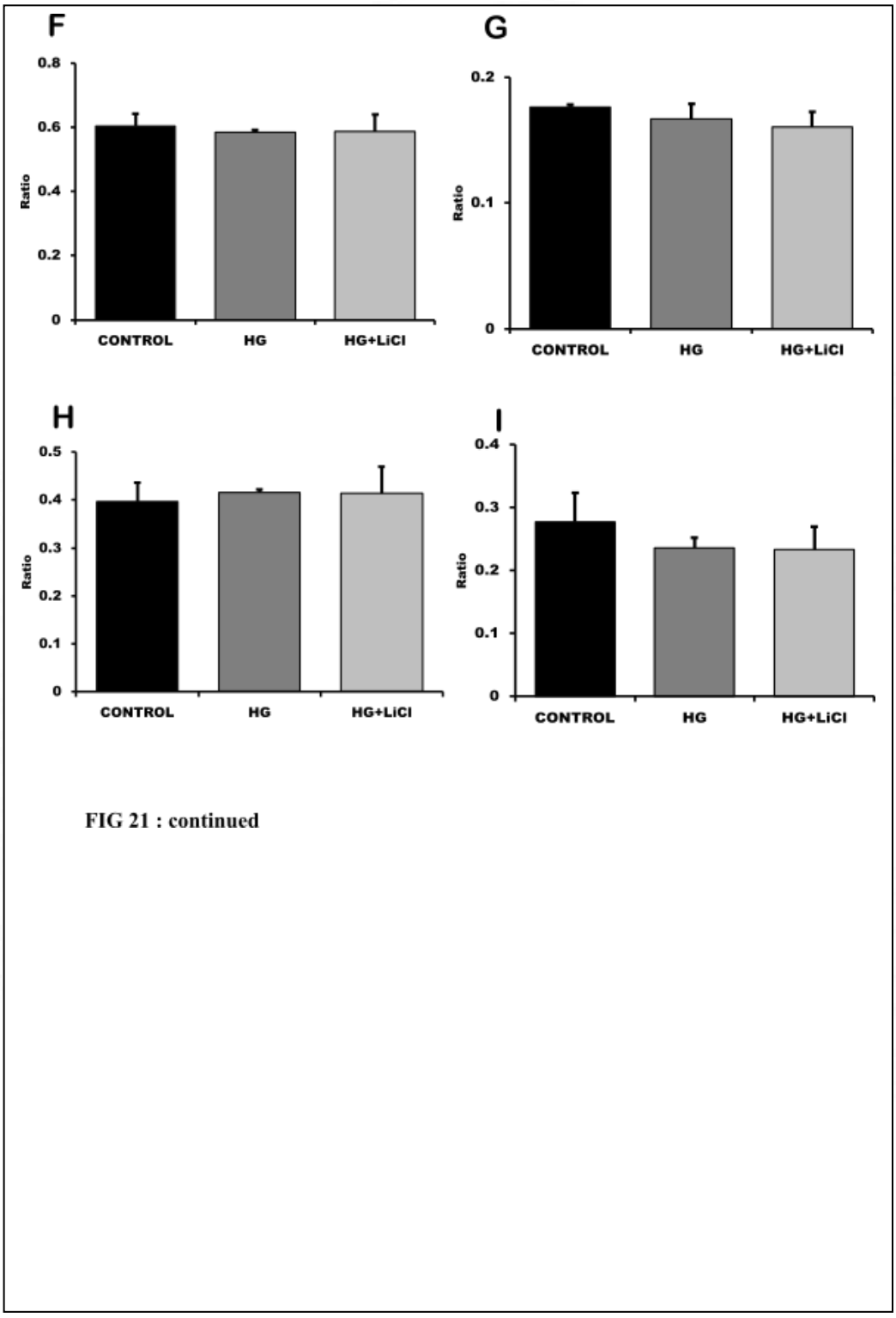

FIG 21 : continued

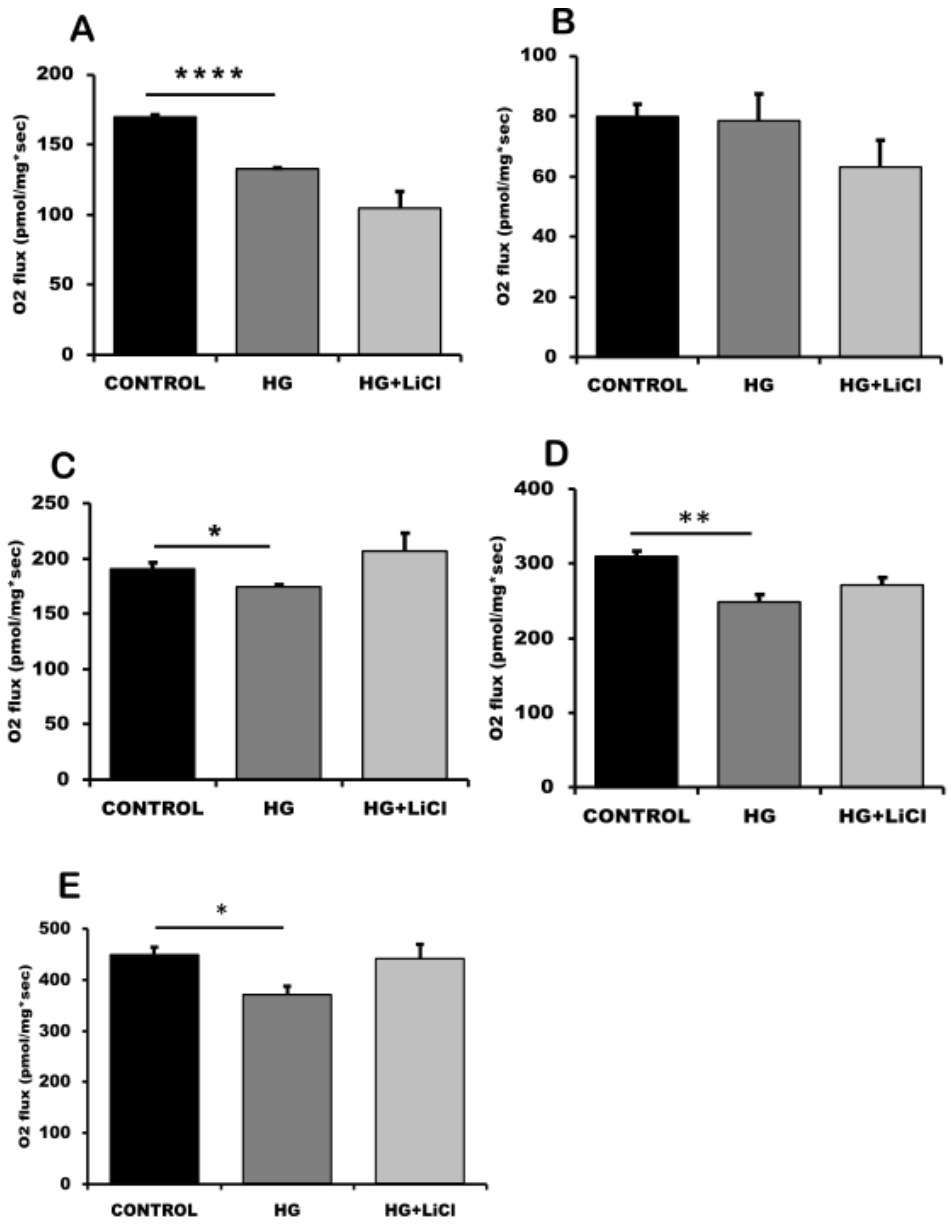

FIG 22 - Mitochondrial States of Respiration

A - State 1 respiration (Routine), **B** - State 2 respiration (following permeabilization with Digitonin, **C** - Glutamate-Malate-State 3, **D** - Complex I- State 3 (Glutamate-Malate-Pyruvate), **E** - Total oxidative phosphorylation capacity (Glutamate-Malate-Pyruvate-Succinate), **F** - Maximal State 3 respiration (following uncoupling), **G** - Complex II Maximal State 3 respiration (following inhibition of Complex I)

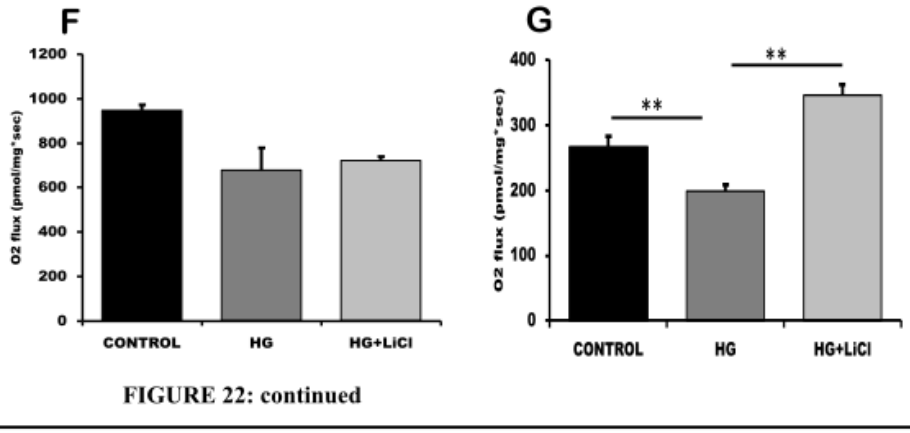

FIGURE 22: continued

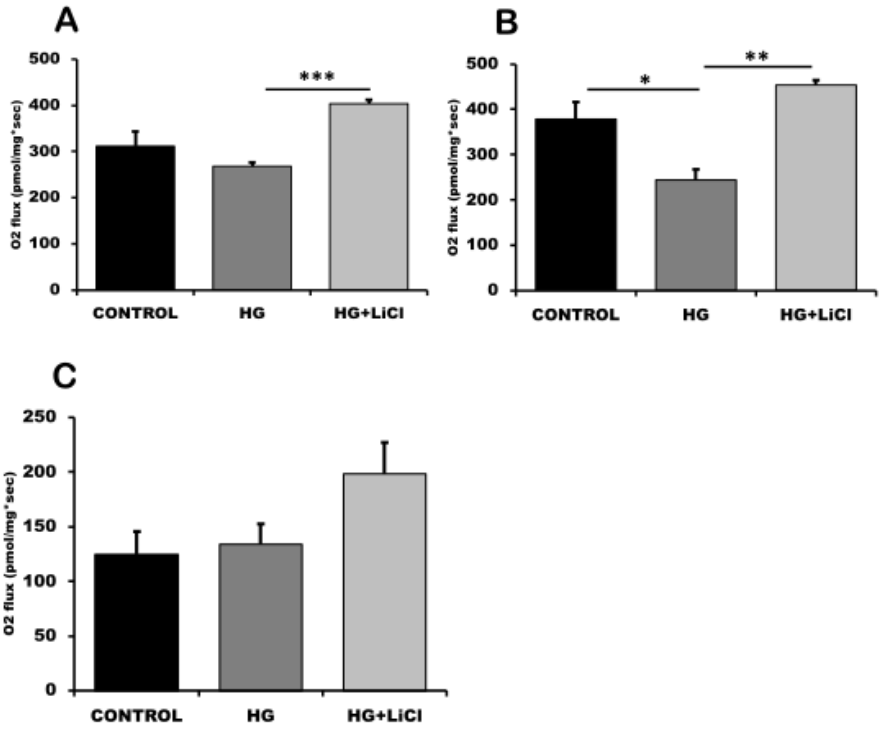

FIG 23 - Activity of Mitochondrial Complexes
A - Complex I function, **B** - Complex II function,
C - Complex IV function

States of Respiration: With the states of respiration, it was observed that there was a mild improvement in the respiration. The State 1 showed a similar decline in respiration with autophagy induction through LiCl (Figure 22A) as observed in the Routine respiration (Fig 21A) as there were no substrates given for both. But following digitonin mediated permeabilization and addition of substrates, State 3 for Glutamate-Malate (Fig 22C), State 3 respiration for complex I mediated substrates (Glutamate-Malate-Pyruvate) (Fig 22D) both showed a mild increase, suggesting a possibility for better capacity at the Complex I junction. The total OXPHOS (State 3 with both Complex I and Complex II substrates) (Fig 22E) also showed similar mild improvement in the total oxidative phosphorylation although it was not observed with Maximal State 3 respiration (Fig 22F). The Complex II mediated maximal showed significant improvement with LiCl treatment (Fig 22G) suggesting that the succinate accumulation and succinate mediated tumorigenesis can possibly be hindered by autophagy induction with LiCl too.

Activity of mitochondrial complexes: The results with the permeabilized protocol with exogenously given substrates pointed at there being a betterment in the capacity of the mitochondrial electron transport chain enzymes. We thus analysed the activities of individual mitochondrial complexes, and observed that LiCl addition improved the activity of all the three complexes assessed i.e., Complex I, II and IV (Fig 23A-C); with a significantly higher activity for Complex I and Complex II. This confirmed that when substrates were provided exogenously, it was observed that the decline in the complex activities observed in the HG condition was reversed with the autophagy induction by Rapamycin and Torin as well as with LiCl.

5.7 Is there a difference in mitochondrial function with mTOR inhibition and resultant autophagy upregulation and mitochondrial function with autophagy upregulation alone?

We observed that the mitochondrial functional improvement was more pronounced with mTOR inhibition and resultant autophagy activation and with autophagy

activation with LiCl. We thus believe that Rapamycin and Torin had a synergistic impact on the mitochondrial metabolism. We next assessed if there was any significant difference between the autophagy activation alone and between autophagy activation along with mTOR inhibition.

5.7.1 Glucose consumption and Lactate secretion:

The glucose consumption showed significant increase between mTOR inhibitors and LiCl and LiCl mediated glucose consumption was similar to that observed in HG (Fig 24A). This same trend was observed in the lactate secreted by the cells (Fig 24B). This suggests that mTOR inhibition but not autophagy activation alters the glucose uptake and lactate secretion in the cells.

5.7.2 Mitochondrial Respiration measurements:

Intact cell respiration: The measurements of parameters if intact cell respiration showed that there isn't any significant change in the respiratory parameters measured with mTOR inhibition and autophagy activation (Fig 25A, B, C, D), except for the Reserve capacity (Fig 25E) in which there was observable decline in the reserve capacity of mTOR inhibitors when compared to HG while none in LiCl when compared to HG. The coupling control ratios showed no difference between the mTOR inhibitor groups and LiCl group (Fig 25F, G, H, I).

States of Respiration: Any significant difference was not observed between the mTOR inhibitors and the LiCl treated groups for State 1 respiration (Fig 26A). But with permeabilization and addition of substrates there was significant difference between the respiration in these groups with mTOR inhibitors showing increased respiration for Complex I State 3 (Fig 26D), total OXPHOS (Fig 26E), Maximal State 3 respiration (Fig 26F) and Complex II maximal State 3 respiration (Fig 26G) as compared to the respiration with autophagy activation through LiCl.

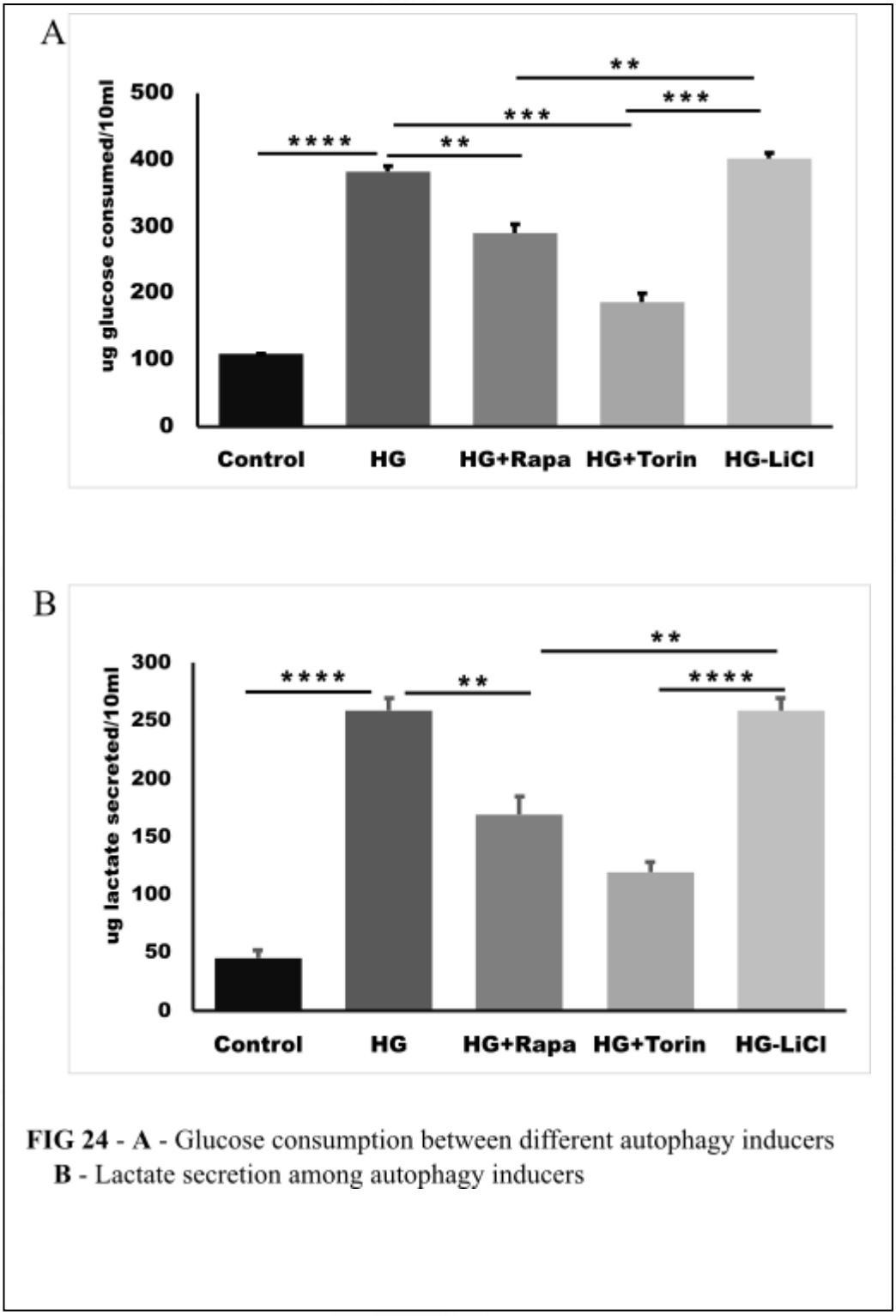

FIG 24 - **A** - Glucose consumption between different autophagy inducers
B - Lactate secretion among autophagy inducers

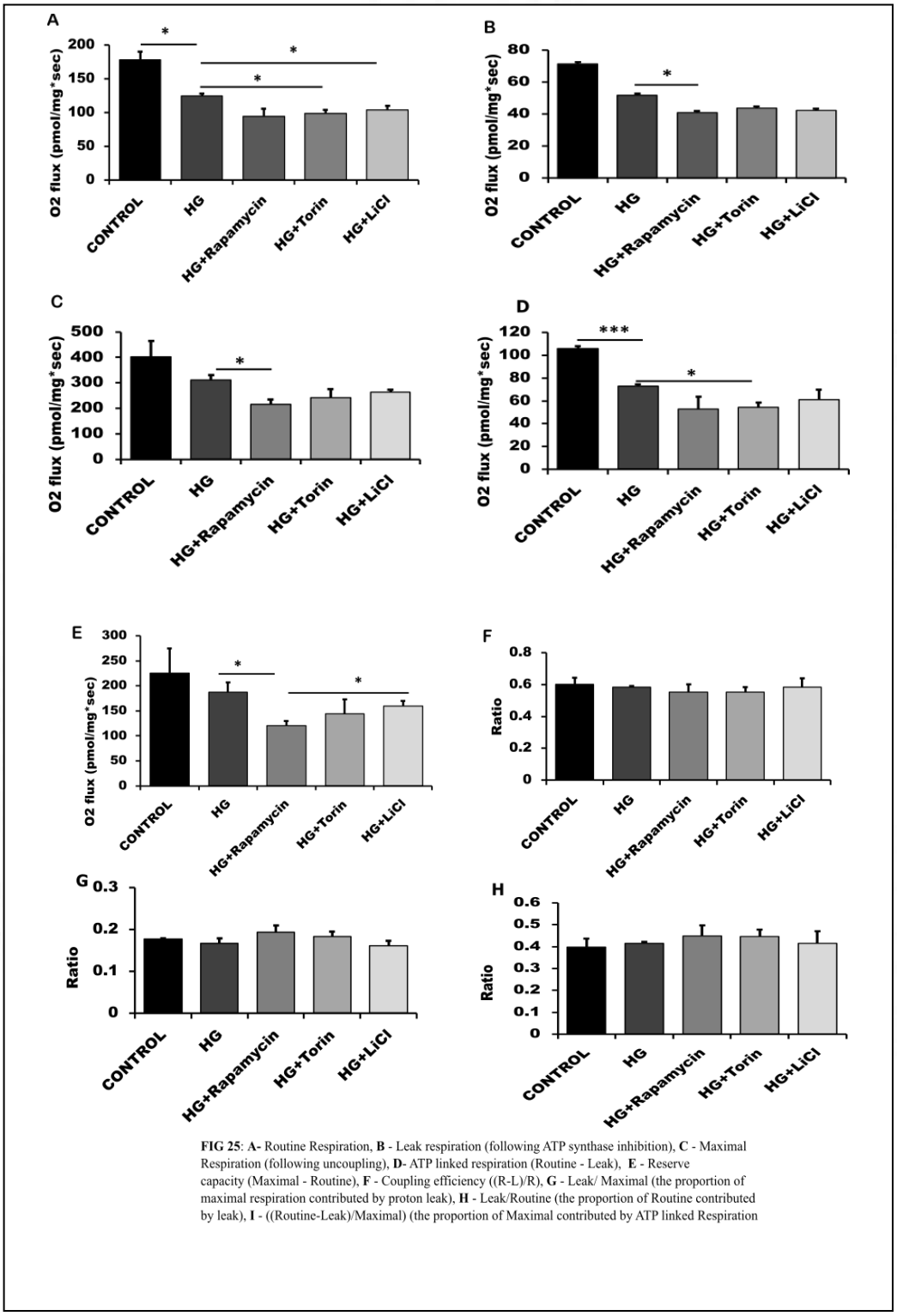

FIG 25: **A-** Routine Respiration, **B** - Leak respiration (following ATP synthase inhibition), **C** - Maximal Respiration (following uncoupling), **D**- ATP linked respiration (Routine - Leak), **E** - Reserve capacity (Maximal - Routine), **F** - Coupling efficiency ((R-L)/R), **G** - Leak/ Maximal (the proportion of maximal respiration contributed by proton leak), **H** - Leak/Routine (the proportion of Routine contributed by leak), **I** - ((Routine-Leak)/Maximal) (the proportion of Maximal contributed by ATP linked Respiration

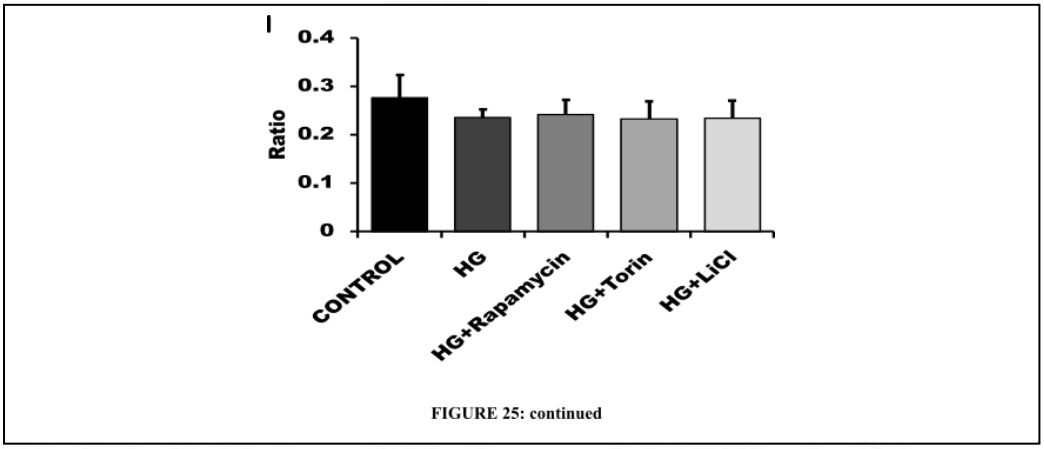

FIGURE 25: continued

Activity of mitochondrial complexes: The activity of individual complexes was assessed between the two groups and it was observed that the autophagy activation by both mTOR mediated and independent mechanism improved respiration as compared to the HG group (Fig 27A-C). There were no significant differences observed between the mTOR inhibitor and LiCl groups in all three Complexes assessed – I, II, IV.

5.8 Discussion:

It was observed that the autophagy was lowered under the HG state. The autophagy mediating the healthy mitochondrial population is relatively known and thus we expected that with the lowering of autophagy there could be decline in the mitochondrial metabolism. Our results indeed point out to that as the autophagy induction had a tendency towards the improvement of mitochondrial metabolism. We observed that the improvement was more pronounced with the autophagy activation through mTOR inhibition as compared to that with LiCl mediated autophagy activation, as mTOR has its own effects on the mitochondrial metabolism (Ramanathan and Schreiber, 2009), (Schieke et al., 2006), (Cunningham et al., 2007, p. 1), (Morita et al., 2015). Fornai et al., observed that Lithium acted as an autophagy inducer has a positive effect on metabolism by eliminating damaged mitochondria and inducing new mitochondrial biogenesis in the in vitro model for amyotrophic lateral

sclerosis (Fornai et al., 2008). Lithium has also shown to influence the metabolism by influencing mitophagy through the modulation of ROS and P38 MAPK pathways (Aminzadeh et al., 2014).

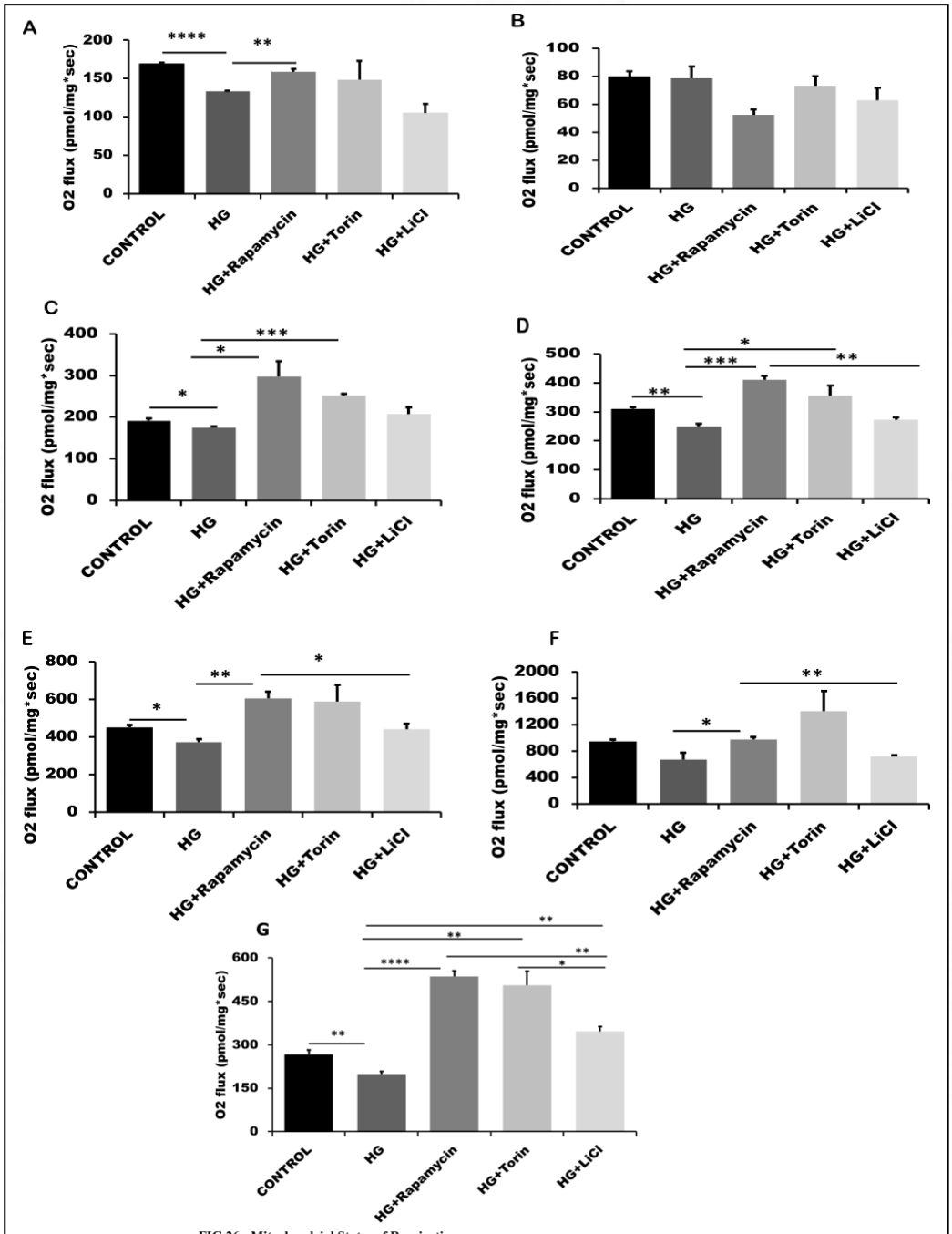

FIG 26 - Mitochondrial States of Respiration
A - State 1 respiration (Routine), **B** - State 2 respiration (following permeabilization with Digitonin, **C** - Glutamate-Malate-State 3, **D** - Complex I- State 3 (Glutamate-Malate-Pyruvate), **E** - Total oxidative phosphorylation capacity (Glutamate-Malate-Pyruvate-Succinate), **F** - Maximal State 3 respiration (following uncoupling), **G** - Complex II Maximal State 3 respiration (following inhibition of Complex I)

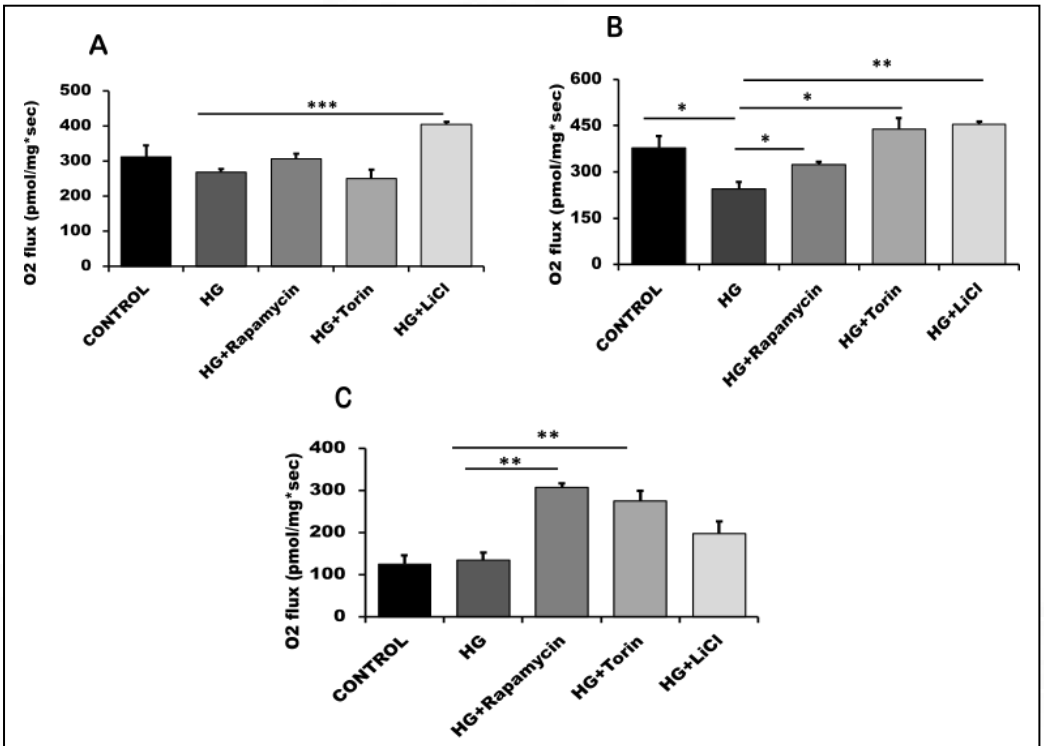

FIG 27 - Activity of Mitochondrial Complexes
A - Complex I function, **B** - Complex II function,
C - Complex IV function

The study by Johnson et. al. tested the effect of Rapamycin on the mitochondrial metabolism in the mitochondria disease (Johnson et al., 2013). they used the mice with Complex I deficiency as their model system and observed that a high dose of Rapamycin resulted in improvement in the mitochondrial function. Although they did not check the autophagy mediated contribution in the mitochondrial functional improvement, it naturally follows that there would be autophagy activation in their treated mice. Our findings correlate with their study showing improved mitochondrial efficiency with Rapamycin. Figueroa et al., observed in a chondrocyte; which formed non-transformed model system, that the autophagic decline with genetic interventions have a significant impact on mitochondrial metabolism and mitochondria showed reduced capacity with the same (López de Figueroa et al., 2015). With autophagic induction with Rapamycin and Torin, the mitochondrial function showed considerable

improvement and it also protected mitochondrial dysfunction which they induced with oligomycin treatment; suggesting that autophagy induction improved mitochondrial metabolism.

It is known that mTOR exists as aggregates at the mitochondrial membrane and are thus visualized as puncta in imaging studies. The study by Schieke et. al. has demonstrated that this mTOR can have profound effects on the mitochondrial metabolism and its inhibition changed the phosphor-proteome within the cells (Schieke et al., 2006). It thus becomes apparent that the inhibition of mTOR would have a more profound impact on the mitochondrial metabolism and our results have also shown so. Both Rapamycin and Torin have been assessed for their efficacy in cancer therapy, for used for glioblastoma, it was observed that the treatment reduced the invasive phenotype, even with a marked reduction in the expression of the stem-cell markers like nestin, Sox2, Oct4, etc. (Chandrika et al., 2017). The mTOR inhibition in glioma in yet another study reconfirmed that it affects the glioma aggressiveness; by mediating the autophagy activation and not apoptosis. This decline if further augmented by upstream regulators of mTOR like Protein Kinase B (Akt) showed a synergistic anti-tumour effect (Takeuchi et al., 2005). Although not mitochondrial metabolism was not assessed in these studies; the studies which show a metabolic implication of mTOR inhibition are numerous (Ramanathan and Schreiber, 2009), (Schieke et al., 2006), (Cunningham et al., 2007).

Another important aspect with the autophagy activation in HG condition and mitochondrial functional analysis showed that here is considerable improvement in the Complex II mediated respiration. There are reports that have shown with compensating for the defective SDH gene, there is a decline in the hypoxia like phenotype mediated by HIF1-α and an increased mitochondrial metabolism. The cells under HG when given autophagy activators show improved SDH activity; and the above study correlates with our analysis that with an improvement in the previously declined SDH activity in the glioma cells under HG through autophagy, the overall mitochondrial metabolism showed improvement.

Although not proven by us, there are numerous studies that have demonstrated that these compounds that we used as autophagy activators have potent anti-tumour effects. We thus believe that autophagy activation can potentially curb the HG mediated increased aggressiveness observed in glioma.

5.9 Conclusion:

Our hypothesis that autophagy would be declined in the HG state owing to a nutrient excess state was shown to be likely. The decline in the cellular autophagy had an impact on the mitochondrial pool within the cells making them less efficient at oxidative phosphorylation. The improved Warburg effect observed under the HG state seems likely due to the decline in autophagy mediated through the mTOR and not likely the autophagy alone; as the autophagy activation with LiCl did not change the glucose uptake and lactate secretion in the media when compared with the HG alone group. We thus conclude that the autophagy activation mediates the enhanced mitochondrial reliance.

Are the changes in mitochondrial function under hyperglycaemia mediated by mitochondrial fission?

5.10 Introduction:

Mitochondrial function is influenced by a number of internal and external inputs, one of such intracellular process that modulates mitochondrial function being the mitochondrial network. Mitochondria were once considered static organelles due to the electron microscopy and other microscopic techniques that can only visualize the end point. With the invention of high resolution and microscopes with lower capture times, it became possible to capture images in seconds, thus bringing forth for the first time the dynamic nature of the mitochondrial population within cells. Mitochondrial dynamics is the ever-changing architecture of the mitochondria due to the fission and fusion within the mitochondrial fragments based on the cellular needs. This dynamic

greatly modifies the mitochondrial behaviour and function upon exposure to metabolic activity and stimuli like stress. One such cellular stress that is known to change mitochondrial network is hyperglycaemia.

5.11 Review of Literature:

It has been well documented that HG causes more fragmentation in the mitochondrial populations (Wu et al., 2021), (Kobayashi et al., 2020), (Chen et al., 2020). The mitochondria with good quality and membrane potential tends to be fused while the ones with either defective mitochondrial complex functions or increased superoxide production or reduced mitochondrial membrane potential tend to split off from the network. With increased glucose uptake due to high glucose availability, there can be increased glucose flow through the mitochondrial TCA cycle and electron transport chain, which cause over-activity induced mitochondrial ROS generation and mitochondrial hyperpolarization (Green et al., 2004), (Brownlee, 2001), (Nishikawa et al., 2000). It is theorised that to save the cells from the detrimental effects of ROS generation, mitochondria undergo fission under HG (Diaz-Morales et al., 2016).

Mitochondrial fission is co-ordinated by multiple fission mediated factors and proteins like Dynamin related protein 1 (Drp1), Mitochondrial fission factor (Mff), mitochondrial dynamics protein of 49 KDa and 51 KDa (MD49, MD51), etc. Drp1 is one of the final proteins to be recruited to and bring about the mitochondrial fission. Once activated through the phosphorylation of Serine 616 residue, Drp1 localizes to the mitochondrial fragment with either reduced membrane potential or with other co-factors suggesting mitochondrial damage, recruits other Drp1 moieties thus forming a ring around the damaged mitochondrial fragment and constricting the mitochondria ultimately breaking it off from the network (Ichishita et al., 2008).

Mitochondrial dynamics has shown to heavily impact the mitochondrial function. When mitochondria are in a network, the sharing of intermediates of the TCA cycle becomes possible between the subunits, making fused mitochondria adept (Twig et al., 2008). The pharmacological inhibition of Drp1 activation phosphorylation is mediated by M-divi which reduces the phosphorylation at serine 616 thus making the Drp1 inactive and accumulating it in the cytoplasm without letting it get recruited to

the mitochondria for completion of fission. Without the recruitment of Drp1 to the mitochondria, the mitochondrial fission cannot be accomplished as depicted in Fig J.

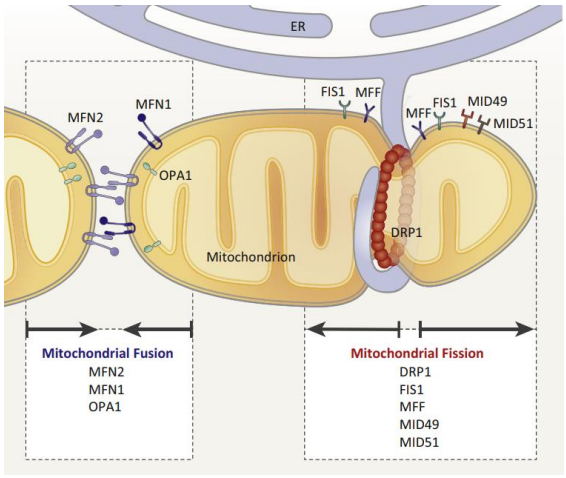

Fig J: Mitochondrial Fission and fusion proteins. Drp1 associated with the mitochondrial membrane and constricts the mitochondrial unit with damaged mitochondrial fragments until it is siphoned off

(Sebastián et al., 2017)

This holds true even when the other mitochondrial fission proteins are active, as without the Drp1 mediated pinching-off of the fragments, mitochondrial fission cannot be achieved.

As the mitochondrial function is dependent upon the mitochondrial architecture, the changes in the fission and fusion processes can impact the mitochondrial function, with fused mitochondria showing better performance under stressed conditions. The HG state has been previously shown to increase fission. We thus hypothesise that HG could be mediating mitochondrial fission even in glioma and this could be a basis of the decline in mitochondrial respiration observed.

5.12 Materials and Methods:

5.12.1 Reagents:

All cell culture reagents were similar to those mentioned in Chapter 2 while all substrates and inhibitors used for mitochondrial functional experiments were same as

that mentioned in Chapter 4. M-divi1 was purchased from Sigma (Sigma Aldrich, MO, USA). Tetramethyl rhodamine ethyl ester (TMRE) dye was purchased from GBiosciences (MO, USA) which localizes into the mitochondria based on the membrane potential and fluoresces red with excitation and emission at 550 nm and 575 nm respectively and Anti-phospho Drp1 with phosphorylation at serine 616 was purchased from Cell Signalling Technology (MA, USA).

5.12.2 Cell Culture and Maintenance:

Cell culture and maintenance techniques were similar to that mentioned in Chapter 4.

5.12.2.1 Reagents used for Cell culture

All reagents used in cell culture mentioned in chapter 3 were used along with HG media containing 5µM M-divi 1 for 72 h was used as a third treatment group for the following experiments.

5.12.3 Mitochondrial fragmentation:

The cells seeded on chambered coverslips from Ibidi (Munich, Germany) and were given Control or HG treatment with 50% confluence for 72h. The mitochondria were stained with membrane permeable TMRE dye that stained all mitochondria with healthy membrane potential at the recommended concentration by the manufacturer while the nuclear stain was achieved with Hoechst at 1:1000 dilution. The cells were washed with PBS to remove excess stain and incubated in the mitochondrial membrane potential buffer for imaging and imaged using fluorescence microscope (Olympus, IX 51, Tokyo, Japan).

5.12.4 Immunoblotting:

Immunoblotting was performed using the same treatment and procedures as mentioned in Chapter 3. The antibody against Drp1(phosphor-Ser616) was used to determine activation phosphorylation Drp1 and normalized with β-actin. The densitometric measurements were performed using ImageJ software.

5.12.5 Determination of M-divi 1 concentration:

M-divi 1 effective concentration was determined using immunoblotting with different concentrations of M-divi 1 and assessing the Drp1(phosphor-ser616) and by MTT measurements to determine cytotoxicity.

5.12.6 Mitochondrial Respiration measurements:

All mitochondrial respiration methods were same as that mentioned in Chapter 4.

5.13 Statistical analysis:

All statistics were performed as mentioned in Chapter 2.

5.14 Results:

5.14.1 Mitochondrial fragmentation:

The mitochondria were analysed following fluorescent staining and it was observed that the control group had more networked mitochondria than the HG group which showed more fragmentation (Fig 28D).

5.14.2 Immunoblotting:

Immunoblotting with phosphor-Drp1 (Ser616) showed marked increase in the HG group as compared to the control (Fig 28A) suggesting increased activation of Drp1 and thus a concomitant recruitment onto the mitochondria that could result in increased fragmentation.

5.14.3 M-divi concentration:

Following the cytotoxicity assay with MTT mediated colourimetric detection of tetrazolium salt formation, it was observed that 2.5 and 5 µM M-divi 1 resulted in low cell death while any increase from this caused high cell death (Fig 28C). The immunoblotting showed that at 5µM concentration there was reduced expression of phosphor-Drp (ser616) expression (Fig 28B) suggesting that at this concentration there was sufficient M-divi effect and thus 5 µM concentration was utilized for all further experiments.

5.14.4 Mitochondrial Respiration measurements:

The mitochondrial respiration parameters measured were intact cell respiration and substrate mediated states of respiration.

Intact cell respiration: All respiratory parameters measured within the Control, HG and HG with M-divi show a trend towards a decline in the respiration with mitochondrial fission inhibition with M-divi 1 mediated phosphor-Drp1 suppression. The Routine respiration showed decline (Figure 29 A) with a significantly lower leak respiration (Figure 29 B) suggesting a lowering of overall respiration. The maximal respiration (Figure 29 C), ATP linked respiration (Figure 29D) and Reserve Capacity (Figure 29E) also showed steady decline with mitochondrial fission suppression. The coupling control ratios were observed to be similar to the ones seen in Control and HG (Figure 29 F-I) suggesting that although the declined the mitochondria may not have any damage associated.

States of Respiration: The State 1 respiration showed similar pattern with the Routine respiration observed in the bioenergetics protocol (Figure 30A) as no substrates were added but upon permeabilization with digitonin and addition of substrates, the states of respiration showed improvement in the M-divi group. State 3 for Glutamate-Malate (Fig 30C), State 3 respiration for complex I mediated substrates (Glutamate-Malate-Pyruvate) (Fig 30D) both showed improvement suggesting improvement in the respiration at the Complex I junction. The total OXPHOS (State 3 with both Complex I and Complex II substrates) (Fig 30E) showed significant improvement in the at the total oxidative electron transport chain capacity also seen with Maximal State 3 respiration (Fig 30F) which although not significant showed a marked trend towards improvement with M-divi 1 group. The Complex II mediated maximal showed significant improvement with M-divi 1 supplementation (Fig 30G) suggesting that the succinate accumulation and succinate mediated tumorigenesis would be hindered.

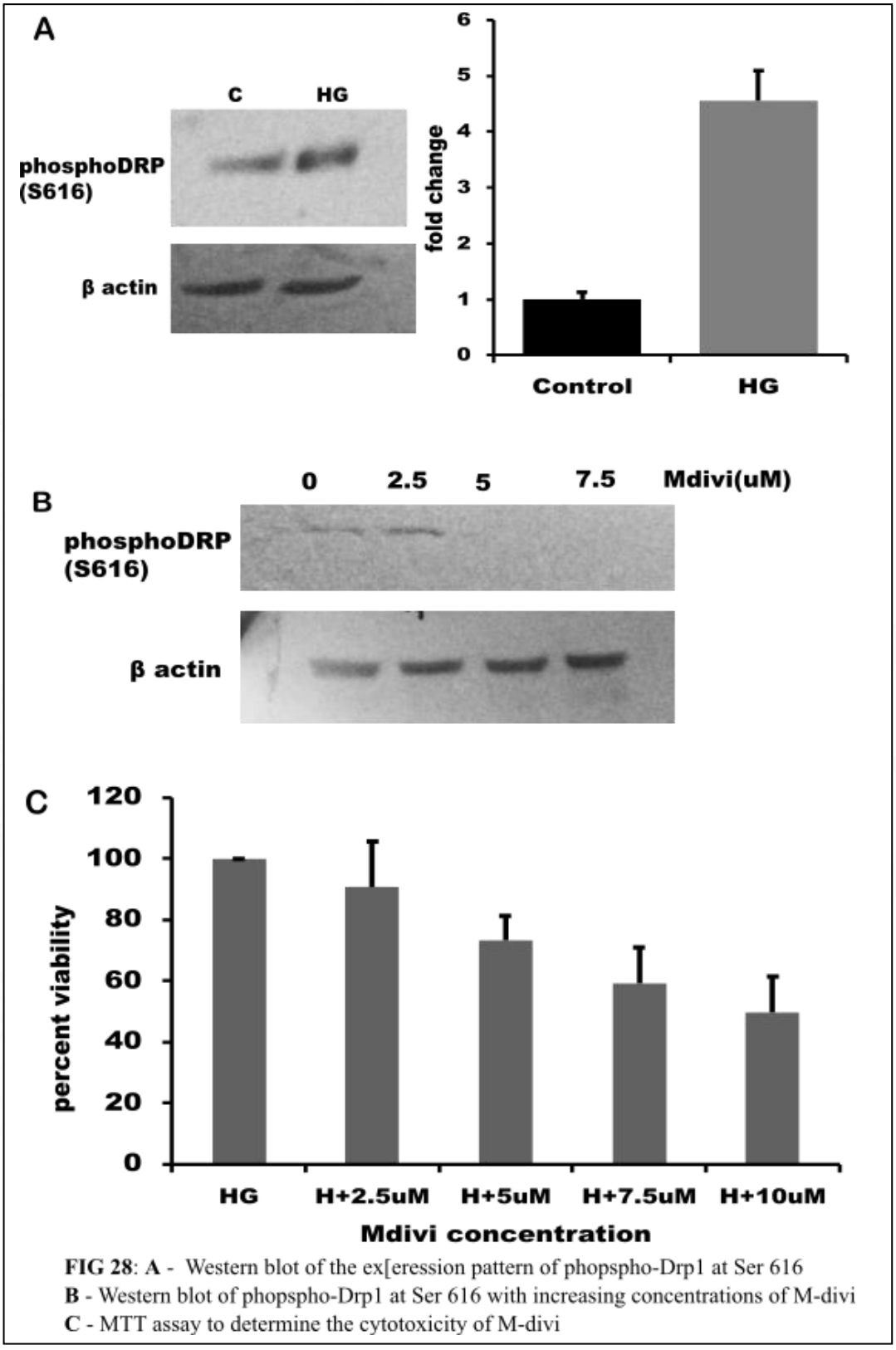

FIG 28: **A** - Western blot of the ex[eression pattern of phopspho-Drp1 at Ser 616
B - Western blot of phopspho-Drp1 at Ser 616 with increasing concentrations of M-divi
C - MTT assay to determine the cytotoxicity of M-divi

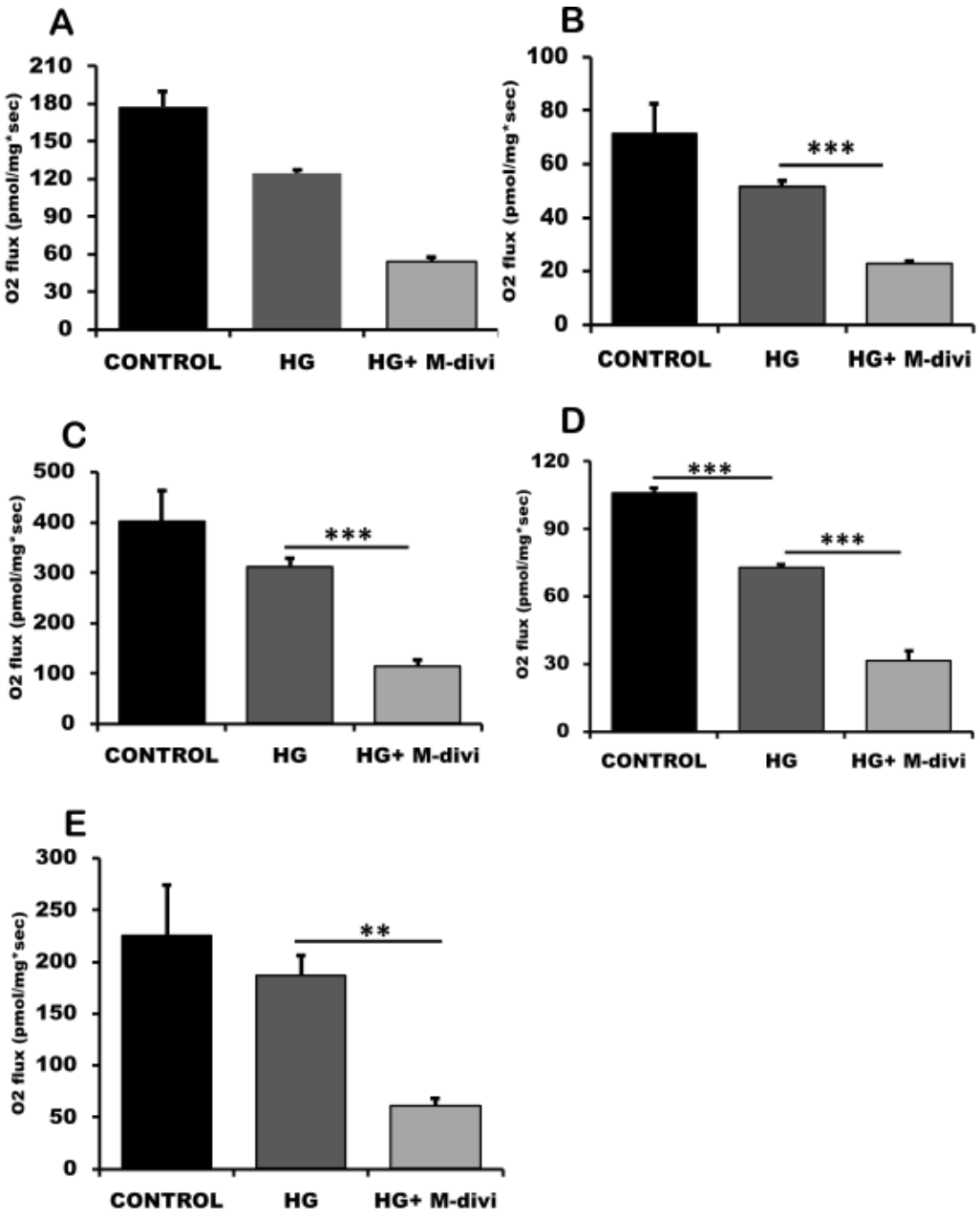

FIG 29: **A-** Routine Respiration, **B** - Leak respiration (following ATP synthase inhibition), **C** - Maximal Respiration (following uncoupling), **D**- ATP linked respiration (Routine - Leak), **E** - Reserve capacity (Maximal - Routine), **F** - Coupling efficiency ((R-L)/R), **G** - Leak/ Maximal (the proportion of maximal respiration contributed by proton leak), **H** - Leak/Routine (the proportion of Routine contributed by leak), **I** - ((Routine-Leak)/Maximal) (the proportion of Maximal contributed by ATP linked Respiration

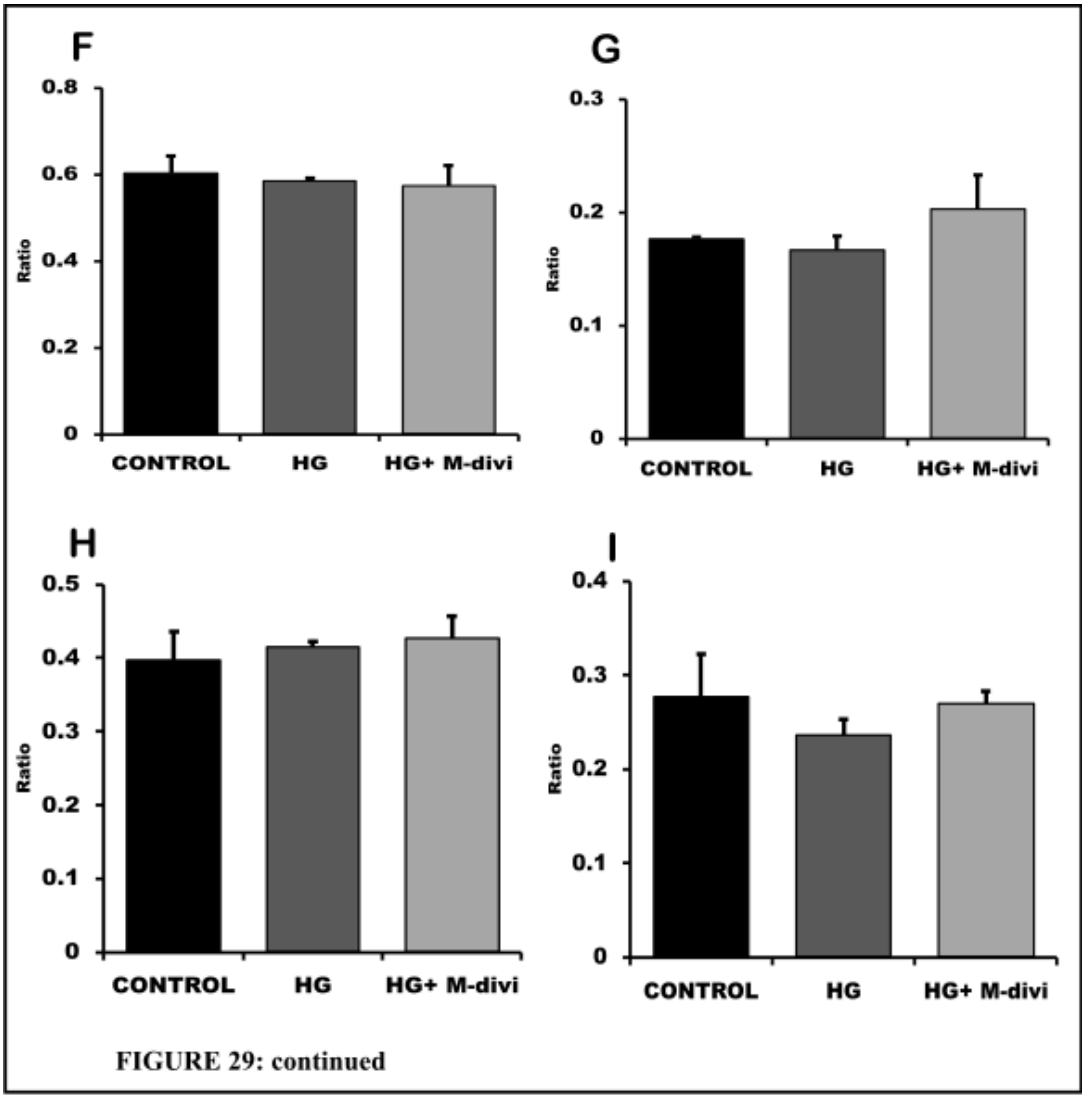

FIGURE 29: continued

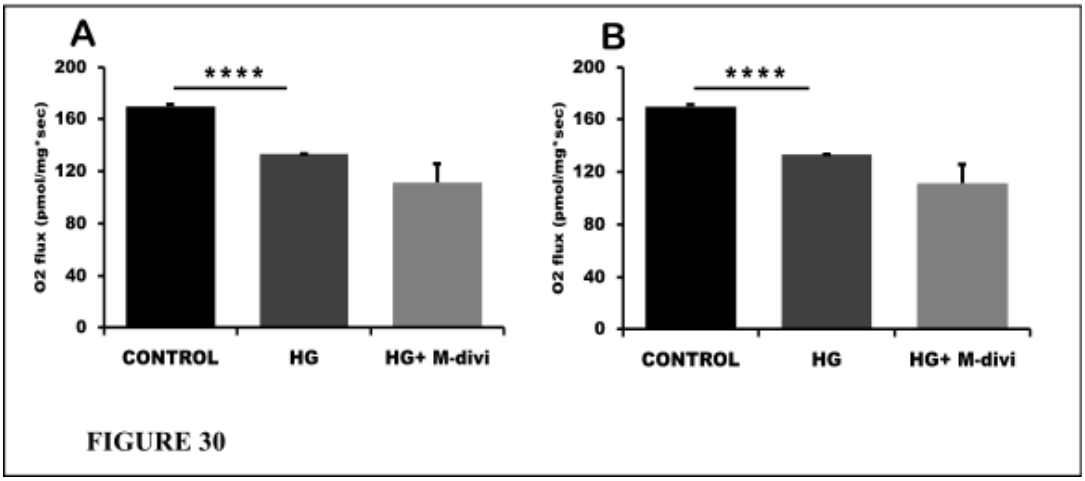

FIGURE 30

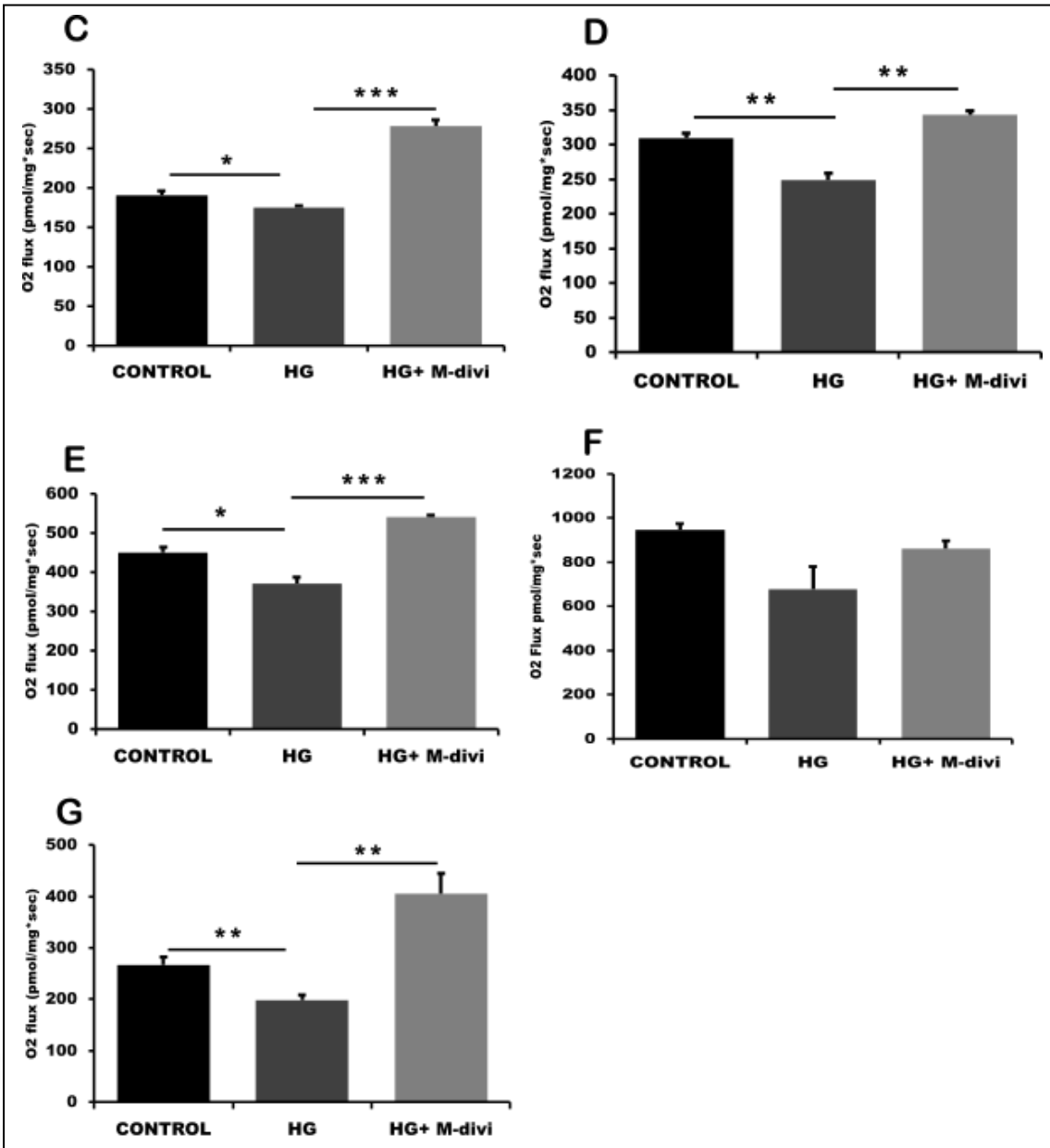

FIG 30 - Mitochondrial States of Respiration

A - State 1 respiration (Routine), **B** - State 2 respiration (following permeabilization with Digitonin, **C** - Glutamate-Malate-State 3, **D** - Complex I- State 3 (Glutamate-Malate-Pyruvate), **E** - Total oxidative phosphorylation capacity (Glutamate-Malate-Pyruvate-Succinate), **F** - Maximal State 3 respiration (following uncoupling), **G** - Complex II Maximal State 3 respiration (following inhibition of Complex I)

5.15 Discussion:

It was observed that the mitochondrial fission a consequence of the HG treatment and the expected mitochondrial fission also had an effect on the mitochondrial metabolism. The mitochondrial fission was inhibited through Drp1 phosphorylation inhibition; thus, the mitochondrial network was forcefully retained. We observed that the mitochondrial network maintenance through fission inhibition had reduced intact cell respiration and reduced bioenergetics. This correlated with the previous studies on mitochondrial fission inhibition and mitochondrial functional analysis (Dai et al., 2020), (Ruiz et al., 2018). This could be due to the reduction of available metabolites (although it was expected that the fused state of the mitochondria would make better available the metabolic intermediates). The permeabilised protocol showed that the mitochondrial electron transport capacity improved with the inhibition of mitochondrial fission, suggesting that there was improved capacity of the mitochondria. It was intriguing to observe that the results were similar to those obtained following autophagy induction.

With analysing the literature it was found that the inhibitor used in our study had a direct effect on the mitochondrial electron transport chain complexes (Bordt et al., 2017). The Complex I inhibition is observed with its use. There are also reports this suggest that it can have a modulation of cellular autophagy due to affecting some upstream regulators of autophagy which are as of yet not conclusively identified (Aishwarya et al., 2020). Thus, the effects that were observed could be due to these pleiotropic effects and not necessarily due to the inhibition of mitochondrial fission.

5.16 Conclusion:

The mitochondrial fission when blocked under the HG condition showed an improvement in the mitochondrial electron transport chain capacity. But the methodology utilized for mitochondrial fission was with the use of pharmacological inhibitor M-divi 1.

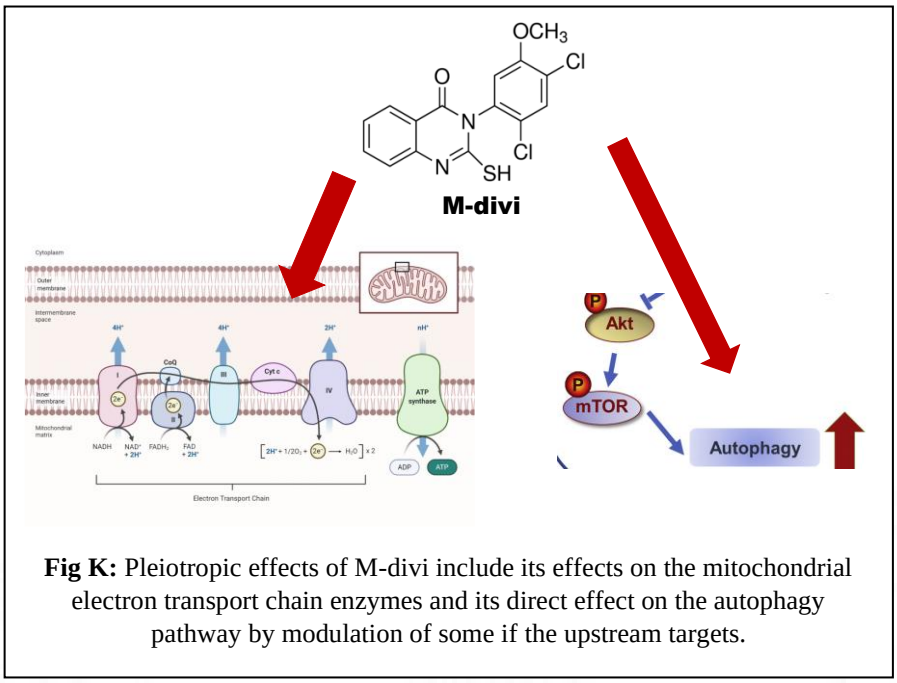

Fig K: Pleiotropic effects of M-divi include its effects on the mitochondrial electron transport chain enzymes and its direct effect on the autophagy pathway by modulation of some if the upstream targets.

This molecule has shown pleiotropic effects which could be confounding variables in the analysis as depicted in Fig K. The M-divi 1 mediated mitochondrial fission inhibition formed an inefficient model for the present study, and thus no conclusive inference could be made with respect to the inhibition of mitochondrial fission under hyperglycaemia and its impact on mitochondrial metabolism in glioma cells.

Does Nitric Oxide Cause Hyperglycaemia Mediated Changes in the Mitochondrial Function?

5.17 Introduction:

There are many common denominators among cancer and metabolic syndrome (Bredt, 1999). One of the factors that has been shown to be critically associated in both is Nitric Oxide (NO). Nitric oxide mediated signalling alterations have been time and again reported under hyperglycaemia, although mostly in the vascular and endothelial cells. There are reports of compromised cellular bioavailability of NO in tissues under diabetic conditions. NO has proven Complex IV reversible inhibitor and thus affects

mitochondrial metabolism. NO has also been shown to be involved in tumour progression under certain conditions. It thus seemed possible that the two effects that were observed with regard to mitochondrial metabolism and induction of tumour aggressiveness could be regulated by NO production under HG condition.

5.18 Review of Literature:

Nitric oxide is an endogenously produced gaseous molecule that plays a role as a signalling agent. It has a very short half-life of 0.1 to 2 sec, has reactivity towards metals and metal co-factors of enzymes. Being highly diffusible, it can have effects on surrounding cells and tissues even with the extremely short half-life (Thomas, 2015). Based on the time of release and the concentration available, in cancer cells, NO can have dual effects as both a tumour initiator and as an anti-tumour agent inducing apoptosis and reducing the invasive capacity in transformed cells (Korde Choudhari et al., 2013).

NO affects cellular metabolism by its direct interaction with the complexes of the electron transport chain enzymes and indirectly by its effects on the mitochondrial biogenesis regulation. Depending on the duration of exposure, NO can have an inhibitory effect on the mitochondria at Complex I (Brown and Borutaite, 2004), Complex III (Cadenas, 2004), (Poderoso et al., 1996) and Complex IV (Brown and Cooper, 1994), (Cleeter et al., 1994). The Complex IV is first affected. Complex IV is the site of terminal electron acceptor and uses this to reduce molecular oxygen to H_2O. It is also involved in generation of the proton gradient across the mitochondrial membrane that drive the generation of ATP by Complex V. NO has a structural similarity to O_2 and thus competitively binds to Complex IV and inhibit its activity.

Endogenously NO can be produced by any of the three forms of nitric oxide syntheses; inducible NOS (iNOS), neuronal NOS (nNOS) and endothelial NOS (eNOS) from arginine as the substrate. L-NAME (N(G) nitro-L-arginine methyl ester) is a general nitric oxide inhibitor and blocks all three forms if nitric oxide synthases as depicted in Fig L. It has been shown that when any specific isoform of NOS is blocked either pharmacologically or by RNA interference experiments, the other isoforms of NOS can take over and thus there may not be any reduction of total NO generation, thus L-NAME was used in all experiments.

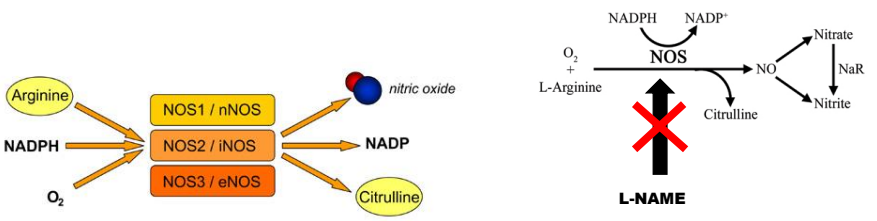

Fig L: Cellular Nitric Oxide is produced by three isoforms of Nitric Oxide Synthases and L-NAME is a generic suppressor that blocks NO generation from all three isoforms.

Nitric oxide generation has been demonstrated under the HG condition and there are also multiple studies that have proven a decline in mitochondrial functional capacity with NO. We thus hypothesize that the glioma cells under the HG condition produce NO and this could be the mechanism by which the mitochondrial functional decline is observed under HG state.

5.19 Materials and Methods:

5.19.1 Reagents:

All cell culture reagents were similar to those mentioned in Chapter 2 while all substrates and inhibitors used for mitochondrial functional experiments were same as that mentioned in Chapter 4. L-NAME was purchased from Cayman Chemicals (MI, USA). Sodium Nitrate was obtained from Sigma (Sigma Aldrich, MO, USA) while DAF-FM fluorescent dye was obtained from Thermo (ThermoFisher Scientific, MA, USA).

5.19.2 Cell Culture and Maintenance:

The cell culture and maintenance techniques were similar to that mentioned in Chapter 4.

5.19.2.1 Reagents used for Cell culture

All reagents used in cell culture were same as mentioned in chapter 3 along with HG media containing 6 mM L-NAME for 72 h as a third treatment group for nitric oxide inhibition; while as a nitric oxide donor, 200 µM Sodium Nitrate ($NaNO_3$) along with L-NAME in the high glucose media was given for the following experiments.

5.19.3 Determination of L-NAME concentration:

L-NAME effective concentration was determined using MTT measurements to determine cytotoxicity.

5.19.4 Glucose consumption and Lactate secretion:

The methodology was same as that mentioned in Chapter 4.

5.19.5 Mitochondrial Respiration measurements:

All mitochondrial respiration methods were same as that mentioned in Chapter 4.

5.20 Statistical analysis:

Statistical assessments were performed as mentioned in Chapter 2.

5.21 Results:

5.21.1 Determination of Nitric Oxide generation:

Cells were cultured at same density and upon reaching 80% confluence, the cells were given control or HG treatment. As NO is a gas with extremely low half-life, we analysed the NO generation at 6 h and 12 h post treatment. The cells were incubated with DAF-FM stain dissolved at the manufacturer's recommendations in the respective media for 30 min. The cells were washed in PBS and imaged using Olympus IX 51 fluorescent microscope (Tokyo, Japan).

5.21.2 Determining L-NAME concentration:

Following the cytotoxicity assay with MTT mediated colourimetric detection of tetrazolium salt formation, it was observed that 6mM L-NAME resulted in low cell death while any increase from this caused high cell death (Fig 31B). With this concentration given under both HG and control conditions, it was observed that under HG the total cell viability dropped closer to the control while under the Control with L-NAME the viability was minimally reduced (Fig 31C). Thus, 6 mM concentration was utilized for all further experiments.

5.21.3 Glucose consumption and Lactate secretion:

The glucose concentration in the L-NAME containing group showed a marked decline as compared to the HG group. Although the glucose consumption and Lactate secreted were not close to that observed in the Control group, there was a significant decline in these values when NO was blocked under HG condition (Fig 32 A-B).

5.21.4 Mitochondrial Respiration measurements:

Intact cell respiration: All respiratory parameters measured within the Control, HG and HG with L-NAME showed there was no change in respiration with inhibition of NO production with L-NAME as observed in the values for Routine respiration (Fig 33A), leak respiration (Fig 33B), maximal respiration (Fig 33C), ATP linked respiration (Fig 33D) and Reserve Capacity (Fig 33E). The coupling control ratios were also observed to be similar to the ones seen in Control and HG (Figure 33F-I).

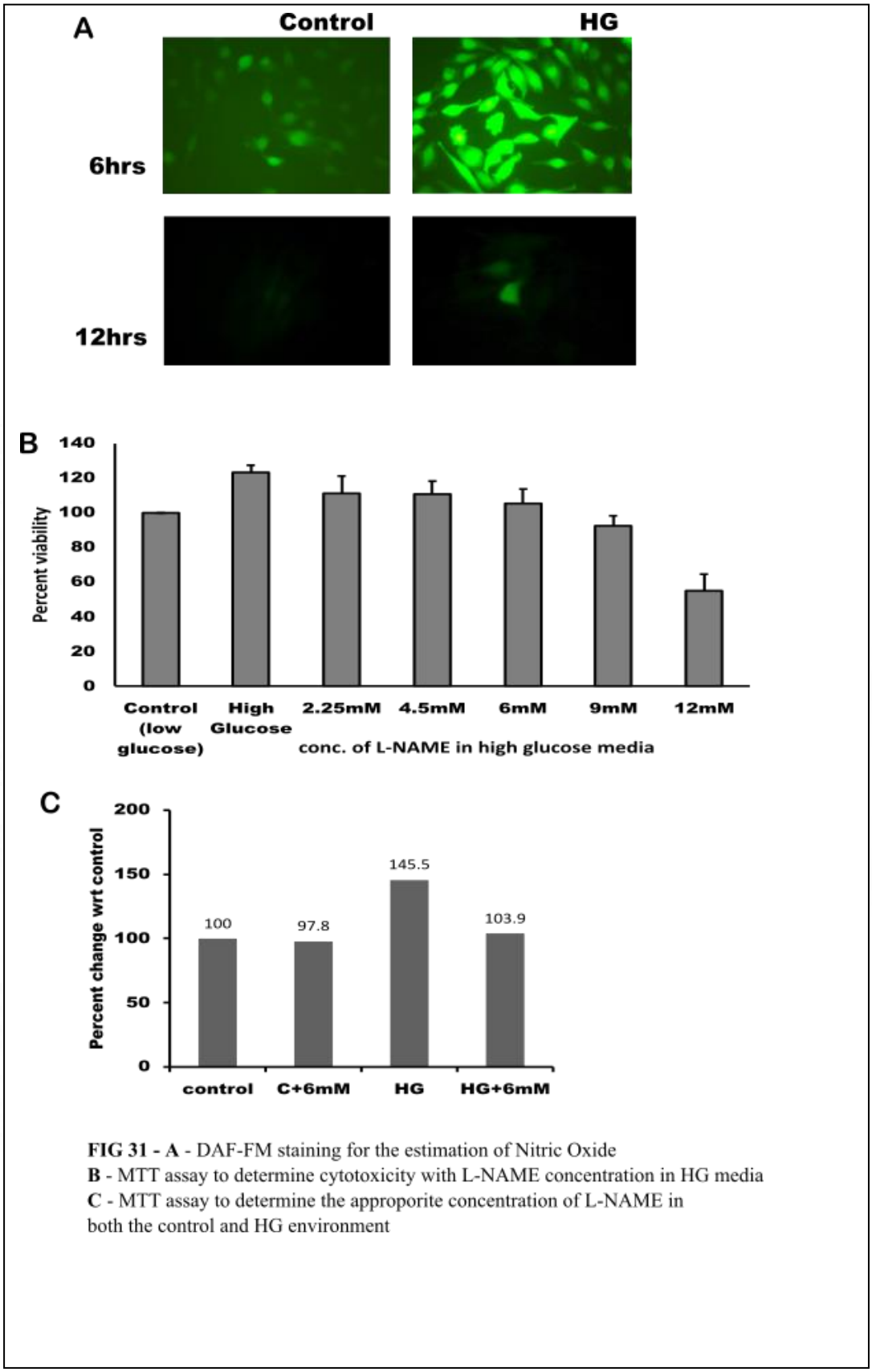

FIG 31 - A - DAF-FM staining for the estimation of Nitric Oxide
B - MTT assay to determine cytotoxicity with L-NAME concentration in HG media
C - MTT assay to determine the approporite concentration of L-NAME in both the control and HG environment

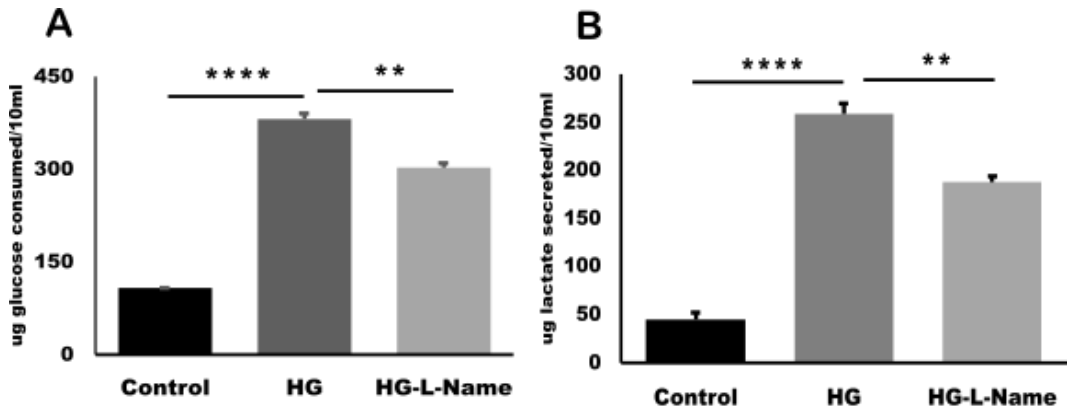

FIG 32 - A - Glucose Consumption, **B** - Lactate secretion

States of Respiration: The State 1 respiration showed similar pattern with the Routine respiration observed in the bioenergetics protocol (Figure 34A) as no substrates were added but upon permeabilization with digitonin and addition of substrates, the states of respiration showed a trend towards improvement in the L-NAME group. State 3 for Glutamate-Malate (Fig 34C), State 3 respiration for complex I mediated substrates (Glutamate-Malate-Pyruvate) (Fig 34D) both showed some betterment in respiration suggesting a potential improvement in the respiration at the Complex I junction. The total OXPHOS (State 3 with both Complex I and Complex II substrates) (Fig 34E) showed mild improvement in the total oxidative electron transport chain capacity also observed with Maximal State 3 respiration (Fig 34F) which although not significant showed a trend towards improvement. The Complex II mediated maximal showed significant improvement with L-NAME supplementation (Fig 34G) suggesting that the succinate accumulation and succinate mediated tumorigenesis can possibly be hindered.

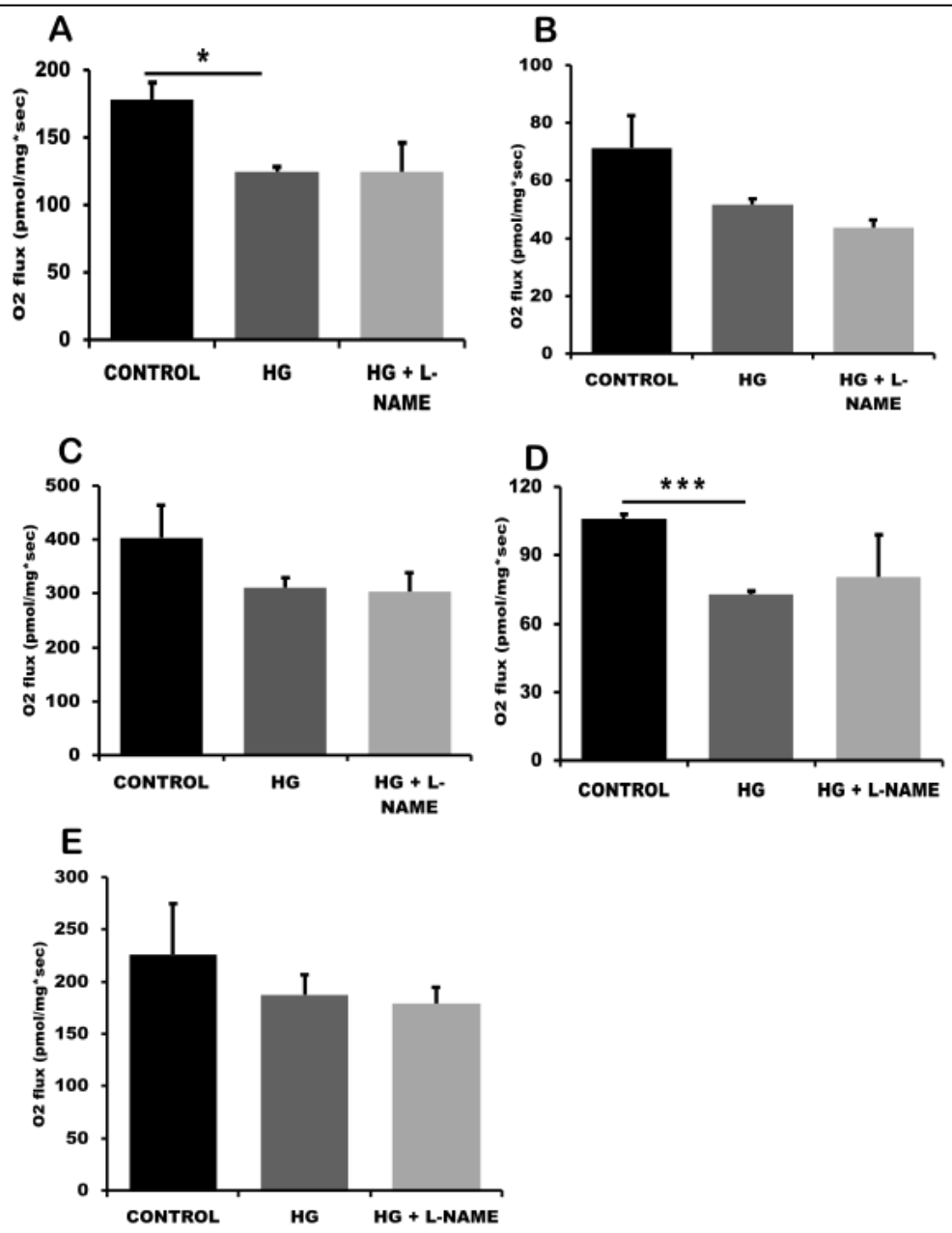

FIG 33: **A-** Routine Respiration, **B** - Leak respiration (following ATP synthase inhibition), **C** - Maximal Respiration (following uncoupling), **D**- ATP linked respiration (Routine - Leak), **E** - Reserve capacity (Maximal - Routine), **F** - Coupling efficiency ((R-L)/R), **G** - Leak/ Maximal (the proportion of maximal respiration contributed by proton leak), **H** - Leak/Routine (the proportion of Routine contributed by leak), **I** - ((Routine-Leak)/Maximal) (the proportion of Maximal contributed by ATP linked Respiration

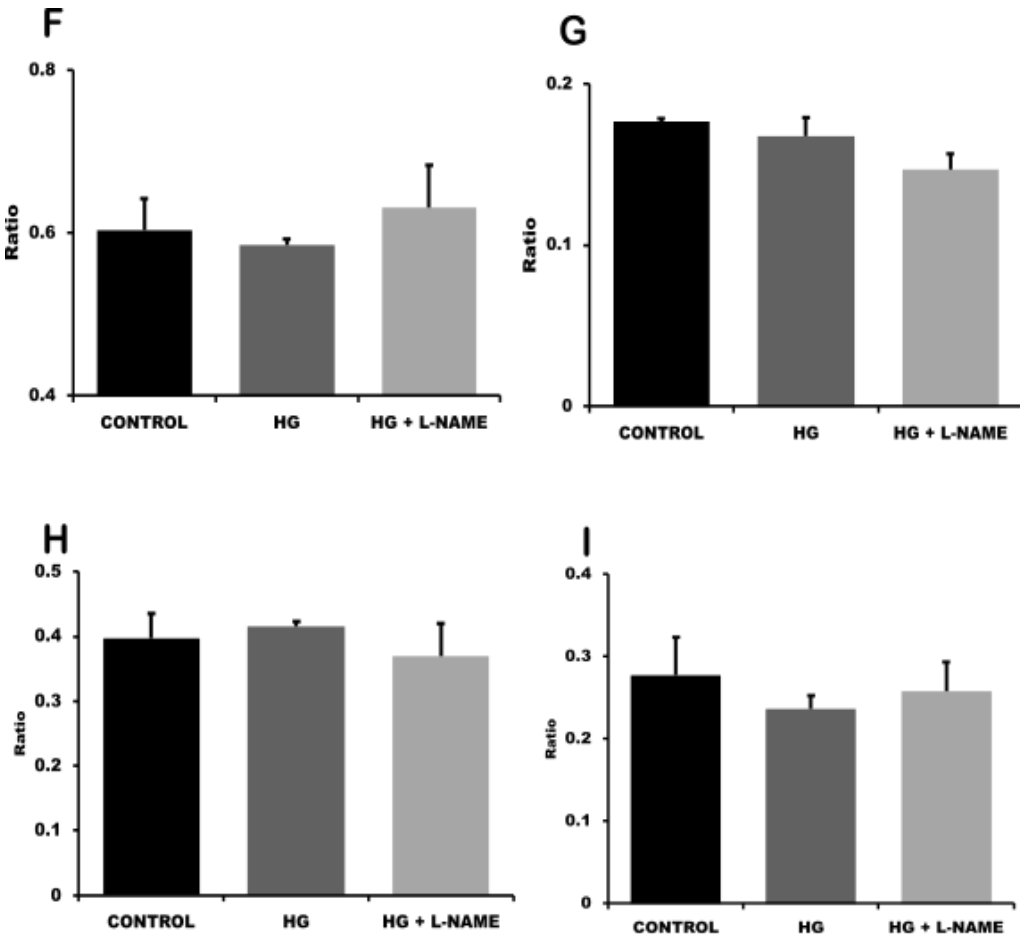

FIGURE 33: continued

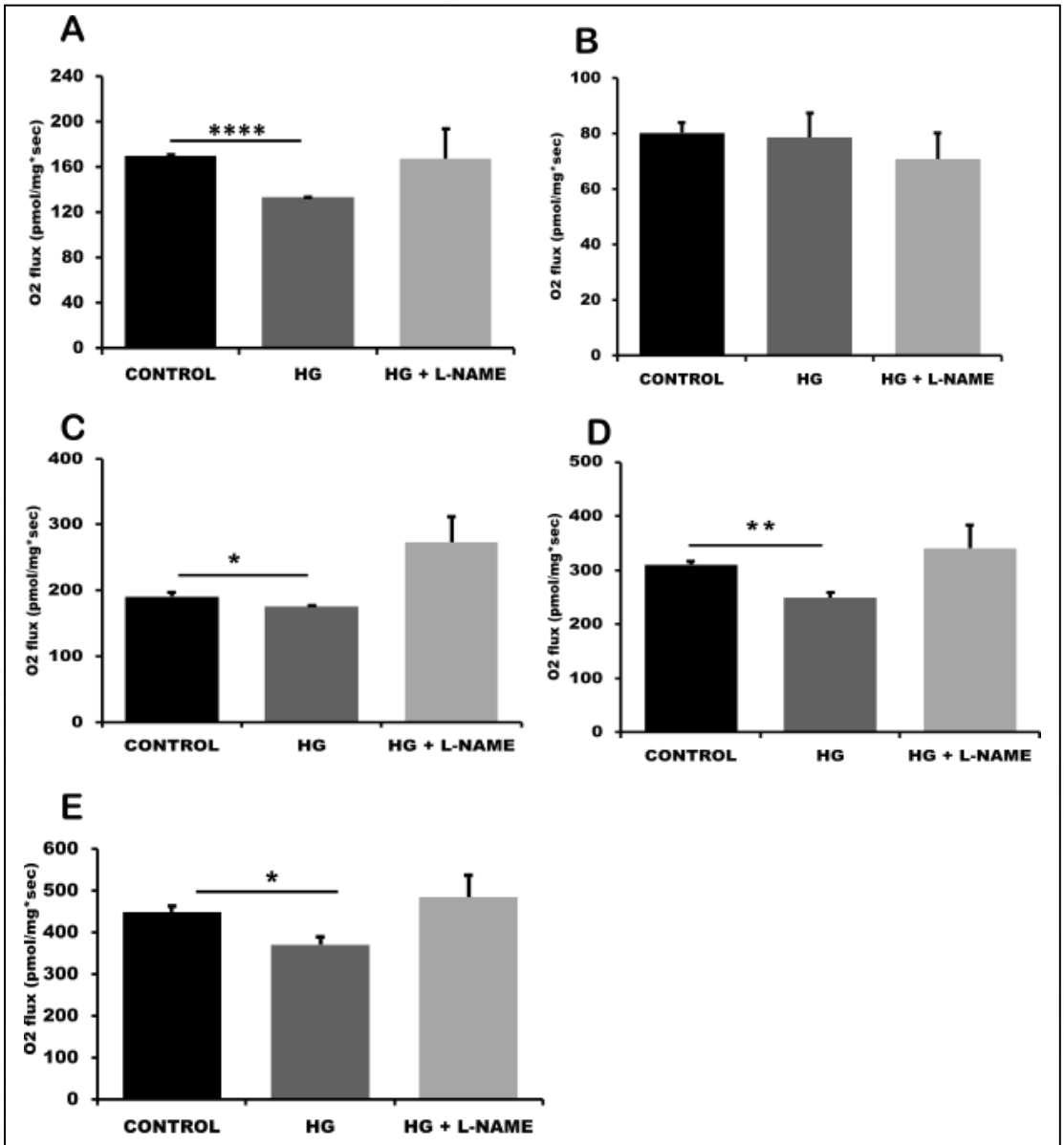

FIG 34 - Mitochondrial States of Respiration

A - State 1 respiration (Routine), **B** - State 2 respiration (following permeabilization with Digitonin, **C** - Glutamate-Malate-State 3, **D** - Complex I- State 3 (Glutamate-Malate-Pyruvate), **E** - Total oxidative phosphorylation capacity (Glutamate-Malate-Pyruvate-Succinate), **F** - Maximal State 3 respiration (following uncoupling), **G** - Complex II Maximal State 3 respiration (following inhibition of Complex I)

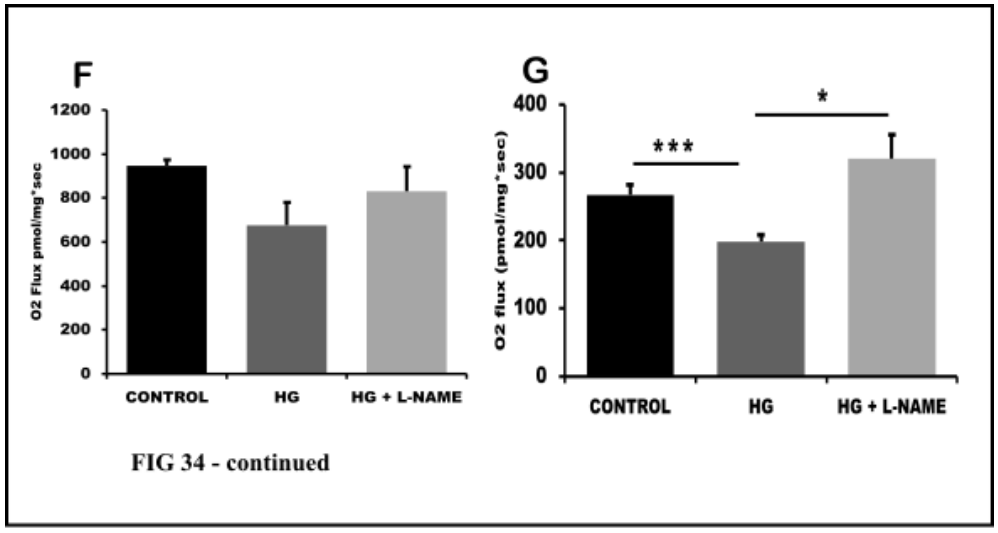

FIG 34 - continued

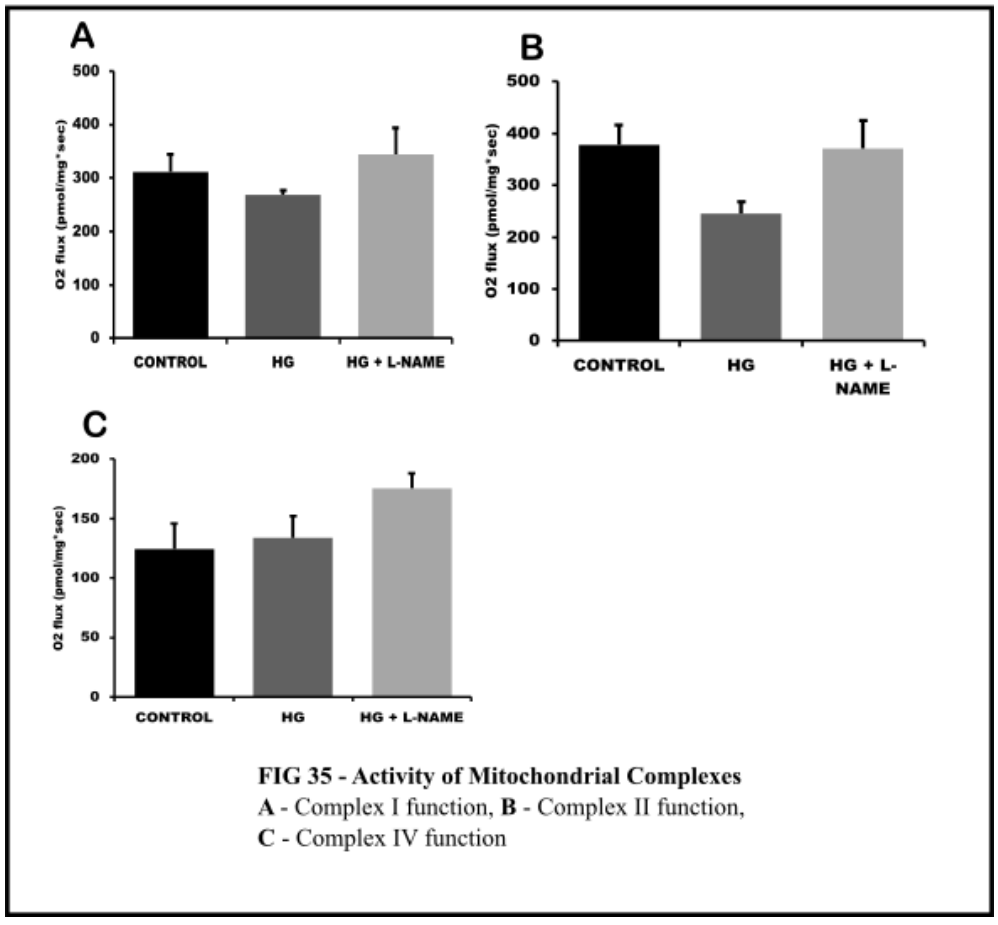

FIG 35 - Activity of Mitochondrial Complexes
A - Complex I function, **B** - Complex II function,
C - Complex IV function

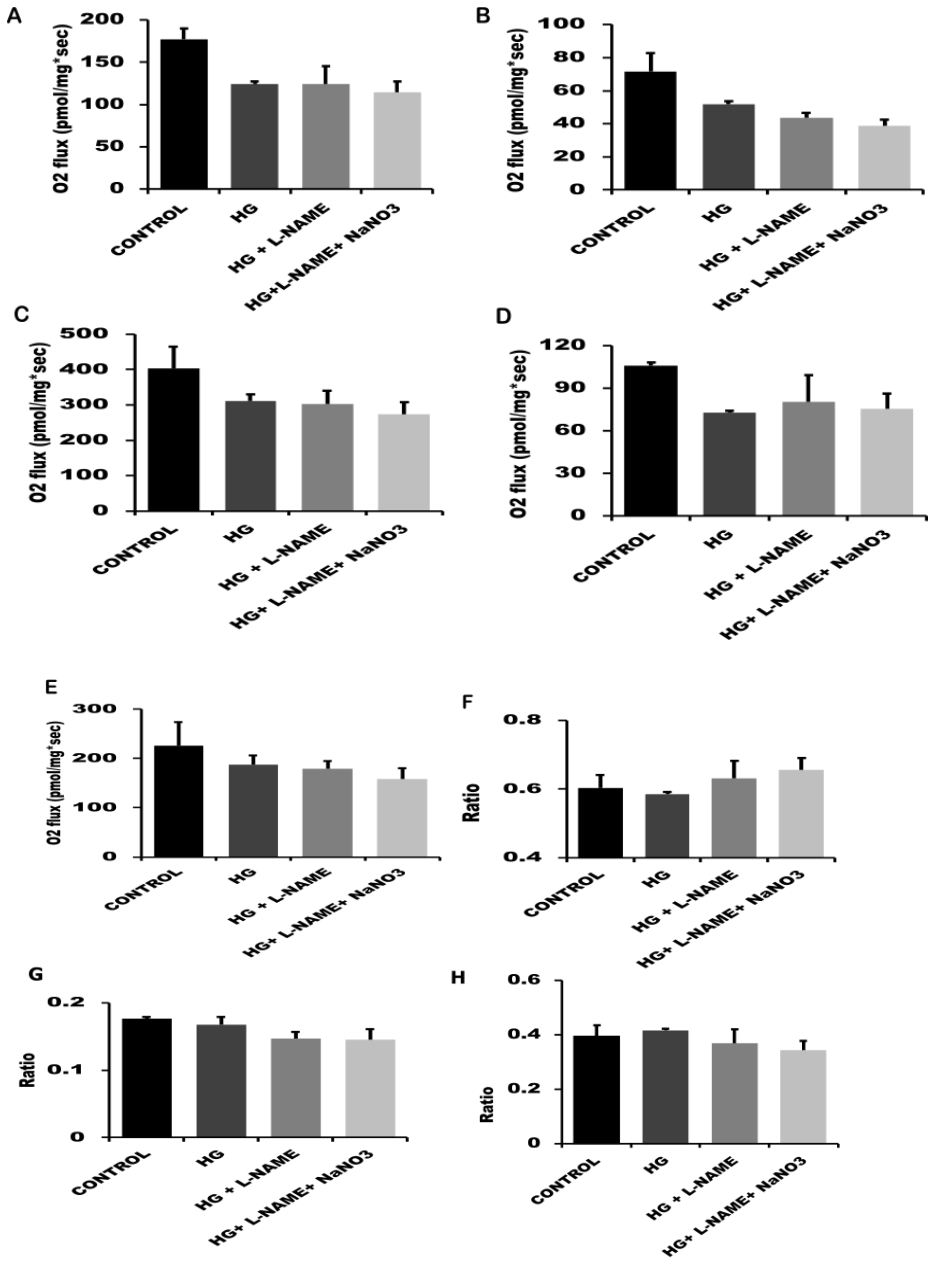

FIG 36: **Intact Cell Respiration (Cellular Bioenergitics)**
A- Routine Respiration, **B** - Leak respiration (following ATP synthase inhibition), **C** - Maximal Respiration (following uncoupling), **D**- ATP linked respiration (Routine - Leak), **E** - Reserve capacity (Maximal - Routine), **F** - Coupling efficiency ((R-L)/R), **G** - Leak/ Maximal (the proportion of maximal respiration contributed by proton leak), **H** - Leak/Routine (the proportion of Routine contributed by leak), **I** - ((Routine-Leak)/Maximal) (the proportion of Maximal contributed by ATP linked Respiration

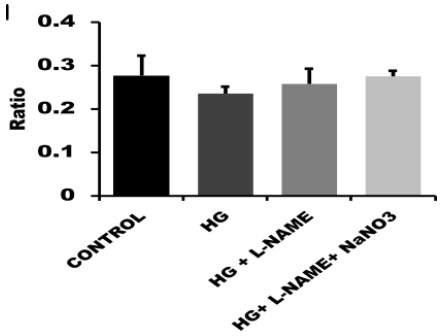

FIGURE 36: continued

Activities of mitochondrial complexes: The results with the permeabilized protocol with exogenously given substrates pointed at there being a betterment in the capacity of the mitochondrial electron transport chain enzymes. We thus analysed the activities of individual mitochondrial complexes, and observed that the L-NAME addition improved the activity of all the three complexes assessed i.e., Complex I, II and IV (Fig 35A-C). Although not statistically significant, it was observed that the decline in the complex activities observed in the HG condition was reversed with the inhibition of NO.

5.21.5 Estimation of the mitochondrial function with Nitric Oxide donor.

It needed to be determined if the effects observed on the mitochondrial function were due to the L-NAME mediated inhibition of NO generation or some pleiotropic effects of the L-NAME itself. Towards that end, we added a NO donor as the fourth group which was treated with HG containing 6mM L-NAME and 200 µM $NaNO_3$ and performed mitochondrial functional experiments as mentioned above.

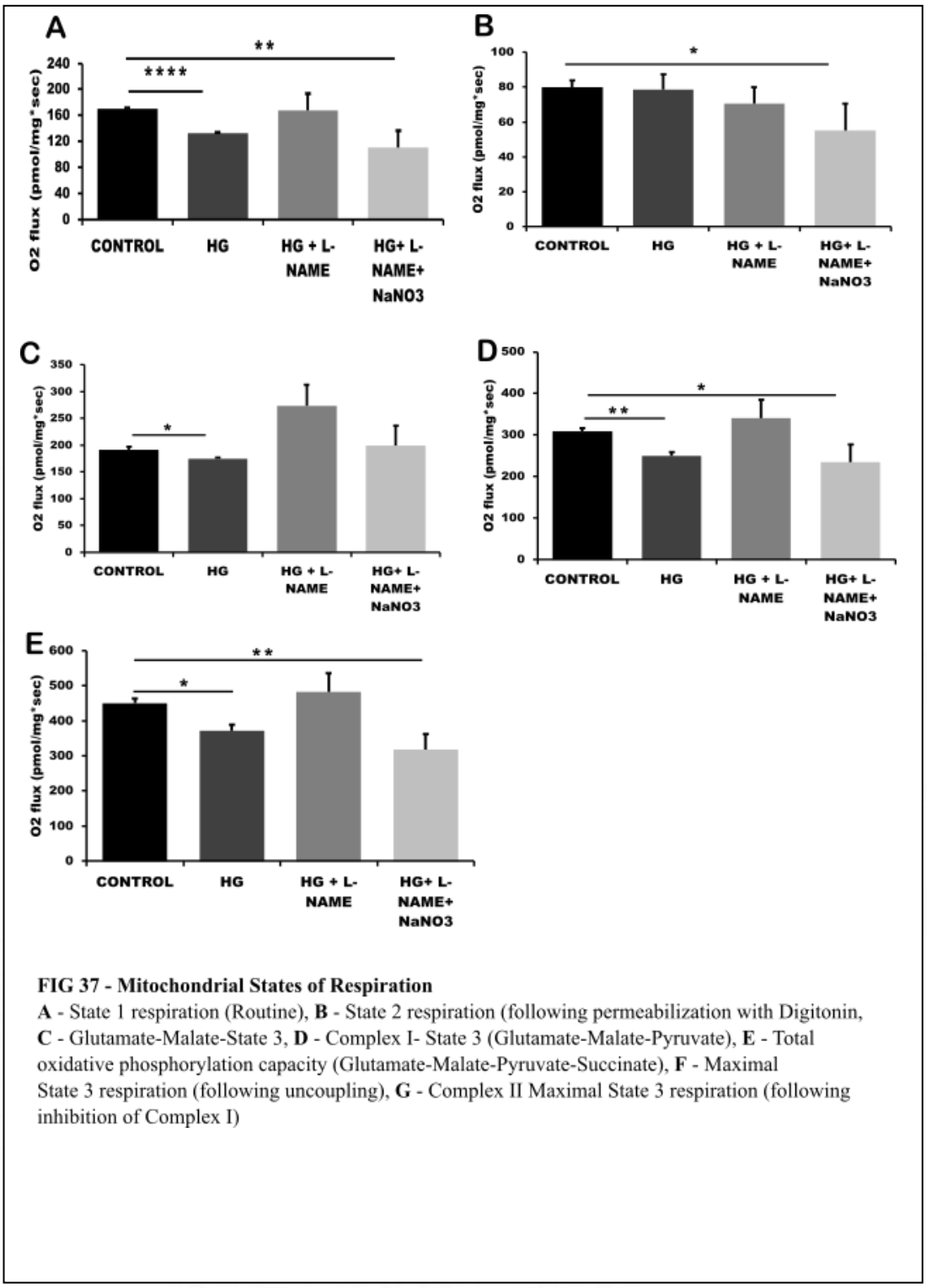

FIG 37 - Mitochondrial States of Respiration

A - State 1 respiration (Routine), **B** - State 2 respiration (following permeabilization with Digitonin, **C** - Glutamate-Malate-State 3, **D** - Complex I- State 3 (Glutamate-Malate-Pyruvate), **E** - Total oxidative phosphorylation capacity (Glutamate-Malate-Pyruvate-Succinate), **F** - Maximal State 3 respiration (following uncoupling), **G** - Complex II Maximal State 3 respiration (following inhibition of Complex I)

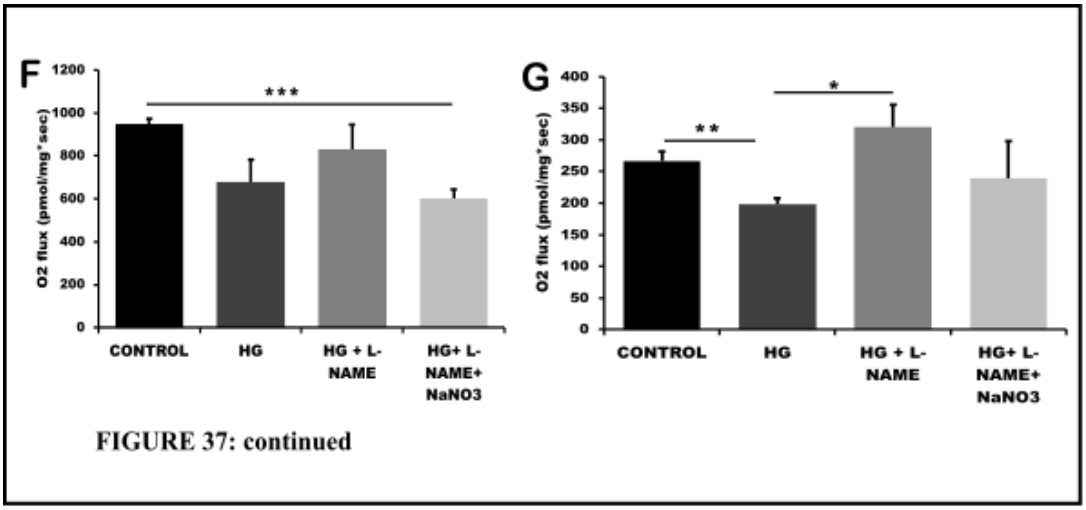

FIGURE 37: continued

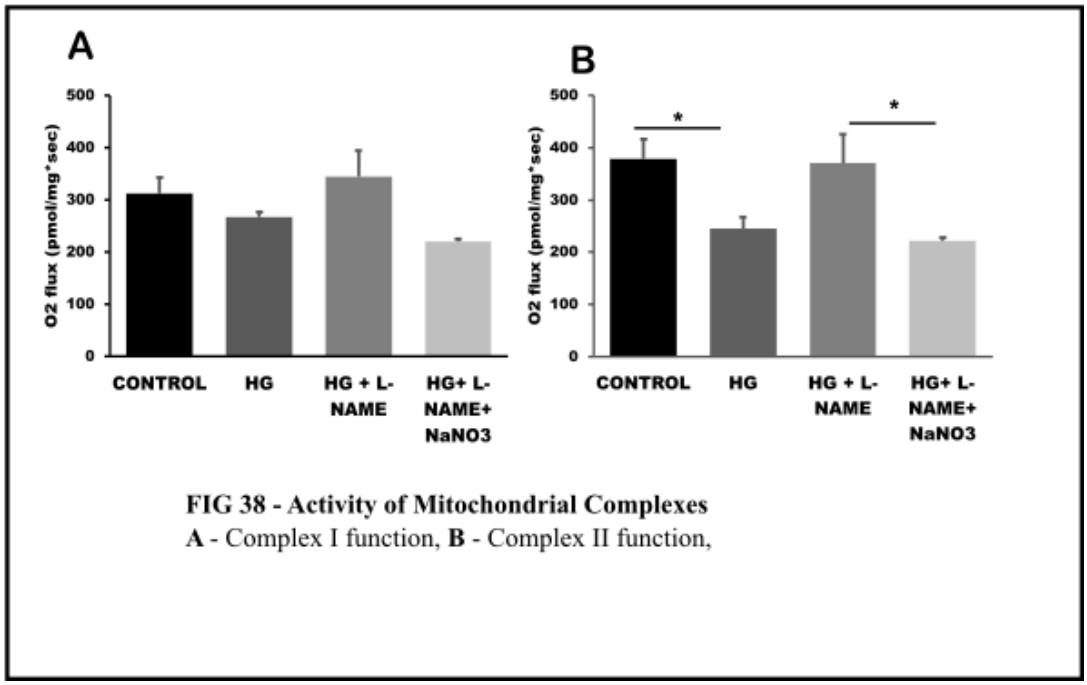

FIG 38 - Activity of Mitochondrial Complexes
A - Complex I function, **B** - Complex II function,

Intact cell respiration: With the NO donor addition, there was not much effect in the respiratory parameters measured with intact cell respiration as observed with the Routine respiration (Fig 36A), leak (Fig 36B), maximal respiration (Fig 36C), ATP linked respiration (Fig 36D), Reserve capacity (Fig 36E). The coupling control ratios also did not give much change suggesting that there may not be damage to the mitochondria (Fig 36F-I).

States of Respiration: The states of respiration with $NaNO_3$ supplementation showed results similar to the ones obtained for the corresponding HG group. This was consistently observed in across all parameters assessed like State 1 respiration (Fig 37A), State 3 for Glutamate-Malate (Fig 37C), State 3 for complex I mediated substrates Glutamate-Malate-Pyruvate (Fig 37D), Total OXPHOS (Fig 37E), Maximal State 3 respiration (Fig 37F) as well as Complex II maximal State 3 (Fig 37G).

Activities of mitochondrial complexes: The assessment of individual mitochondrial complexes also showed a similar pattern with the $NaNO_3$ group showing activity similar to that seen in the HG alone condition (Fig 38A-B).

5.22 Discussion:

It was observed that the cells under HG condition have increased generation of NO and this has profound metabolic implications. It is well established that the NO levels have an inhibitory effect on the mitochondrial OXPHOS. Our results correlated with these previous findings. With the nitric oxide production decreased using general NO synthase inhibitor, it was observed that the nitric oxide suppression under HG resulted in the increased reliance on mitochondrial metabolism as shown by improvement of respiration following substrates given exogenously. It was further cross validated that these effects were indeed due to NO suppression by providing a NO donor and observing that the beneficial changes in mitochondrial capacity were undone. There are reports that have confirmed that the NO production was linked to increased metastatic capacity in tumour cells by enhancing Wnt signalling (Du et al., 2013).

Also, studies have shown that NO decreased the OXPHOS and enhanced the glycolytic levels such that the energy demands for ATP are met with the glycolytic ATP production (Caneba et al., 2014). They thus proved that the NO can potentially increase the Warburg effect in the ovarian cancer models (Caneba et al., 2014).

The results that we observed show that the pattern of mitochondrial metabolism by L-NAME treatment was similar to that observed by the autophagy inducers Rapamycin and Torin. Studies have shown that NO can be engaged in a feed-forward loop and that its generation can potentially induce HIF1α through mTOR meditated signalling (Roy and Awasthi, 2019). there are also reports suggesting that the mTOR mediated signalling affects the NO levels by modulating NOS (Kim et al., 2012). This points towards an interconnected signalling wherein both the mTOR and NO signalling converge and affect each other. Arginine is a potent activator of mTOR and one study shows that could be by the generation of NO from arginine and which later activates mTOR (Wang et al., 2018). In effect multiple studies points towards mTOR activation with NO, which would mean that autophagy decline with NO levels. Thus, our results of L-NAME mediated improvement in mitochondrial function being similar to Rapamycin and Torin mediated improvement in mitochondrial function could be due to a common mechanism of autophagy activation.

5.23 Conclusion:

Hyperglycaemia increased cellular nitric oxide generation. With the Nitric oxide synthesis inhibited under HG condition, the mitochondrial dependency improved. When Nitric oxide donor was supplemented with the Nitric oxide inhibition, the effects of Nitric oxide inhibition on mitochondrial function were reversed suggesting that HG mediated NO generation contributes to the HG mediated decline in mitochondrial dependency. Also, other studies have shown there to be a link between NO and autophagy pathway potentially regulating autophagy by upstream regulator. Though not performed in our work, this could theoretically implicate that the autophagy decline in HG is ultimately the contributor to the reduced mitochondrial dependency and increased glycolysis in glioma.

Chapter 6

Objective 4: Does Hyperglycaemia affect Mitochondrial Quality?

6. 1 Introduction:

Mitochondria are the seat for ATP synthesis through oxidative phosphorylation which results in transfer of electrons through the electron transport chain system and finally reducing molecular oxygen to water at complex IV. This causes mitochondria to become susceptible to damage through production of mitochondrial reactive oxygen species. The mitochondrial DNA and the mitochondrial enzymes of are at an increased risk for the damage associated with mitochondrial ROS generation. This requires systematic clearance of the damaged parts of the mitochondria to maintain quality of the healthy mitochondrial pool. Mitochondrial health is mediated by fission mediated separation of the damaged subunit of the mitochondrial network followed by mitochondrial degradation through lysosomal route. Although multiple lysosomal degradative pathways for mitochondrial degradation have been identified, the most common is the bulk degradation of mitochondria through autophagy (mitophagy).

With autophagy declined in the HG condition, and concomitant mitochondrial dependency reduced; it becomes vital to assess the quality of the mitochondrial population in the HG condition. Towards that end mitochondrial membrane potential and mitochondrial network were assessed.

6. 2 Review of Literature:

The biggest determinant of mitochondrial quality is its increased ability to generate ATP and a controlled ability to generate ROS. ATP generation is dependent upon the potential gradient generated between the mitochondrial matrix and the intermembrane space ($\Delta\psi_m$) by the activity of electron transport chain complexes, particularly Complex I, III and IV (Ataullakhanov and Vitvitsky, 2002), as depicted in Fig M. Studies also point towards this potential gradient serving another critical function with negative potential on the inside and positive potential outside sue to proton pumping in the intermembrane space. This draws inward transport of cations like Ca^{2+} and Fe^{2+}. This Ca^{2+} plays critical role in mitochondrial stress response while Fe^{2+} forms the component of $Fe^{2+}S$ (iron-sulphur) clusters required for electron transport chain enzyme complexes (Gunter and Pfeiffer, 1990), (Hansford and Zorov, 1998), (Gunter et al., 2004).

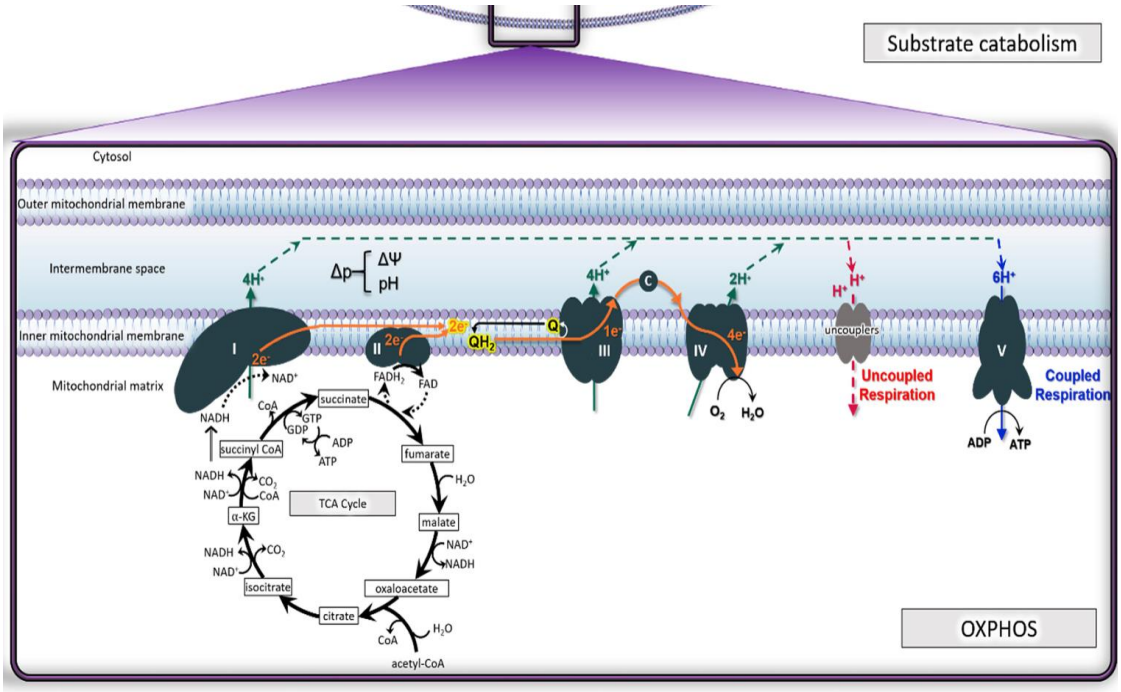

Fig M - Mitochondrial electron transport chain generates the potential gradient $\Delta\psi_m$ by proton pumping in the intermembrane space by Complexes I, III, IV

(Nolfi-Donegan et al., 2020)

6. 3 Materials and Methods:

6. 3. 1 Reagents:

MitoTracker Green dye was purchased from Invitrogen (MA, USA), PGC1-α and β-actin antibody was obtained from Cell Signalling Technology (MA, USA). DNA isolation was performed using Qiagen's DNA extraction Kit (Hilden, Germany). The Primers for mitochondrial-DNA $tRNA^{Leu(UUR)}$ and nuclear-DNA β2-microglobulin were purchased from Metabion (Martinsried, Germany), while SYBR Green was obtained from Applied Biosystems (MA, USA). TMRE mitochondrial membrane potential kit was obtained from GBioscineces (MO, USA).

6. 3. 2 Cell Culture and Maintenance:

The cell culture and maintenance techniques were similar to that mentioned in Chapter 2.

6. 3. 2. 1 Reagents used for Cell culture:

The Reagents used for Cell culture were same as that mentioned in Chapter 4. The specific treatments for autophagy activation and Nitric oxide inhibition were similar to that mentioned in chapters 5 and 7 respectively.

6. 3. 2 Mitochondrial Content:

Fluorescence Imaging: Cells were cultured in 8 chambered coverslips from Ibidi (Munich, Germany) and upon 50% confluence were given treatment. Mitochondrial Dye MitoTracker Green was used following the Control and HG treatment for 72 h and incubated for 15 mins with MitoTracker Green at manufacturer's recommended dilution with 1:1000 dilution for Hoechst. The cells were washed with PBS to eliminate any surplus dye and reduce background signal and the fluorescence was measured with excitation at 480 nm and emission at 510 nm with Olympus Fluorescent microscope. Multiple fields were captured for each treatment group. The fluorescent intensity was quantified using ImageJ and the average intensity values were obtained for both the groups.

qPCR: Cells were cultured and treatments were given as mentioned previously. The total cellular DNA including the mitochondrial and nuclear DNA was isolated using Qiagen DNA extraction kit following manufacturer's instructions. The DNA quality and purity was assessed using the 260/280 ratio for absorbance for double stranded DNA. The primers were diluted such that each forward and reverse primer was at a final concentration of 0.5 µM. The mitochondrial and nuclear DNA estimations were done in separate reaction tubes for each sample set. The reactions preparation was under a laminar hood and was as follows: 5 µl of 2x SYBR Green, 1 µl of 5 µM forward primer, 1 µl of 5 µM reverse primer, 3 µl of 0.1 ng/µl template DNA making the final reaction volume 10 µl.

Gene	Primer Sequence (5'- 3')	Amplicon size (bp)	Annealing Temp. (°C)
	F CACCCAAGAACAGGGTTTGT	107	62

mitochondrial-DNA $tRNA^{Leu(UUR)}$	**R** TGGCCATGGGTATGTTGTTA		
nuclear-DNA β2-microglobulin	**F** TGCTGTCTCCATGTTTGATGTATCT	86	62
	R TCTCTGCTCCCCACCTCTAAGT		

Primers used for mitochondrial DNA copy number analysis through qPCR

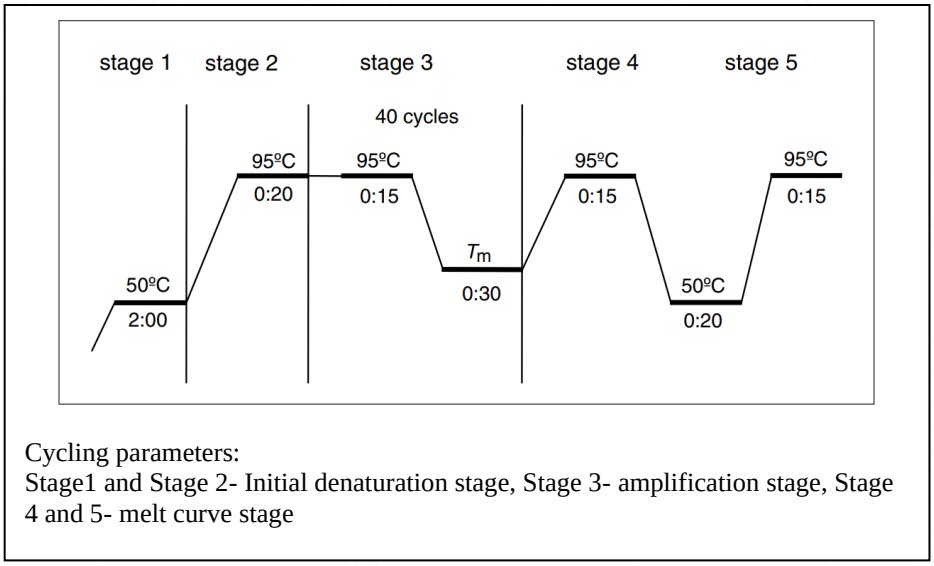

Cycling parameters:
Stage1 and Stage 2- Initial denaturation stage, Stage 3- amplification stage, Stage 4 and 5- melt curve stage

The cycling parameters were as mentioned above with annealing performed at 62°C and the success of the PCR was determined through no amplification signal in the negative control (having same components of the reaction mix but with nuclease free water instead of template DNA) and a single amplification curve in the melt curve stage for both the nuclear and the mitochondrial sample sets. The mitochondrial DNA content was calculated by the following equation,

Mitochondrial DNA content = $2 \times 2^{(\Delta CT)}$

where ΔCT is the difference of C_T values between β2-Myoglobulin gene and the $tRNA^{Leu(UUR)}$ (C_T of β2-M - C_T of $tRNA^{Leu(UUR)}$).

Relative mitochondrial DNA content = mtDNA of treated / mtDNA of control

6. 3. 3 Immunoblotting for the expression of PGC1-α:

Total protein isolation, protein quantification and the SDS-PAGE and immunoblotting was performed following the treatment period as mentioned in Chapter 3. The levels of PGC1-α were assessed using densitometry with ImageJ and relative values normalized to β-actin were graphically represented.

6. 3. 4 Mitochondrial Membrane Potential:

Cells were cultured in 8 chambered coverslips from Ibidi (Munich, Germany) and upon 50% confluence were given treatment. The mitochondrial membrane potential was determined using TMRE MMP (mitochondrial membrane potential) Kit following the manufacture's guidelines. Following incubation with the dye for the recommended time, the excess was washed off using PBS and the cells were kept in the MMP imaging buffer provided in the kit. The cells were imaged using Olympus microscope with excitation at 550 nm and emission at 580 nm respectively. Multiple fields were captured and fluorescent intensity was calculated using ImageJ and values averaged and graphically represented.

6. 3. 5 Mitochondrial Architecture:

The mitochondrial architecture was determined for the cells with the TMRE staining of the healthy mitochondrial population and compared between the treatment groups.

6. 4. Statistical analysis:

All statistical analysis were performed as mentioned in Chapter 2.

6. 5 Results:

6. 5. 1 Mitochondrial Content:

The MitoTracker imaging showed an increase in the total mitochondrial mass in the HG treated cells as compared to the control (Fig 39A-B).

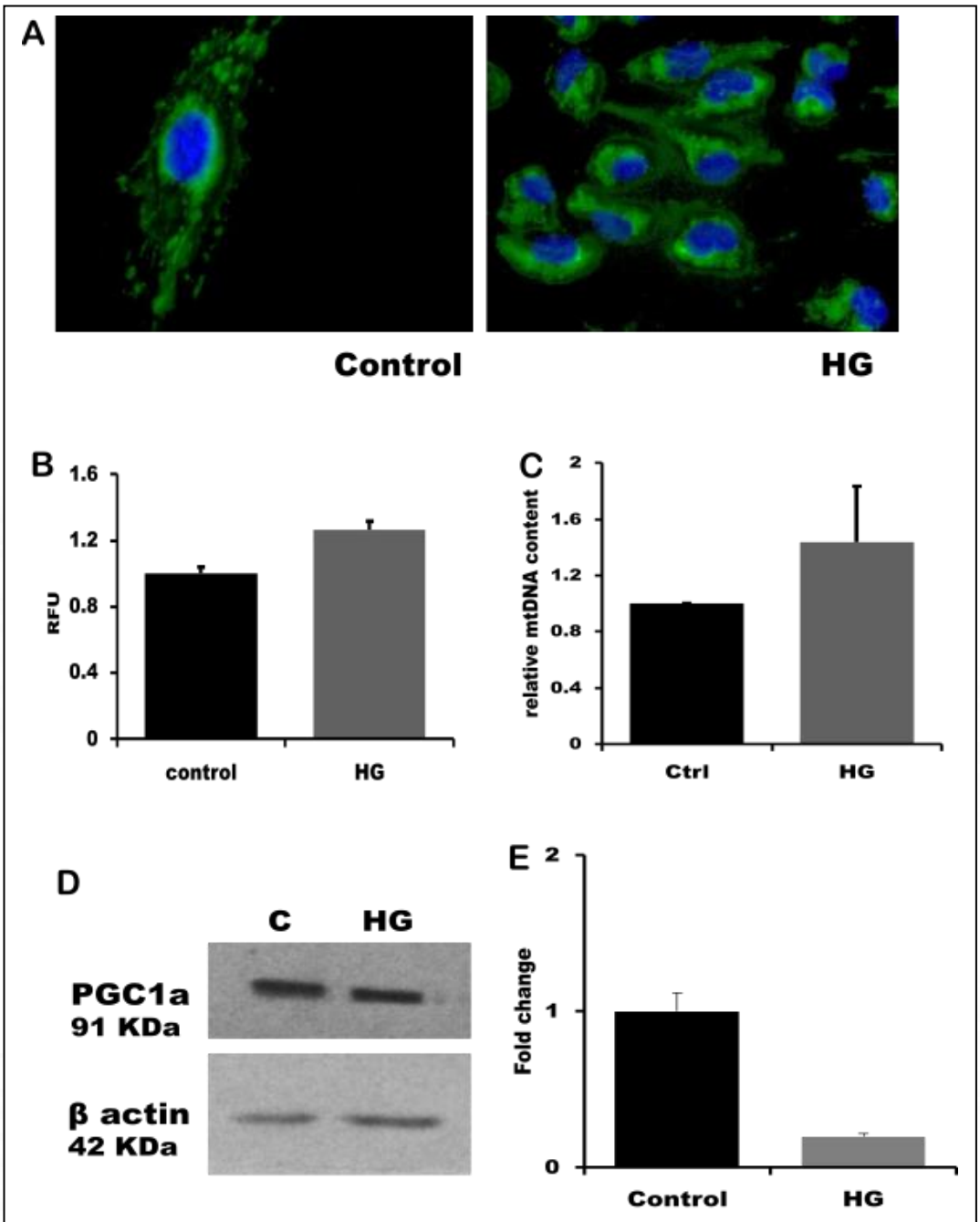

Fig 39: Analysis of mitochondrial content:
A - MitoTracker green imaging, **B** - Quantification of the MitoTracker fluorescent image, **C** - qPCR data for the quantification of the mitochondrial content, **D** - Western Blotting for the experssion analysis of PGC1-alpha

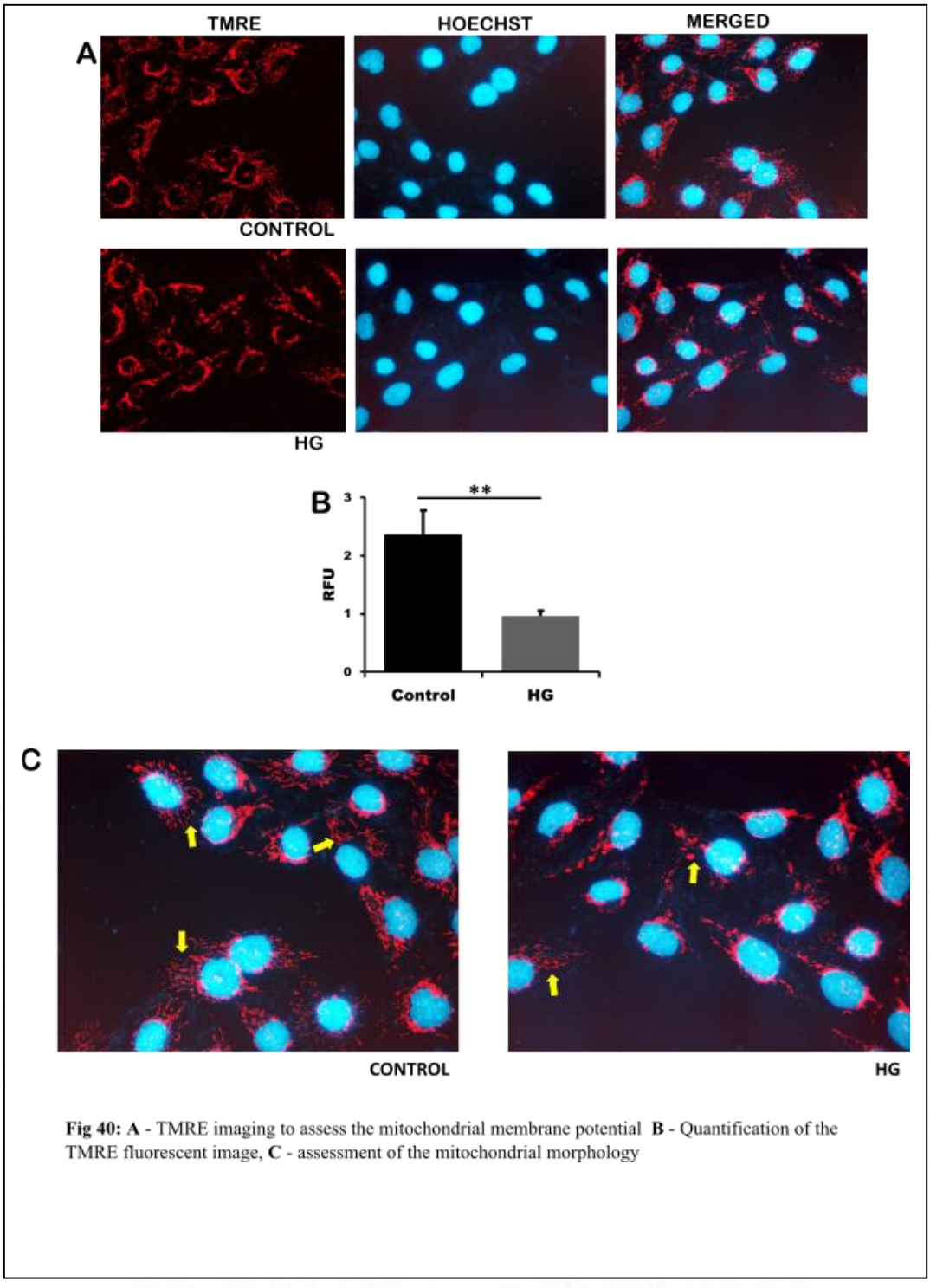

Fig 40: A - TMRE imaging to assess the mitochondrial membrane potential **B** - Quantification of the TMRE fluorescent image, **C** - assessment of the mitochondrial morphology

This was cross verified using qPCR-based analysis of total mitochondrial content normalized to total number of cells and again it was observed that the HG cells had increased mitochondrial mass (Fig 39C) confirming that there is higher mitochondrial content in HG treated cells.

6. 5. 2 Immunoblotting for the expression of PGC1-α:

To assess if the mitochondrial content increment was due to the accumulation of old mitochondria or due to the formation of new one, the expression pattern of the master regulator of mitochondrial biogenesis was determined. The PGC1-α was found to be declined under the HG state (Fig 39D-E) suggesting decreased mitochondrial biogenesis. This also points out to there being increase in mitochondrial accumulation leading to mitochondrial content rise.

6. 5. 3 Mitochondrial Membrane Potential:

The mitochondrial quality and health were determined through the determination of mitochondrial membrane potential, as the membrane potential is the driver for the ATP generation in the mitochondria and thus of mitochondrial efficiency. The TMRE dye localizes only in the mitochondria with optimum membrane potential and fluoresces. It was observed that the HG treated cells had reduced TMRE fluorescence (Fig 40A-B). This points to the fact that although greater in quantity, the mitochondrial population in the HG is not healthy.

6. 5. 4 Mitochondrial Architecture:

The mitochondrial architecture was assessed only for the mitochondria with healthy membrane potential as that is the only mitochondrial pool that is capable to contribute in the electron transport chain and ATP synthesis. The TMRE fluorescence images were analysed for the same and it was observed that the mitochondrial network was modified in the HG group with mitochondria more fragmented than that in the control. The control group had filamentous mitochondria suggesting that there would be more mitochondria in a network (Fig 40C).

6. 6 If Autophagy decline mediates accumulation of inefficient mitochondria and disruption of the mitochondrial network, then do the interventions that enhanced autophagy reverse that?

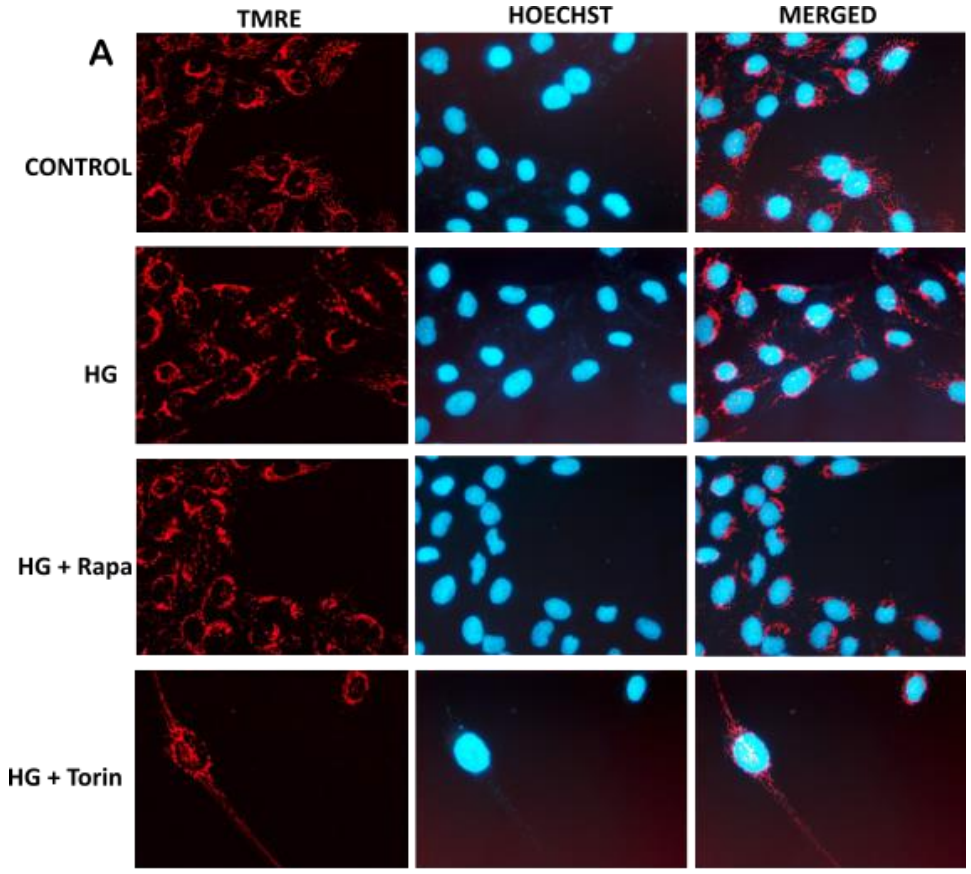

Fig 41: A - TMRE imaging to assess the mitochondrial membrane potential **B** - Quantification of the TMRE fluorescent image

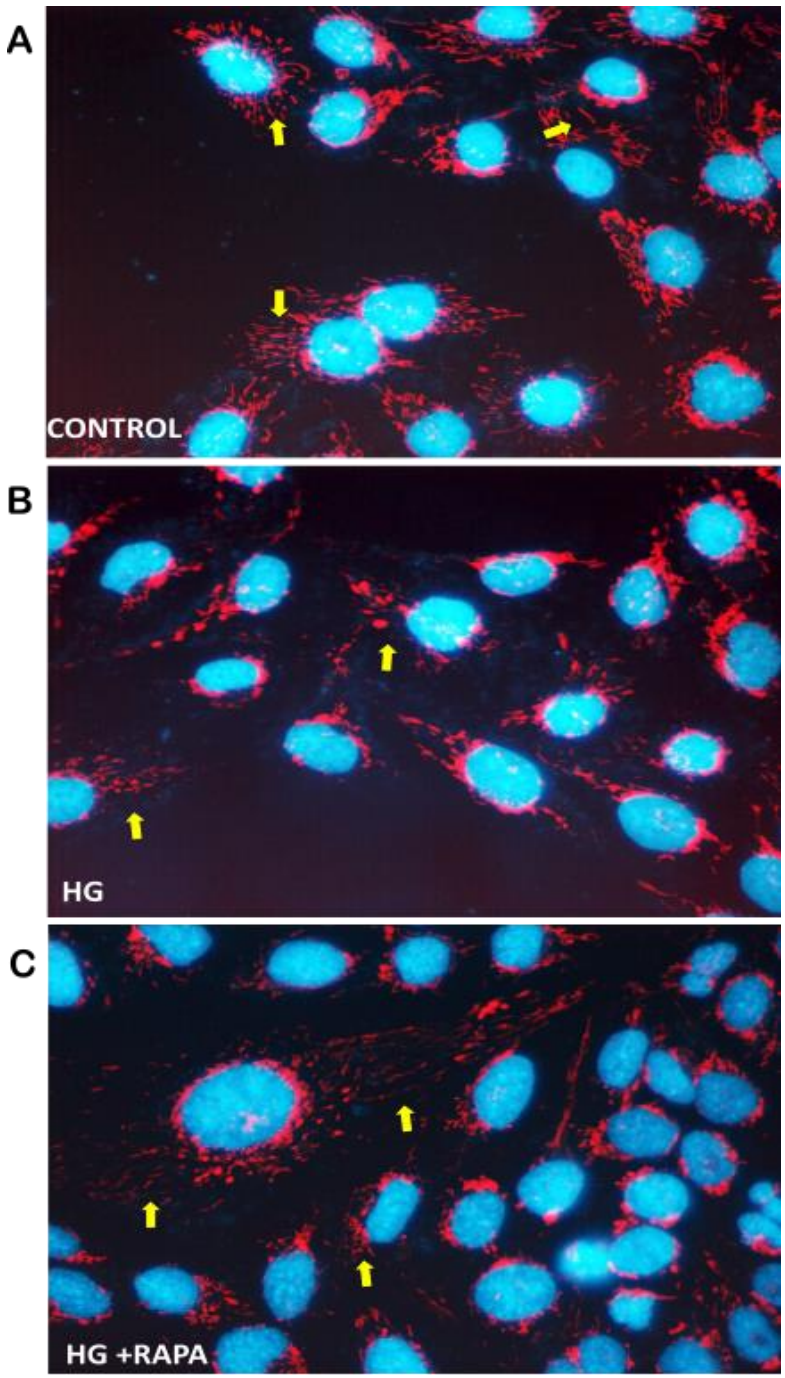

Fig 42: Estimation of mitochondrial network and connectedness among Control, HG and HG + Rapamycin groups

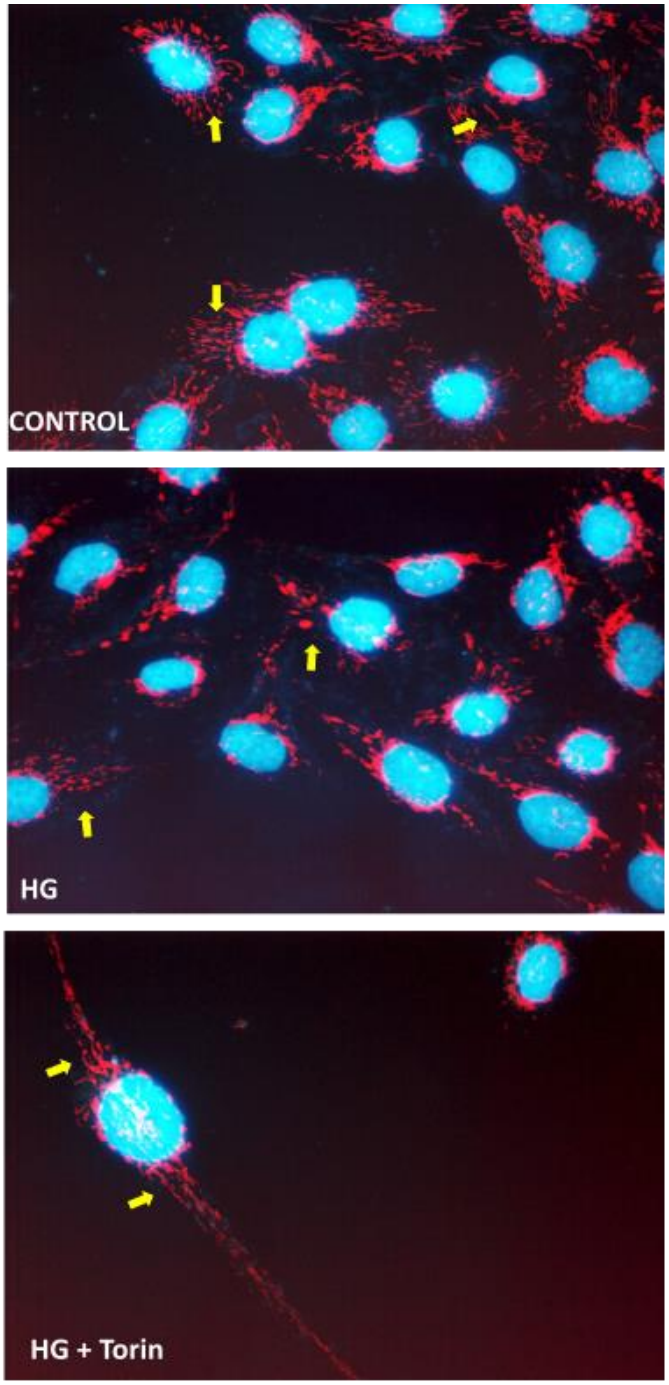

Fig 43: Estimation of mitochondrial network and connectedness among Control, HG and HG + Torin groups

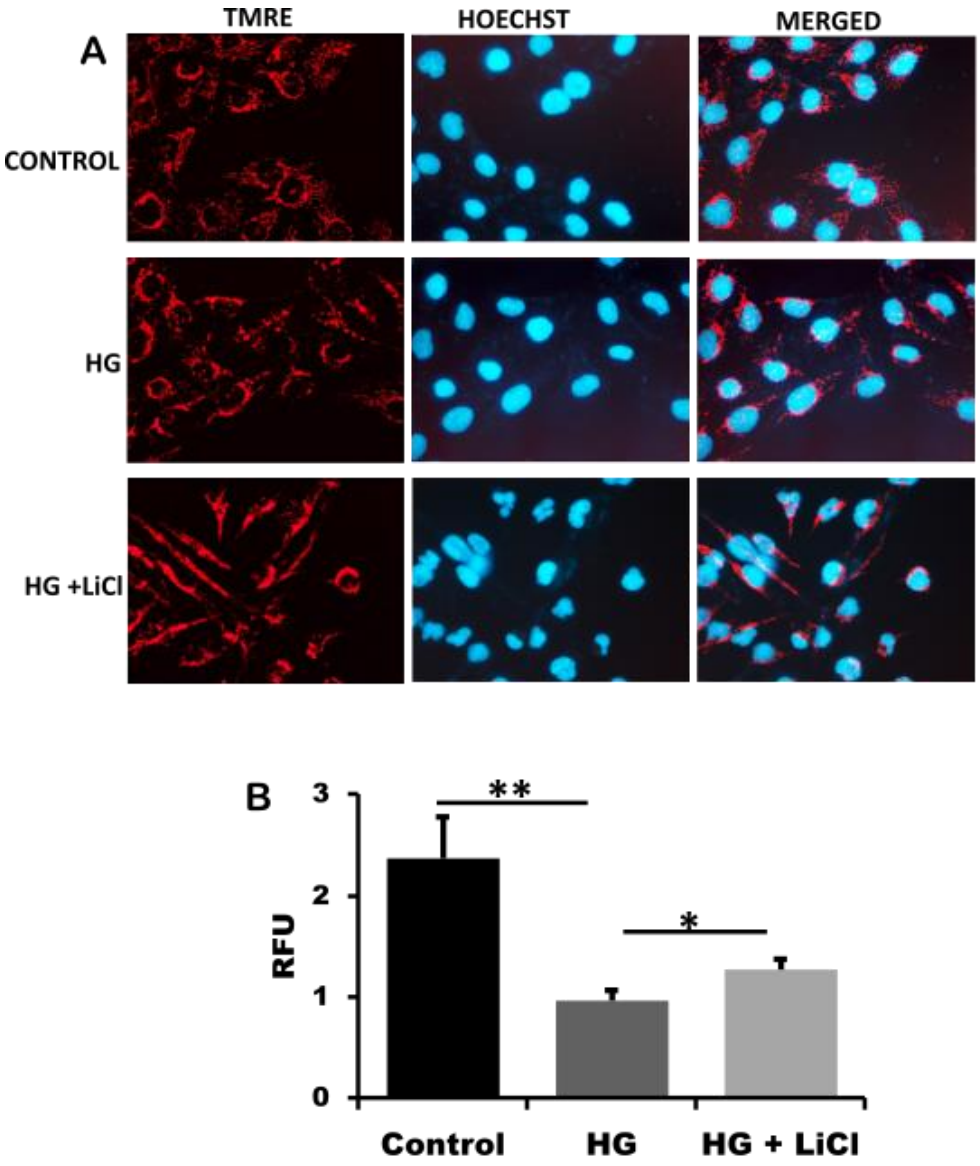

Fig 44: A - TMRE staninig for the estimation of mitochondrial membrane potential among Control, HG and HG + LiCl groups, **B** - the quantification of the TMRE fluorescence

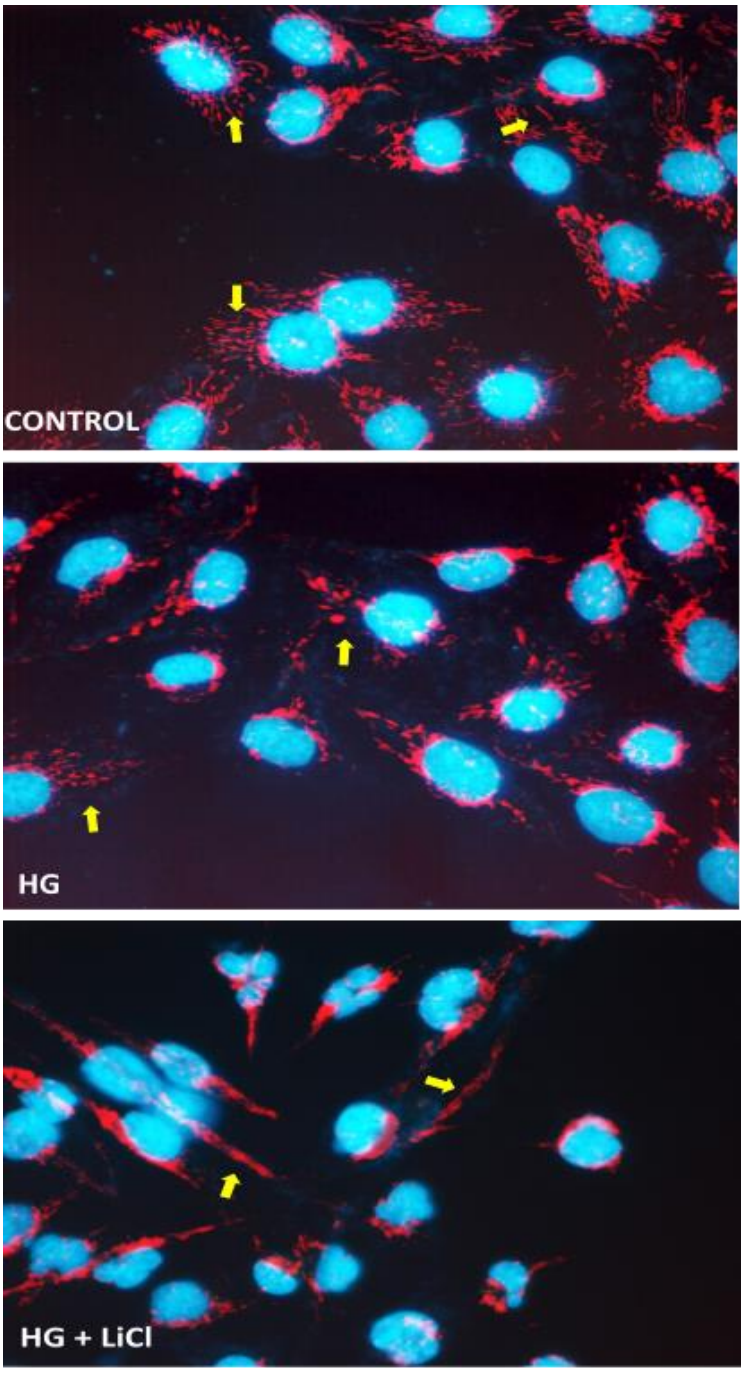

Fig 45: Estimation of mitochondrial network and connectedness among Control, HG and HG + LiCl groups

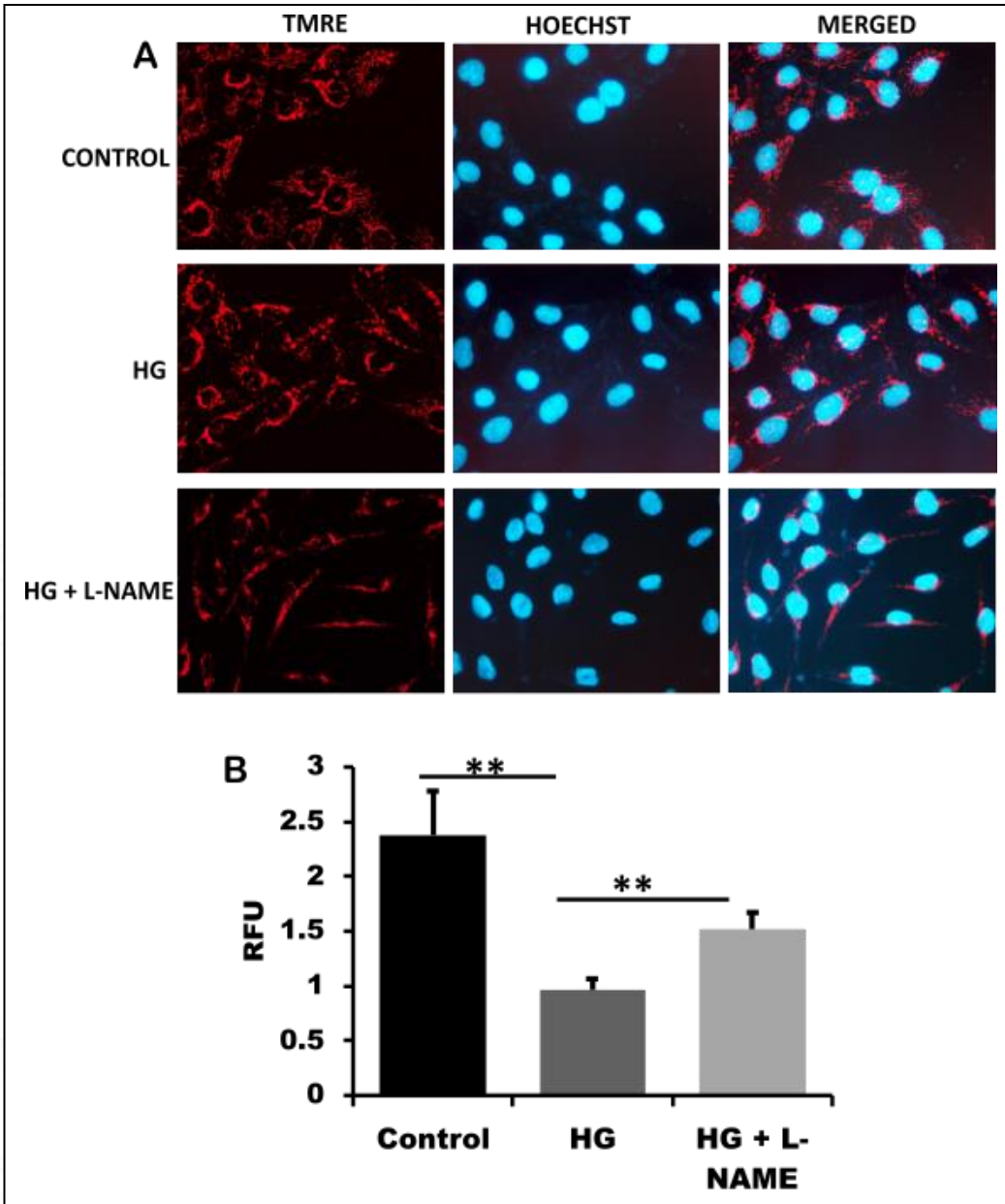

Fig 46: A - TMRE staninig for the estimation of mitochondrial membrane potential among Control, HG and HG + L-NAME groups, **B** - the quantification of the TMRE fluorescence

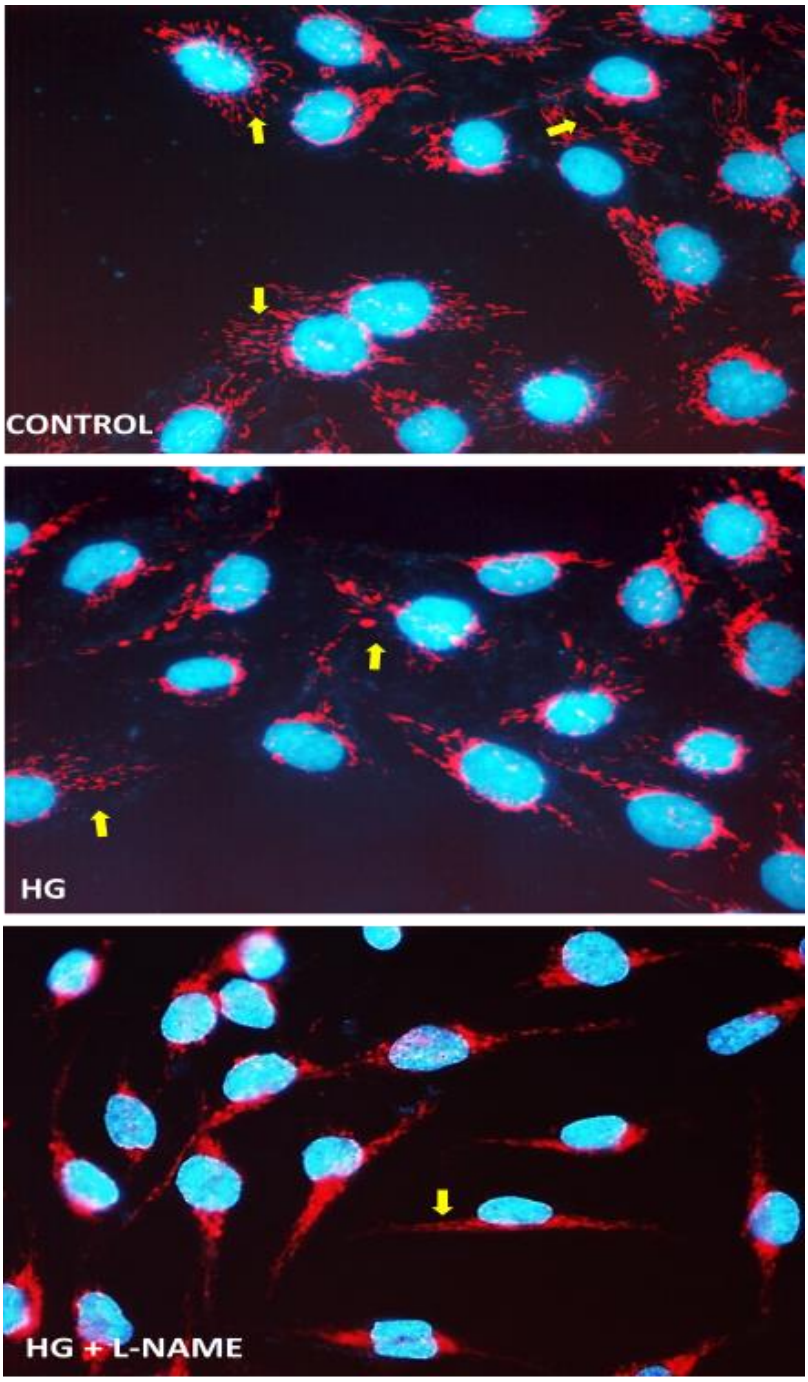

Fig 47: Estimation of mitochondrial network and connectedness among Control, HG and HG + L-NAME groups

6. 6. 1 Mitochondrial membrane potential and mitochondrial architecture following autophagy induction by Rapamycin and Torin:

The cells were cultured in chambered coverslips the treatments given as mentioned previously. The TMRE staining was performed as mentioned above. It was observed that in the HG with Rapamycin and HG with Torin, the TMRE fluorescence was improved as compared to that seen under HG alone (Fig 41). The mitochondria appeared more networked with the Rapamycin and Torin treatments (Fig 42, Fig 43).

6. 6. 2 Mitochondrial membrane potential and mitochondrial architecture following autophagy induction by LiCl:

It was observed that in the HG with LiCl, the TMRE fluorescence was significantly improved as compared to that seen under HG alone (Fig 44), also the mitochondria appeared more networked (Fig 45).

6. 6. 3 Mitochondrial membrane potential and mitochondrial architecture following autophagy induction by Nitric oxide inhibition through L-NAME:

It was observed that in the HG with L-NAME, the TMRE fluorescence was significantly improved as compared to that seen under HG alone (Fig 46), also the mitochondria appeared more networked (Fig 47).

6. 7 Discussion:

It is observed that HG caused reduction in autophagy. This could potentially impact the quality control mechanisms of the mitochondria. It was observed that such was indeed the case as there was an increase in the total mitochondrial pool even in the absence of signal for mitochondrial biogenesis; thus, implying that there may be accumulation of mitochondria due to lack of degradation. Also, the previous results show that under HG condition there is a decline in the efficiency of mitochondria with decline in mitochondrial function observed through various parameters. Taken together, HG caused the accumulation of inefficient mitochondria. Many studies support the notion that mitophagy dysregulation is associated with tumour formation

(as shown in the Fig N), and mutations in the genes for mitophagy adaptor proteins is found in various cancers (Letessier et al., 2007, p. 2), (Burrell et al., 2013).

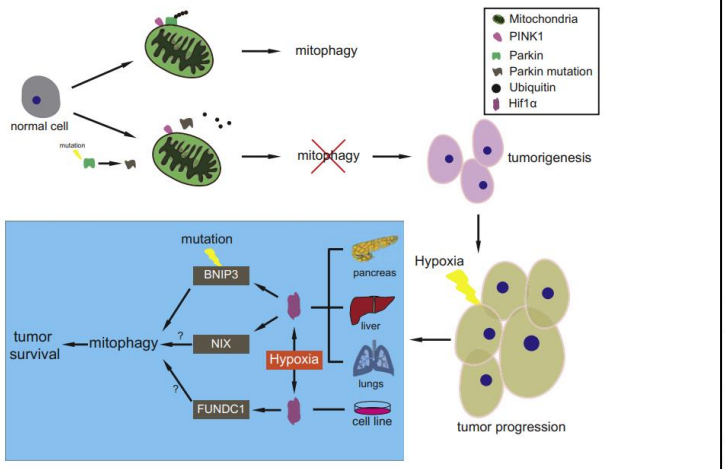

Fig N - The dysregulation of clearing mechanism of the mitochondria affects basal cellular metabolism and results in pro-tumorigenic phenotype.

(Chang et al., 2017)

Pharmacological studies on the effects of compound that work by mTOR activation have demonstrated that mTOR activation causes mitophagy decline. Vigabatrin, the anti-epileptic drug, causes mTOR activation (which inadvertently cause generalized autophagy decline) and has shown to result in increased mitochondrial pool with poor metabolic profile in C57BL/J6 mice brain and eye extracts, which got corrected by the supplementation of Torin (Vogel et al., 2015). This reduced mitochondrial efficiency was accompanied with a reduction in the mean mitochondrial size, suggesting mitochondrial fragmentation and reduced mitochondrial antioxidant capacity implying an accumulation of damaged mitochondria.

Mitochondrial membrane potential serves as potential energy stored that is later harnessed by the ATP synthase for ATP generation. Thus, it forms the source of mitochondrially derived ATP (Mitchell, 2011). If the fluctuation in this potential gradient becomes prolonged, it becomes damaging as in the absence of this potential difference, the ATP synthase acts in reverse and utilizes cellular ATP generated through other means like glycolysis to form ADP + P_i, which becomes detrimental to cell survival (Zamzami et al., 1995), (Yaniv et al., 2010), (Zorov et al., 2014),

(Izyumov et al., 2004). As we had observed that the activity of mitochondrial complexes was declined, it seemed reasonable to expect there may be a decline in the mitochondrial membrane potential, which is created by the activity of Complexes I, III and IV. The observations of the decline in mitochondrial membrane potential observed with TMRE fluorescence under HG correlate with this hypothesis.

Mitochondrial network plays a role in the mitochondrial behaviour, with increase in fragmentation being associated with mitochondrial functional abnormalities, increased ROS generation, increased susceptibility to apoptotic cell death; while mitochondria fused in filamentous network is associated with decreased mtDNA mutations, decreased apoptotic cell death and increase in the bioenergetic efficiency (Casuso and Huertas, 2020). Our results show a decline in mitochondrial fragmentation suggesting a decline in the mitochondrial efficiency. Also, as there were less population of mitochondria with optimum membrane potential, it seems likely that those fragments with reduced potential would have been fragmented off from the network. To assess the interconnectedness between the healthy mitochondria with optimal membrane potential, TMRE stained mitochondria were assessed for the interconnectivity.

To substantiate the claim that these effects would be observed due to lack of clearance mechanisms in the cell, the autophagy inducers were used under HG condition and mitochondrial membrane potential and mitochondrial network assessed. The results suggest that the autophagy decline under the HG group drove the decline in the total mitochondrial quality. Morita et al., presented that mTOR controls mitochondrial fission and apoptosis by increasing the expression of mitochondrial fission proteins and recruitment of Drp1; and potent mTOR inhibitors created hyperfused mitochondria by regulating the transcription factor 4E-Binding Protein 1, the downstream target of mTOR which in turn diminished the pro-fission proteins causing unopposed fusion (Morita et al., 2017).

6. 8 Conclusion:

We conclude that HG causes a decline in the mitochondrial clearance mechanisms due to a decline in the generalized autophagy in the glioma cells. This causes accumulation

of inefficient mitochondria within the cells. There is also evidence that the accumulation of inefficient mitochondria caused a negative impact on the entire mitochondrial population within the cells, reducing the mitochondrial pool with healthy membrane potential and destabilizing the mitochondrial network. This also brought down the mitochondrial functional efficiency as estimated by mitochondrial respiration studies.

Chapter 7

Conclusion

We assessed the metabolic effects of high glucose on the glioblastoma in an in vitro model. We had hypothesised that the high glucose would affect the glioma cells and this effect would be visible in the metabolic profile of the cells.

It was first determined if the HG had any effect on the tumour formation capacity of the glioma cells. For the same, HG stress was given in the glioma cell lines and it was observed that there were increase in aggressiveness. The HG increased the capacity of the cells for proliferate thus suggesting modulation of the cell cycle; there was increased capacity for migration and increased secretion of invasion specific makers like MMP2 and MMP9. This suggested a potential for increase in the capacity for migration hinting towards a more metastatic phenotype in the HG state. But the tumour cells need to acquire the ability to survive in an attachment free state for being able to initiate secondary growth. The anoikis resistance was increased in HG suggesting a higher capacity for tumorigenesis.

With the assessment of the metabolism of cells under HG, it was revealed that it created a more glycolytic environment in the cells. There was an increase in the glucose consumption but there was a concomitant increase in the lactate secreted in the extracellular media validated with the pH decline, suggesting that the consumed glucose took the glycolytic route for energy generation. there was a substantial decline in the mitochondrial oxidative phosphorylation in cells under HG pointing at an augmentation of the Warburg effect with the HG treatment. This lowering of the mitochondrial capacity is mediated by the decline in the mitochondrial quality which was observed with there being limited mitochondria with optimal membrane potential. The mitochondrial network also showed dysregulation with observable fragmentation in the HG state.

It was also observed that there was a decline in the autophagy under the HG state. Autophagy being the major recycling pathway in the cell, any deviation from the basal levels has an impact on the cell. This decline in the generalized autophagy might also reduce the mitochondrial clearance and it was observed that there was an accumulation of inefficient mitochondrial population in the cells under HG. With the lack of proper clearance of the damaged fraction of the mitochondrial population, though more in

content, the total mitochondrial population becomes impacted possibly by some feedback mechanism which would decline the mitochondrial oxidative phosphorylation with the accumulation of damaged mitochondria in the cell as a means to protect the cell from ROS and Ca^{2+} leakage mediated detrimental effects. It thus seems likely that this decline in autophagy could be the means by which the cells under HG had reduced mitochondrial reliance. The decline in oxidative phosphorylation is the hallmark of the Warburg effect. Thus, the decline in autophagy could be potentially associated with the augmentation of this effect observed under HG. This increased Warburg effect is beneficial for cancer cell survival and thus could be the basis of increased aggressiveness of glioma.

Our study suggests that this decline in autophagy causes the accumulation of inefficient mitochondria, as the interventions that we used that had an effect of autophagy activation also had the capacity to affect the mitochondrial metabolism. It was observed that with increased autophagy under the HG condition there was an improvement in the mitochondrial OXPHOS with a concomitant decline in the glucose utilization and lactate secretion. This signifies that the autophagy activation caused a decline in the otherwise overactive Warburg effect under the HG stress. Our data point out that with the autophagy activation, there is a potential improvement of mitochondrial transmembrane gradient, mitochondrial network along with improved mitochondrial respiration.

There are many interventions that target the autophagy in cancer cells. There are numerous autophagy modulators easily available and some even have FDA clearance, thus could be a potential agent of targeted therapy. It thus seems worthwhile to further determine the role the autophagy modulators would have on the aggressiveness of the glioma under HG state and to identify the targets in the autophagy pathway that could serve as chemotherapy adjuvants.

Limitations of the study:

The study analysed the hyperglycaemia mediated changes in the mitochondrial function of glioma cells for which high grade glioma cell lines were used. Glioma can have IDH mutations that can alter the metabolic response to the glucose and glutamine. The IDH mutant phenotype could have been checked with IDH mutant plasmid insertion and the effects of HG could be better understood that could be more appropriate to the real-life scenario.

Also, the augmented autophagy resulted in the healthy mitochondrial population as assessed by the mitochondrial membrane potential and mitochondrial network remodelling. It could shed light on the mechanism of this observation if the types of mitophagy could also be assessed. The mitochondrial degradation is carried with various adaptor molecules playing a role. These specific types of mitophagy can have different associated signalling pathways getting activated. Accurate interventions could be planned with the knowledge of the activation or decline of any specific mitophagy pathway with HG stress.

Future directions:

The study explored the hyperglycaemia induced changes in mitochondrial function. It was observed that the autophagy decline in the HG condition caused the mitochondrial functional changes. It is was also observed that when autophagy was augmented by mTOR inhibition (with the use of Rapamycin and Torin) the mitochondrial functional improvement was more substantial than when autophagy was augmented with LiCl. This suggests the involvement of mTOR pathway. This study showed important leads for the involvement of the mTOR pathway and it would be interesting to analyse the upstream regulators of the mTOR pathway that get modulated by the HG stress. That would give a comprehensive idea of the pathway that gets activated and the sequence of the downstream regulators that get modified following HG stimulation which later leads to augmented Warburg Effect.

Graphical Abstract

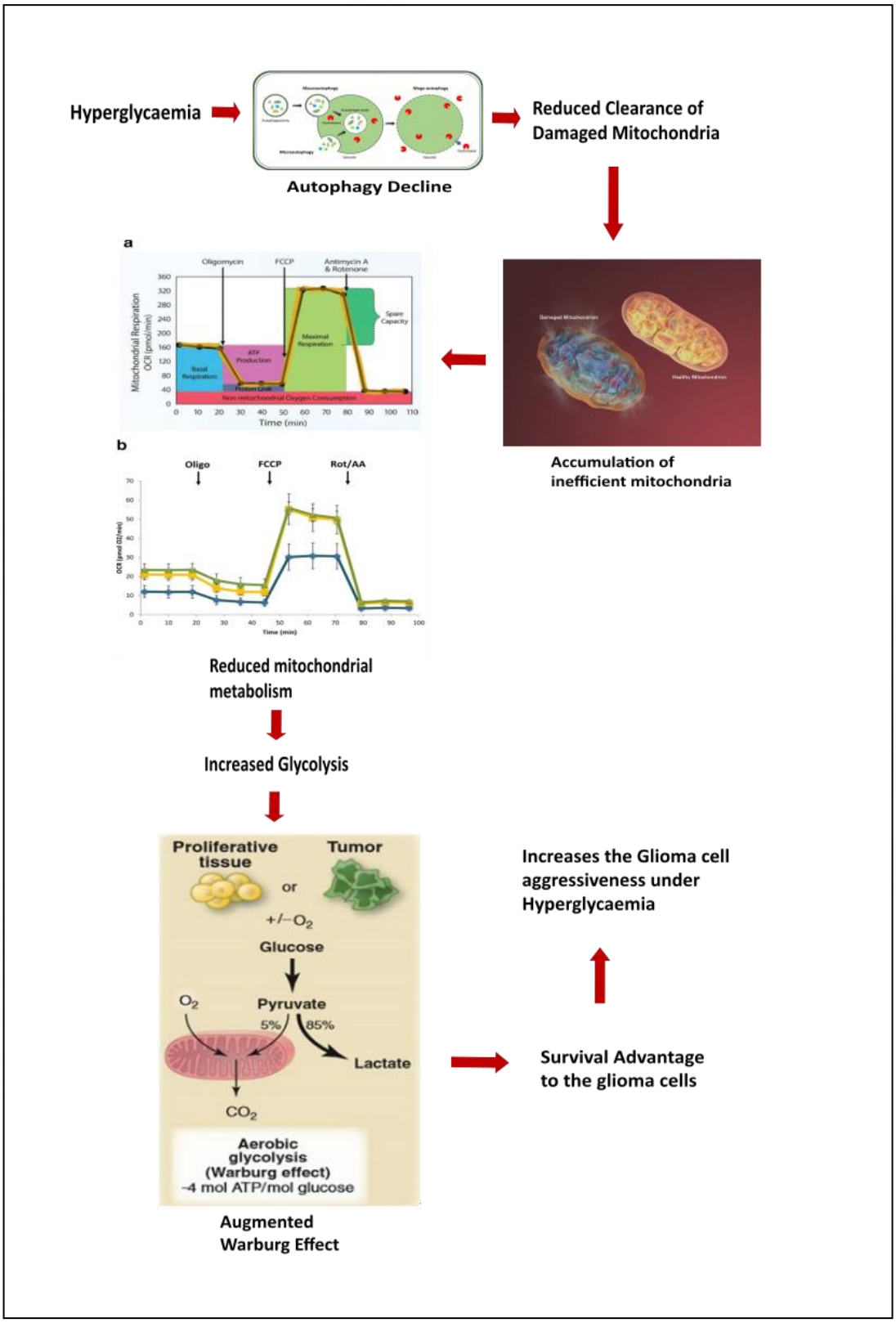

References:

A Spectroscopic Approach to Investigate the Molecular Interactions between the Newly Approved Irreversible ErbB blocker “Afatinib” and Bovine Serum Albumin [WWW Document], n.d. URL https://journals.plos.org/plosone/article?id=10.1371/journal.pone.0146297 (accessed 6.15.21).

Adami, H.-O., McLaughlin, J., Ekbom, A., Berne, C., Silverman, D., Hacker, D., Persson, I., 1991. Cancer risk in patients with diabetes mellitus. Cancer Causes Control 2, 307–314. https://doi.org/10.1007/BF00051670

Ahmad, F., Dixit, D., Sharma, V., Kumar, A., Joshi, S.D., Sarkar, C., Sen, E., 2016. Nrf2-driven TERT regulates pentose phosphate pathway in glioblastoma. Cell Death Dis. 7, e2213–e2213. https://doi.org/10.1038/cddis.2016.117

Aishwarya, R., Alam, S., Abdullah, C.S., Morshed, M., Nitu, S.S., Panchatcharam, M., Miriyala, S., Kevil, C.G., Bhuiyan, M.S., 2020. Pleiotropic effects of mdivi-1 in altering mitochondrial dynamics, respiration, and autophagy in cardiomyocytes. Redox Biol. 36, 101660. https://doi.org/10.1016/j.redox.2020.101660

Aminzadeh, A., Dehpour, A.R., Safa, M., Mirzamohammadi, S., Sharifi, A.M., 2014. Investigating the Protective Effect of Lithium Against High Glucose-Induced Neurotoxicity in PC12 Cells: Involvements of ROS, JNK and P38 MAPKs, and Apoptotic Mitochondria Pathway. Cell. Mol. Neurobiol. 34, 1143–1150. https://doi.org/10.1007/s10571-014-0089-y

Apicella, M., Giannoni, E., Fiore, S., Ferrari, K.J., Fernández-Pérez, D., Isella, C., Granchi, C., Minutolo, F., Sottile, A., Comoglio, P.M., Medico, E., Pietrantonio, F., Volante, M., Pasini, D., Chiarugi, P., Giordano, S., Corso, S., 2018. Increased Lactate Secretion by Cancer Cells Sustains Non-cell-autonomous Adaptive Resistance to MET and EGFR Targeted Therapies. Cell Metab. 28, 848-865.e6. https://doi.org/10.1016/j.cmet.2018.08.006

Ataullakhanov, F.I., Vitvitsky, V.M., 2002. What determines the intracellular ATP concentration. Biosci. Rep. 22, 501–511. https://doi.org/10.1023/a:1022069718709

Atchison, E.A., Gridley, G., Carreon, J.D., Leitzmann, M.F., McGlynn, K.A., 2011. Risk of cancer in a large cohort of U.S. veterans with diabetes. Int. J. Cancer 128, 635–643. https://doi.org/10.1002/ijc.25362

Bangsbo, J., Gibala, M.J., Krustrup, P., González-Alonso, J., Saltin, B., 2002. Enhanced pyruvate dehydrogenase activity does not affect muscle O2 uptake at onset of intense exercise in humans. Am. J. Physiol.-Regul. Integr. Comp. Physiol. 282, R273–R280. https://doi.org/10.1152/ajpregu.2002.282.1.R273

Bao, Z., Chen, K., Krepel, S., Tang, P., Gong, W., Zhang, M., Liang, W., Trivett, A., Zhou, M., Wang, J.M., 2019. High Glucose Promotes Human Glioblastoma Cell Growth by Increasing the Expression and Function of Chemoattractant and Growth Factor Receptors. Transl. Oncol. 12, 1155–1163. https://doi.org/10.1016/j.tranon.2019.04.016

Bordt, E.A., Clerc, P., Roelofs, B.A., Saladino, A.J., Tretter, L., Adam-Vizi, V., Cherok, E., Khalil, A., Yadava, N., Ge, S.X., Francis, T.C., Kennedy, N.W., Picton, L.K., Kumar, T., Uppuluri, S., Miller, A.M., Itoh, K., Karbowski, M., Sesaki, H., Hill, R.B., Polster, B.M., 2017. The Putative Drp1 Inhibitor mdivi-1 Is a Reversible Mitochondrial Complex I Inhibitor that Modulates Reactive Oxygen Species. Dev. Cell 40, 583-594.e6. https://doi.org/10.1016/j.devcel.2017.02.020

Boudina, S., Sena, S., Theobald, H., Sheng, X., Wright, J.J., Hu, X.X., Aziz, S., Johnson, J.I., Bugger, H., Zaha, V.G., Abel, E.D., 2007. Mitochondrial energetics in the heart in obesity-related diabetes: direct evidence for increased uncoupled respiration and activation of uncoupling proteins. Diabetes 56, 2457–2466. https://doi.org/10.2337/db07-0481

Bredt, D.S., 1999. Endogenous nitric oxide synthesis: Biological functions and pathophysiology. Free Radic. Res. 31, 577–596. https://doi.org/10.1080/10715769900301161

Brière, J.-J., Favier, J., Bénit, P., Ghouzzi, V.E., Lorenzato, A., Rabier, D., Di Renzo, M.F., Gimenez-Roqueplo, A.-P., Rustin, P., 2005. Mitochondrial succinate is instrumental for HIF1α nuclear translocation in SDHA-mutant fibroblasts under normoxic conditions. Hum. Mol. Genet. 14, 3263–3269. https://doi.org/10.1093/hmg/ddi359

Brown, G.C., Borutaite, V., 2004. Inhibition of mitochondrial respiratory complex I by nitric oxide, peroxynitrite and S-nitrosothiols. Biochim. Biophys. Acta BBA - Bioenerg., EBEC 2004 1658, 44–49. https://doi.org/10.1016/j.bbabio.2004.03.016

Brown, G.C., Cooper, Chris.E., 1994. Nanomolar concentrations of nitric oxide reversibly inhibit synaptosomal respiration by competing with oxygen at cytochrome oxidase. FEBS Lett. 356, 295–298. https://doi.org/10.1016/0014-5793(94)01290-3

Brownlee, M., 2001. Biochemistry and molecular cell biology of diabetic complications. Nature 414, 813–820. https://doi.org/10.1038/414813a

Bugger, H., Boudina, S., Hu, X.X., Tuinei, J., Zaha, V.G., Theobald, H.A., Yun, U.J., McQueen, A.P., Wayment, B., Litwin, S.E., Abel, E.D., 2008. Type 1 diabetic akita mouse hearts are insulin sensitive but manifest structurally abnormal mitochondria that remain coupled despite increased uncoupling protein 3. Diabetes 57, 2924–2932. https://doi.org/10.2337/db08-0079

Burrell, R.A., McClelland, S.E., Endesfelder, D., Groth, P., Weller, M.-C., Shaikh, N., Domingo, E., Kanu, N., Dewhurst, S.M., Gronroos, E., Chew, S.K., Rowan, A.J., Schenk, A., Sheffer, M., Howell, M., Kschischo, M., Behrens, A., Helleday, T., Bartek, J., Tomlinson, I.P., Swanton, C., 2013. Replication stress links structural and numerical cancer chromosomal instability. Nature 494, 492–496. https://doi.org/10.1038/nature11935

Cadenas, E., 2004. Mitochondrial free radical production and cell signaling. Mol. Aspects Med., Oxidative Stress in Aging and Disease - Mitochondrial Aging, Neuronal Fuction and Neurodegeneration, and Oxidative Metabolic Disorders and Diseases 25, 17–26. https://doi.org/10.1016/j.mam.2004.02.005

Calle, E.E., Thun, M.J., Petrelli, J.M., Rodriguez, C., Heath, C.W., 1999. Body-mass index and mortality in a prospective cohort of U.S. adults. N. Engl. J. Med. 341, 1097–1105. https://doi.org/10.1056/NEJM199910073411501

Campbell, P.T., Newton, C.C., Patel, A.V., Jacobs, E.J., Gapstur, S.M., 2012. Diabetes and cause-specific mortality in a prospective cohort of one million U.S. adults. Diabetes Care 35, 1835–1844. https://doi.org/10.2337/dc12-0002

Caneba, C.A., Yang, L., Baddour, J., Curtis, R., Win, J., Hartig, S., Marini, J., Nagrath, D., 2014. Nitric oxide is a positive regulator of the Warburg effect in ovarian cancer cells. Cell Death Dis. 5, e1302. https://doi.org/10.1038/cddis.2014.264

Cantin, A.M., Paquette, B., Richter, M., Larivée, P., 2000. Albumin-mediated regulation of cellular glutathione and nuclear factor kappa B activation. Am. J. Respir. Crit. Care Med. 162, 1539–1546. https://doi.org/10.1164/ajrccm.162.4.9910106

Casuso, R.A., Huertas, J.R., 2020. The emerging role of skeletal muscle mitochondrial dynamics in exercise and ageing. Ageing Res. Rev. 58, 101025. https://doi.org/10.1016/j.arr.2020.101025

Chandrika, G., Natesh, K., Ranade, D., Chugh, A., Shastry, P., 2017. Mammalian target of rapamycin inhibitors, temsirolimus and torin 1, attenuate stemness-associated properties and expression of mesenchymal markers promoted by phorbol-myristate-acetate and oncostatin-M in glioblastoma cells. Tumor Biol. 39, 1010428317695921. https://doi.org/10.1177/1010428317695921

Chang, J., Yi, H., Kim, H.-W., Shong, M., 2017. Dysregulation of mitophagy in carcinogenesis and tumor progression. Biochim. Biophys. Acta Bioenerg. https://doi.org/10.1016/j.bbabio.2016.12.008

Chen, Z., Ma, Y., Yang, Q., Hu, J., Feng, J., Liang, W., Ding, G., 2020. AKAP1 mediates high glucose-induced mitochondrial fission through the phosphorylation of Drp1 in podocytes. J. Cell. Physiol. 235, 7433–7448. https://doi.org/10.1002/jcp.29646

Cicuttini, F.M., Hurley, S.F., Forbes, A.B., Donnan, G.A., Salzberg, M., Giles, G.G., McNeil, J.J., 1997. Association of adult glioma with medical conditions, family and reproductive history. Int. J. Cancer 203–207. https://doi.org/10.1002/(SICI)1097-0215(19970410)71:2<203::AID-IJC13>3.0.CO;2-I

Cleeter, M.W.J., Cooper, J.M., Darley-Usmar, V.M., Moncada, S., Schapira, A.H.V., 1994. Reversible inhibition of cytochrome c oxidase, the terminal enzyme of the mitochondrial respiratory chain, by nitric oxide: Implications for neurodegenerative diseases. FEBS Lett. 345, 50–54. https://doi.org/10.1016/0014-5793(94)00424-2

Cunningham, J.T., Rodgers, J.T., Arlow, D.H., Vazquez, F., Mootha, V.K., Puigserver, P., 2007. mTOR controls mitochondrial oxidative function through a YY1–PGC-1α transcriptional complex. Nature 450, 736–740. https://doi.org/10.1038/nature06322

Currie, E., Schulze, A., Zechner, R., Walther, T.C., Farese, R.V., 2013. Cellular Fatty Acid Metabolism and Cancer. Cell Metab. 18, 153–161. https://doi.org/10.1016/j.cmet.2013.05.017

Dai, W., Wang, G., Chwa, J., Oh, M.E., Abeywardana, T., Yang, Y., Wang, Q.A., Jiang, L., 2020. Mitochondrial division inhibitor (mdivi-1) decreases oxidative metabolism in cancer. Br. J. Cancer 122, 1288–1297. https://doi.org/10.1038/s41416-020-0778-x

de la Cruz López, K.G., Toledo Guzmán, M.E., Sánchez, E.O., García Carrancá, A., 2019. mTORC1 as a Regulator of Mitochondrial Functions and a Therapeutic Target in Cancer. Front. Oncol. 9, 1373. https://doi.org/10.3389/fonc.2019.01373

Diaz-Morales, N., Rovira-Llopis, S., Bañuls, C., Escribano-Lopez, I., de Marañon, A.M., Lopez-Domenech, S., Orden, S., Roldan-Torres, I., Alvarez, A., Veses, S., Jover, A., Rocha, M., Hernandez-Mijares, A., Victor, V.M., 2016. Are Mitochondrial Fusion and Fission Impaired in Leukocytes of Type 2 Diabetic Patients? Antioxid. Redox Signal. 25, 108–115. https://doi.org/10.1089/ars.2016.6707

Du, Q., Zhang, Xinglu, Liu, Q., Zhang, Xianghong, Bartels, C.E., Geller, D.A., 2013. Nitric oxide production upregulates Wnt/β-catenin signaling by inhibiting Dickkopf-1. Cancer Res. 73, 6526–6537. https://doi.org/10.1158/0008-5472.can-13-1620

Edick, M.J., Cheng, C., Yang, W., Cheok, M., Wilkinson, M.R., Pei, D., Evans, W.E., Kun, L.E., Pui, C.-H., Relling, M.V., 2005. Lymphoid gene expression as a predictor of risk of secondary brain tumors. Genes. Chromosomes Cancer 42, 107–116. https://doi.org/10.1002/gcc.20121

Ferlay, J., Soerjomataram, I., Dikshit, R., Eser, S., Mathers, C., Rebelo, M., Parkin, D.M., Forman, D., Bray, F., 2015. Cancer incidence and mortality worldwide: sources, methods and major patterns in GLOBOCAN 2012. Int. J. Cancer 136, E359-386. https://doi.org/10.1002/ijc.29210

Fornai, F., Longone, P., Ferrucci, M., Lenzi, P., Isidoro, C., Ruggieri, S., Paparelli, A., 2008. Autophagy and amyotrophic lateral sclerosis: The multiple roles of lithium. Autophagy 4, 527–530. https://doi.org/10.4161/auto.5923

Gao, P., Yang, C., Nesvick, C.L., Feldman, M.J., Sizdahkhani, S., Liu, H., Chu, H., Yang, F., Tang, L., Tian, J., Zhao, S., Li, G., Heiss, J.D., Liu, Y., Zhuang, Z., Xu, G., 2016. Hypotaurine evokes a malignant phenotype in glioma through aberrant hypoxic signaling. Oncotarget 7, 15200–15214. https://doi.org/10.18632/oncotarget.7710

Glick, D., Barth, S., Macleod, K.F., 2010. Autophagy: cellular and molecular mechanisms. J. Pathol. 221, 3–12. https://doi.org/10.1002/path.2697

Green, K., Brand, M.D., Murphy, M.P., 2004. Prevention of mitochondrial oxidative damage as a therapeutic strategy in diabetes. Diabetes 53 Suppl 1, S110-118. https://doi.org/10.2337/diabetes.53.2007.s110

Gunter, T.E., Pfeiffer, D.R., 1990. Mechanisms by which mitochondria transport calcium. Am. J. Physiol. 258, C755-786. https://doi.org/10.1152/ajpcell.1990.258.5.C755

Gunter, T.E., Yule, D.I., Gunter, K.K., Eliseev, R.A., Salter, J.D., 2004. Calcium and mitochondria. FEBS Lett. 567, 96–102. https://doi.org/10.1016/j.febslet.2004.03.071

Guo, D., Bell, E.H., Chakravarti, A., 2013. Lipid metabolism emerges as a promising target for malignant glioma therapy. CNS Oncol. 2, 289–299. https://doi.org/10.2217/cns.13.20

GUPPY, M., LEEDMAN, P., ZU, X., RUSSELL, V., 2002. Contribution by different fuels and metabolic pathways to the total ATP turnover of proliferating MCF-7 breast cancer cells. Biochem. J. 364, 309–315. https://doi.org/10.1042/bj3640309

Gupta, K., Kalra, I., Salunke, P., Vasishta, R.K., 2011. Lipidized glioblastoma: A rare differentiation pattern. Neuropathology 31, 93–97. https://doi.org/10.1111/j.1440-1789.2010.01141.x

Hansford, R.G., Zorov, D., 1998. Role of mitochondrial calcium transport in the control of substrate oxidation. Mol. Cell. Biochem. 184, 359–369.

Heiden, M.G.V., Cantley, L.C., Thompson, C.B., 2009. Understanding the Warburg Effect: The Metabolic Requirements of Cell Proliferation. Science. https://doi.org/10.1126/science.1160809

Hjalgrim, H., Frisch, M., Ekbom, A., Kyvik, K.O., Melbye, M., Green, A., 1997. Cancer and diabetes--a follow-up study of two population-based cohorts of diabetic patients. J. Intern. Med. 241, 471–475. https://doi.org/10.1111/j.1365-2796.1997.tb00004.x

Ichishita, R., Tanaka, K., Sugiura, Y., Sayano, T., Mihara, K., Oka, T., 2008. An RNAi Screen for Mitochondrial Proteins Required to Maintain the Morphology of the Organelle in Caenorhabditis elegans. J. Biochem. (Tokyo) 143, 449–454. https://doi.org/10.1093/jb/mvm245

Ikuma, H., 1970. Necessary conditions for isolation of tightly coupled higher plant mitochondria. Plant Physiol. 45, 773–781. https://doi.org/10.1104/pp.45.6.773

Izyumov, D.S., Avetisyan, A.V., Pletjushkina, O.Y., Sakharov, D.V., Wirtz, K.W., Chernyak, B.V., Skulachev, V.P., 2004. “Wages of Fear”: transient threefold decrease in intracellular ATP level imposes apoptosis. Biochim. Biophys. Acta BBA - Bioenerg., EBEC 2004 1658, 141–147. https://doi.org/10.1016/j.bbabio.2004.05.007

Johnson, S.C., Yanos, M.E., Kayser, E.-B., Quintana, A., Sangesland, M., Castanza, A., Uhde, L., Hui, J., Wall, V.Z., Gagnidze, A., Oh, K., Wasko, B.M., Ramos, F.J., Palmiter, R.D., Rabinovitch, P.S., Morgan, P.G., Sedensky, M.M., Kaeberlein, M., 2013. mTOR Inhibition Alleviates Mitochondrial Disease in a Mouse Model of Leigh Syndrome. Science. https://doi.org/10.1126/science.1244360

Kane, M.S., Paris, A., Codron, P., Cassereau, J., Procaccio, V., Lenaers, G., Reynier, P., Chevrollier, A., 2018. Current mechanistic insights into the CCCP-induced cell survival response. Biochem. Pharmacol. 148, 100–110. https://doi.org/10.1016/j.bcp.2017.12.018

Kim, J., Jang, H.-J., Martinez-Lemus, L.A., Sowers, J.R., 2012. Activation of mTOR/p70S6 kinase by ANG II inhibits insulin-stimulated endothelial nitric oxide synthase and vasodilation. Am. J. Physiol.-Endocrinol. Metab. 302, E201–E208. https://doi.org/10.1152/ajpendo.00497.2011

King, A., Selak, M.A., Gottlieb, E., 2006. Succinate dehydrogenase and fumarate hydratase: linking mitochondrial dysfunction and cancer. Oncogene 25, 4675–4682. https://doi.org/10.1038/sj.onc.1209594

Kitahara, C.M., Linet, M.S., Brenner, A.V., Wang, S.S., Melin, B.S., Wang, Z., Inskip, P.D., Beane Freeman, L.E., Braganza, M.Z., Carreón, T., Feychting, M., Gaziano, J.M., Peters, U., Purdue, M.P., Ruder, A.M., Sesso, H.D., Shu, X.-O., Waters, M.A., White, E., Zheng, W., Hoover, R.N., Fraumeni, J.F., Chatterjee, N., Yeager, M., Chanock, S.J., Hartge, P., Rajaraman, P., 2014. Personal history of diabetes, genetic susceptibility to diabetes, and risk of brain glioma: a pooled analysis of observational studies. Cancer Epidemiol. Biomark. Prev. Publ. Am. Assoc. Cancer Res. Cosponsored Am. Soc. Prev. Oncol. 23, 47–54. https://doi.org/10.1158/1055-9965.EPI-13-0913

Kobayashi, S., Zhao, F., Zhang, Z., Kobayashi, T., Huang, Y., Shi, B., Wu, W., Liang, Q., 2020. Mitochondrial Fission and Mitophagy Coordinately Restrict High Glucose Toxicity in Cardiomyocytes. Front. Physiol. 11, 1596. https://doi.org/10.3389/fphys.2020.604069

Koppenol, W.H., Bounds, P.L., Dang, C.V., 2011. Otto Warburg's contributions to current concepts of cancer metabolism. Nat. Rev. Cancer 11, 325–337. https://doi.org/10.1038/nrc3038

Korde Choudhari, S., Chaudhary, M., Bagde, S., Gadbail, A.R., Joshi, V., 2013. Nitric oxide and cancer: a review. World J. Surg. Oncol. 11, 118. https://doi.org/10.1186/1477-7819-11-118

Layton, D., Symmons, P., 1973. The effect of some uncoupling agents, ionophorous agents and inhibitors on the fluorescence of ANS bound to bovine serum albumin. FEBS Lett. 30, 325–328. https://doi.org/10.1016/0014-5793(73)80680-5

Letessier, A., Garrido-Urbani, S., Ginestier, C., Fournier, G., Esterni, B., Monville, F., Adélaïde, J., Geneix, J., Xerri, L., Dubreuil, P., Viens, P., Charafe-Jauffret, E., Jacquemier, J., Birnbaum, D., Lopez, M., Chaffanet, M., 2007. Correlated break at PARK2/FRA6E and loss of AF-6/Afadin protein expression are associated with poor outcome in breast cancer. Oncogene 26, 298–307. https://doi.org/10.1038/sj.onc.1209772

Lin, H., Patel, S., Affleck, V.S., Wilson, I., Turnbull, D.M., Joshi, A.R., Maxwell, R., Stoll, E.A., 2017. Fatty acid oxidation is required for the respiration and proliferation of malignant glioma cells. Neuro-Oncol. 19, 43–54. https://doi.org/10.1093/neuonc/now128

Ling, S., Brown, K., Miksza, J.K., Howells, L., Morrison, A., Issa, E., Yates, T., Khunti, K., Davies, M.J., Zaccardi, F., 2020. Association of Type 2 Diabetes With Cancer: A Meta-analysis With Bias Analysis for Unmeasured Confounding in 151 Cohorts Comprising 32 Million People. Diabetes Care 43, 2313–2322. https://doi.org/10.2337/dc20-0204

López de Figueroa, P., Lotz, M.K., Blanco, F.J., Caramés, B., 2015. Autophagy Activation and Protection From Mitochondrial Dysfunction in Human Chondrocytes. Arthritis Rheumatol. 67, 966–976. https://doi.org/10.1002/art.39025

MAYNARD, G.D., 1910. A STATISTICAL STUDY IN CANCER DEATH-RATES. Biometrika 7, 276–304. https://doi.org/10.1093/biomet/7.3.276

MiPNet08.09 CellRespiration - Bioblast [WWW Document], n.d. URL https://wiki.oroboros.at/index.php/MiPNet08.09_CellRespiration (accessed 2.19.21).

Mitchell, P., 2011. Chemiosmotic coupling in oxidative and photosynthetic phosphorylation. 1966. Biochim. Biophys. Acta 1807, 1507–1538. https://doi.org/10.1016/j.bbabio.2011.09.018

Mitochondrial electron transport chain, ROS generation and uncoupling (Review) - PubMed [WWW Document], n.d. URL https://pubmed.ncbi.nlm.nih.gov/31115493/ (accessed 3.24.21).

Mizushima, N., Levine, B., Cuervo, A.M., Klionsky, D.J., 2008. Autophagy fights disease through cellular self-digestion. Nature 451, 1069–1075. https://doi.org/10.1038/nature06639

Modrek, A.S., Bayin, N.S., Placantonakis, D.G., 2014. Brain stem cells as the cell of origin in glioma. World J. Stem Cells 6, 43–52. https://doi.org/10.4252/wjsc.v6.i1.43

Morita, M., Gravel, S.-P., Hulea, L., Larsson, O., Pollak, M., St-Pierre, J., Topisirovic, I., 2015. mTOR coordinates protein synthesis, mitochondrial activity and proliferation. Cell Cycle 14, 473–480. https://doi.org/10.4161/15384101.2014.991572

Morita, M., Prudent, J., Basu, K., Goyon, V., Katsumura, S., Hulea, L., Pearl, D., Siddiqui, N., Strack, S., McGuirk, S., St-Pierre, J., Larsson, O., Topisirovic, I., Vali, H., McBride, H.M., Bergeron, J.J., Sonenberg, N., 2017. mTOR Controls Mitochondrial Dynamics and Cell Survival via MTFP1. Mol. Cell 67, 922-935.e5. https://doi.org/10.1016/j.molcel.2017.08.013

Muro, E., Atilla-Gokcumen, G.E., Eggert, U.S., 2014. Lipids in cell biology: how can we understand them better? Mol. Biol. Cell 25, 1819–1823. https://doi.org/10.1091/mbc.e13-09-0516

Nakatogawa, H., Suzuki, K., Kamada, Y., Ohsumi, Y., 2009. Dynamics and diversity in autophagy mechanisms: lessons from yeast. Nat. Rev. Mol. Cell Biol. 10, 458–467. https://doi.org/10.1038/nrm2708

Narendra, D., Tanaka, A., Suen, D.-F., Youle, R.J., 2008. Parkin is recruited selectively to impaired mitochondria and promotes their autophagy. J. Cell Biol. 183, 795–803. https://doi.org/10.1083/jcb.200809125

Nishikawa, T., Edelstein, D., Du, X.L., Yamagishi, S., Matsumura, T., Kaneda, Y., Yorek, M.A., Beebe, D., Oates, P.J., Hammes, H.P., Giardino, I., Brownlee, M., 2000. Normalizing mitochondrial superoxide production blocks three pathways of hyperglycaemic damage. Nature 404, 787–790. https://doi.org/10.1038/35008121

O'Mara, B.A., Byers, T., Schoenfeld, E., 1985. Diabetes mellitus and cancer risk: a multisite case-control study. J. Chronic Dis. 38, 435–441. https://doi.org/10.1016/0021-9681(85)90139-0

Pesta, D., Gnaiger, E., 2012. High-resolution respirometry: OXPHOS protocols for human cells and permeabilized fibers from small biopsies of human muscle. Methods Mol. Biol. Clifton NJ 810, 25–58. https://doi.org/10.1007/978-1-61779-382-0_3

Poderoso, J.J., Carreras, M.C., Lisdero, C., Riobó, N., Schöpfer, F., Boveris, A., 1996. Nitric Oxide Inhibits Electron Transfer and Increases Superoxide Radical Production in Rat Heart Mitochondria and Submitochondrial Particles. Arch. Biochem. Biophys. 328, 85–92. https://doi.org/10.1006/abbi.1996.0146

Ramanathan, A., Schreiber, S.L., 2009. Direct control of mitochondrial function by mTOR. Proc. Natl. Acad. Sci. 106, 22229–22232. https://doi.org/10.1073/pnas.0912074106

Roy, S., Awasthi, A., 2019. ATP Triggers Human Th9 Cell Differentiation via Nitric Oxide-Mediated mTOR-HIF1α Pathway. Front. Immunol. 10, 1120. https://doi.org/10.3389/fimmu.2019.01120

Ruiz, A., Alberdi, E., Matute, C., 2018. Mitochondrial Division Inhibitor 1 (mdivi-1) Protects Neurons against Excitotoxicity through the Modulation of Mitochondrial Function and Intracellular Ca2+ Signaling. Front. Mol. Neurosci. 11, 3. https://doi.org/10.3389/fnmol.2018.00003

Salabei, J.K., Gibb, A.A., Hill, B.G., 2014. Comprehensive measurement of respiratory activity in permeabilized cells using extracellular flux analysis. Nat. Protoc. 9, 421–438. https://doi.org/10.1038/nprot.2014.018

Santos, C.R., Schulze, A., 2012. Lipid metabolism in cancer. FEBS J. 279, 2610–2623. https://doi.org/10.1111/j.1742-4658.2012.08644.x

Schieke, S.M., Phillips, D., McCoy, J.P., Aponte, A.M., Shen, R.F., Balaban, R.S., Finkel, T., 2006. The mammalian target of rapamycin (mTOR) pathway regulates mitochondrial oxygen consumption and oxidative capacity. J. Biol. Chem. 281, 27643–27652. https://doi.org/10.1074/jbc.M603536200

Schlehofer, B., Blettner, M., Becker, N., Martinsohn, C., Wahrendorf, J., 1992. Medical risk factors and the development of brain tumors. Cancer 69, 2541–2547. https://doi.org/10.1002/1097-0142(19920515)69:10<2541::AID-CNCR2820691025>3.0.CO;2-H

Schlehofer, B., Blettner, M., Preston-Martin, S., Niehoff, D., Wahrendorf, J., Arslan, A., Ahlbom, A., Choi, W.N., Giles, G.G., Howe, G.R., Little, J., Ménégoz, F., Ryan, P., 1999. Role of medical history in brain tumour development. Results from the international adult brain tumour study. Int. J. Cancer 82, 155–160. https://doi.org/10.1002/(sici)1097-0215(19990719)82:2<155::aid-ijc1>3.0.co;2-p

Schwartzbaum, J., Jonsson, F., Ahlbom, A., Preston-Martin, S., Malmer, B., Lönn, S., Söderberg, K., Feychting, M., 2005. Prior hospitalization for epilepsy, diabetes, and stroke and subsequent glioma and meningioma risk. Cancer Epidemiol. Biomark. Prev. Publ. Am. Assoc. Cancer Res. Cosponsored Am. Soc. Prev. Oncol. 14, 643–650. https://doi.org/10.1158/1055-9965.EPI-04-0119

Sebastián, D., Palacín, M., Zorzano, A., 2017. Mitochondrial Dynamics: Coupling Mitochondrial Fitness with Healthy Aging. Trends Mol. Med. 23, 201–215. https://doi.org/10.1016/j.molmed.2017.01.003

Seliger, C., Ricci, C., Meier, C.R., Bodmer, M., Jick, S.S., Bogdahn, U., Hau, P., Leitzmann, M.F., 2016. Diabetes, use of antidiabetic drugs, and the risk of glioma. Neuro-Oncol. 18, 340–349. https://doi.org/10.1093/neuonc/nov100

Skogh, T., Magnusson, K.E., Stendahl, O., 1983a. Hydrophobic interaction between DNP-HSA and different tissue structures in vivo assessed by indirect

immunofluorescence microscopy. J. Immunol. Methods 61, 385–390. https://doi.org/10.1016/0022-1759(83)90235-1
Skogh, T., Stendahl, O., Sundqvist, T., Edebo, L., 1983b. Physicochemical properties and blood clearance of human serum albumin conjugated to different extents with dinitrophenyl groups. Int. Arch. Allergy Appl. Immunol. 70, 238–244. https://doi.org/10.1159/000233330
Soutar, M.P.M., Kempthorne, L., Annuario, E., Luft, C., Wray, S., Ketteler, R., Ludtmann, M.H.R., Plun-Favreau, H., 2019. FBS/BSA media concentration determines CCCP's ability to depolarize mitochondria and activate PINK1-PRKN mitophagy. Autophagy 15, 2002–2011. https://doi.org/10.1080/15548627.2019.1603549
Steenland, K., Nowlin, S., Palu, S., 1995. Cancer incidence in the National Health and Nutrition Survey I. Follow-up data: diabetes, cholesterol, pulse and physical activity. Cancer Epidemiol. Prev. Biomark. 4, 807–811.
Stupp, R., Mason, W.P., van den Bent, M.J., Weller, M., Fisher, B., Taphoorn, M.J.B., Belanger, K., Brandes, A.A., Marosi, C., Bogdahn, U., Curschmann, J., Janzer, R.C., Ludwin, S.K., Gorlia, T., Allgeier, A., Lacombe, D., Cairncross, J.G., Eisenhauer, E., Mirimanoff, R.O., European Organisation for Research and Treatment of Cancer Brain Tumor and Radiotherapy Groups, National Cancer Institute of Canada Clinical Trials Group, 2005. Radiotherapy plus concomitant and adjuvant temozolomide for glioblastoma. N. Engl. J. Med. 352, 987–996. https://doi.org/10.1056/NEJMoa043330
Swerdlow, A.J., Laing, S.P., Qiao, Z., Slater, S.D., Burden, A.C., Botha, J.L., Waugh, N.R., Morris, A.D., Gatling, W., Gale, E.A., Patterson, C.C., Keen, H., 2005. Cancer incidence and mortality in patients with insulin-treated diabetes: a UK cohort study. Br. J. Cancer 92, 2070–2075. https://doi.org/10.1038/sj.bjc.6602611
Takeuchi, H., Kondo, Y., Fujiwara, K., Kanzawa, T., Aoki, H., Mills, G.B., Kondo, S., 2005. Synergistic Augmentation of Rapamycin-Induced Autophagy in Malignant Glioma Cells by Phosphatidylinositol 3-Kinase/Protein Kinase B Inhibitors. Cancer Res. 65, 3336–3346. https://doi.org/10.1158/0008-5472.CAN-04-3640
Thomas, D.D., 2015. Breathing new life into nitric oxide signaling: A brief overview of the interplay between oxygen and nitric oxide. Redox Biol. 5, 225–233. https://doi.org/10.1016/j.redox.2015.05.002
Tugnoli, V., Tosi, M.R., Tinti, A., Trinchero, A., Bottura, G., Fini, G., 2001. Characterization of lipids from human brain tissues by multinuclear magnetic resonance spectroscopy. Biopolymers 62, 297–306. https://doi.org/10.1002/bip.10005
Twig, G., Elorza, A., Molina, A.J.A., Mohamed, H., Wikstrom, J.D., Walzer, G., Stiles, L., Haigh, S.E., Katz, S., Las, G., Alroy, J., Wu, M., Py, B.F., Yuan, J., Deeney, J.T., Corkey, B.E., Shirihai, O.S., 2008. Fission and selective fusion govern mitochondrial segregation and elimination by autophagy. EMBO J. 27, 433–446. https://doi.org/10.1038/sj.emboj.7601963
Vogel, K.R., Ainslie, G.R., Jansen, E.E.W., Salomons, G.S., Gibson, K.M., 2015. Torin 1 partially corrects vigabatrin-induced mitochondrial increase in mouse. Ann. Clin. Transl. Neurol. 2, 699–706. https://doi.org/10.1002/acn3.200
Wang, R., Jiao, H., Zhao, J., Wang, X., Lin, H., 2018. L-Arginine Enhances Protein Synthesis by Phosphorylating mTOR (Thr 2446) in a Nitric Oxide-Dependent Manner in C2C12 Cells. Oxid. Med. Cell. Longev. 2018, e7569127. https://doi.org/10.1155/2018/7569127

Warburg, O., 1925. The Metabolism of Carcinoma Cells. J. Cancer Res. 9, 148–163. https://doi.org/10.1158/jcr.1925.148

Welte, M.A., 2015. Expanding Roles for Lipid Droplets. Curr. Biol. 25, R470–R481. https://doi.org/10.1016/j.cub.2015.04.004

Wideroff, L., Gridley, G., Chow, W.-H., Linet, M., Mellemkjaer, L., Olsen, J.H., Keehn, S., Borch-Johnsen, K., 1997. Cancer Incidence in a Population-Based Cohort of Patients Hospitalized With Diabetes Mellitus in Denmark. JNCI J. Natl. Cancer Inst. 89, 1360–1365. https://doi.org/10.1093/jnci/89.18.1360

Wu, Q.-R., Zheng, D.-L., Liu, P.-M., Yang, H., Li, L.-A., Kuang, S.-J., Lai, Y.-Y., Rao, F., Xue, Y.-M., Lin, J.-J., Liu, S.-X., Chen, C.-B., Deng, C.-Y., 2021. High glucose induces Drp1-mediated mitochondrial fission via the Orai1 calcium channel to participate in diabetic cardiomyocyte hypertrophy. Cell Death Dis. 12, 1–15. https://doi.org/10.1038/s41419-021-03502-4

Xu, R., Pelicano, H., Zhou, Y., Carew, J.S., Feng, L., Bhalla, K.N., Keating, M.J., Huang, P., 2005. Inhibition of Glycolysis in Cancer Cells: A Novel Strategy to Overcome Drug Resistance Associated with Mitochondrial Respiratory Defect and Hypoxia. Cancer Res. 65, 613–621.

Yang, Z., Klionsky, D.J., 2010. Mammalian autophagy: core molecular machinery and signaling regulation. Curr. Opin. Cell Biol. 22, 124–131. https://doi.org/10.1016/j.ceb.2009.11.014

Yaniv, Y., Juhaszova, M., Nuss, H.B., Wang, S., Zorov, D.B., Lakatta, E.G., Sollott, S.J., 2010. Matching ATP supply and demand in mammalian heart: in vivo, in vitro, and in silico perspectives. Ann. N. Y. Acad. Sci. 1188, 133–142. https://doi.org/10.1111/j.1749-6632.2009.05093.x

Yu, M., Chen, S., Hong, W., Gu, Y., Huang, B., Lin, Y., Zhou, Y., Jin, H., Deng, Y., Tu, L., Hou, B., Jian, Z., 2019. Prognostic role of glycolysis for cancer outcome: evidence from 86 studies. J. Cancer Res. Clin. Oncol. 145, 967–999. https://doi.org/10.1007/s00432-019-02847-w

Zaidi, N., Royaux, I., Swinnen, J.V., Smans, K., 2012. ATP Citrate Lyase Knockdown Induces Growth Arrest and Apoptosis through Different Cell- and Environment-Dependent Mechanisms. Mol. Cancer Ther. 11, 1925–1935. https://doi.org/10.1158/1535-7163.MCT-12-0095

Zorov, D.B., Juhaszova, M., Sollott, S.J., 2014. Mitochondrial reactive oxygen species (ROS) and ROS-induced ROS release. Physiol. Rev. 94, 909–950. https://doi.org/10.1152/physrev.00026.2013